Electronic Supplementary Material (ESI) for Chemical Science.

Supporting Information

Solvent-controlled E/Z isomerization *vs.* [2+2] photocycloaddition mediated by supramolecular polymerization

Torsten Dünnebacke,[a] Kalathil K. Kartha,[a] Johannes M. Wahl,[a] Rodrigo Q. Albuquerque,[a] Gustavo Fernández*[a]

[a] T. Dünnebacke, Dr. Kalathil K. Kartha, Dr. J. M. Wahl, Dr. R. Q. Albuquerque, Prof. Dr. G. Fernández
Organisch-Chemisches Institut
Westfälische Wilhelms-Universität Münster
Corrensstraße 40, 48149 Münster (Germany)
E-mail: fernandg@uni-muenster.de

Summary of contents

1. Experimental Procedures

1.1. Materials and Methods

General Procedures: All solvents were dried according to standard procedures. Reagents were used as purchased. All air-sensitive reactions were carried out under argon or nitrogen atmosphere. Flash chromatography was performed using silica gel (*Merck Silica 60*, particle size 0.04–0.063 nm).

NMR measurements: ^{1}H and ^{13}C NMR spectra were recorded on a *Bruker Avance 400* (^{1}H: 400 MHz; ^{13}C: 100.6 MHz) and a *Bruker AV300* (^{1}H: 300 MHz; ^{13}C: 100.6 MHz). Additional 1D ^{1}H as well as 2D H,H COSY and 2D H,H ROESY spectra were recorded on an *Agilent DD2 500* (^{1}H: 500 MHz) and an *Agilent DD2 600* (^{1}H: 600 MHz) at a standard temperature of 298 K in deuterated solvents. Deviating temperature is explicitly mentioned when used. The recorded spectra were referenced to the remaining resonance signals of the deuterated solvents ($CDCl_3$: 7.26 ppm (^{1}H); DCM: 5.32 ppm (^{1}H); DMSO: 2.50 ppm (^{1}H,); THF: 1.73 ppm (^{1}H); D_2O: 4.79 (^{1}H); MeOD: 4.87 ppm (^{1}H)). The coupling constant J of the measured spin multiplets is given in Hertz (Hz) and the chemical shifts δ are given in reference to the chemical shift of trimethylsilane (0 ppm). The abbreviations used to analyze the recorded spectra are: *s* (singlet), *d* (doublet), *t* (triplet), *q* (quartet), *m* (multiplet).

Mass spectroscopy: MALDI-mass spectra were recorded on an *Autoflex Speed* manufactured by *Bruker Daltronics*. A *SmartBeamTM* NdYAF-Laser with a wavelength of 335 nm was used. The signals are described by their mass/charge ratio (*m/z*) in Da. ESI accurate masses were measured on a MicroTof (Bruker Daltronics, Bremen) with loop injection. Mass calibration was performed using sodium formate cluster ions immediatley folled by the sample in a quasi internal calibration. ESI mass spectra were recorded on an LTQ Orbitap LTQ XL (Thermo-Fisher Scientific, Bremen) with nano spray (alternatively HPLC, loop injection, syringe pumpe).

UV-Vis spectroscopy: All UV-Vis spectra were recorded on a *V-770* and a *V-750* by the company *JASCO* with a spectral bandwidth of 1.0 nm and a scan rate of 400 nm min^{-1}. Glass cuvettes with a path length of 1 cm, 1 mm and 0.1 mm were used. All measurements have been conducted in solvents from commercial sources from spectroscopic grade.

Fluorescence spectroscopy: The fluorescence spectra were recorded on a *JASCO Spectrofluorometer FP-8500* using quartz cuvettes (*SUPRASIL®, Hellma*) of 1 cm thickness and corrected against photomultiplier (type *R928*) and lamp intensity of the 75 W xenon lamp (type *Ushio UXL-75 XE*).

FT-IR spectroscopy: Solution state FT-IR was measured using a *JASCO-FT-IR-6800* using a CaF_2 cell with a path length of 0.1 mm. For all measurements, spectroscopic grade solvents (*Uvasol*) from Merck were used.

Dynamic Light Scattering: All DLS spectra have been recorded on a *CGS-3 Compact Goniometer System* manufactured by *ALV GmbH*, equipped with a HeNe Laser with a wavelength of 632.8 nm (22 mW) and an *ALV/LSE-5004 Digital Correlator* by *ALV GmbH*.

Atomic force microscopy: The AFM images have been recorded on a *Multimode®8 SPM Systems* manufactured by *Bruker AXS*. The used cantilevers were *AC200TS* by *Oxford Instruments* with an average spring constant of 9 N m^{-1}, an average frequency of 150 kHz, an average length of 200 µM, an average width of 40 µM and an average tip radius of 7 nm. All solutions have been drop-casted onto a MICA surface and the solvents were removed by slow solvent evaporation overnight.

Irradiation Methods: Irradiation-based experiments were performed using a LED *LED Engin LZ1-10UV00-0000* by *Mouser electronics* at 365 nm. For other wavelengths, LEDs by *Conrad Electronics* were used. *HighPower-LED Grün 87 lm 130° 3.8 V 1000 mA Roschwege LSC-G* for measurements using 520 nm wavelength, *HighPower-LED Rot 52 lm 130° 3.5 V 1000 mA Roschwege LSC-R* for measurements using 620 nm wavelength and *HighPower-LED Blau 31 lm 130° 2.3 V 700 mA Roschwege LSC-B* for measurements using 465 nm wavelength.

Lifetime measurements: Steady-state excitation and emission spectra were recorded on a FluoTime300 spectrometer from PicoQuant equipped with a 300 W ozone-free Xe lamp (250-900 nm), a 10 W Xe flash-lamp (250-900 nm, pulse width < 10 µs) with repetition rates of 0.1 – 300 Hz, an excitation monochromator (Czerny-Turner 2.7 nm/mm dispersion, 1200 grooves/mm, blazed at 300 nm), diode lasers (pulse width < 80 ps) operated by a computer-controlled laser driver PDL-820 (repetition rate up to 80 MHz, burst mode for slow and weak decays), two emission monochromators (Czerny-Turner, selectable gratings blazed at 500 nm with 2.7 nm/mm dispersion and 1200 grooves/mm, or blazed at 1250 nm with 5.4 nm/mm dispersion and 600 grooves/mm), Glan-Thompson polarizers for excitation (Xe-lamps) and emission, a Peltier-thermostatized sample holder from Quantum Northwest (-40 °C – 105 °C), and two detectors, namely a PMA Hybrid 40 (transit time spread FWHM < 120 ps, 300 – 720 nm) and a R5509-42 NIR-photomultiplier tube (transit time spread FWHM 1.5 ns, 300-1400 nm) with external cooling (-80 °C) from Hamamatsu. Steady-state and fluorescence lifetimes were recorded in TCSPC mode by a PicoHarp 300 (minimum base resolution 4 ps). Phosphorescence lifetime were recorded in MCS mode by a NanoHarp 250 (minimum base resolution 4 ns). Emission and excitation spectra were corrected for source intensity (lamp and grating) by standard correction curves. Lifetime analysis was performed using the commercial FluoFit software. The quality of the fit was assessed by minimizing the reduced chi squared function ($\chi 2$) and visual inspection of the weighted residuals and their autocorrelation. Luminescence quantum yields were measured with a Hamamatsu Photonics absolute PL quantum yield measurement system (C9920-02) equipped with a L9799-01 CW Xenon light source (150 W), monochromator, C7473 photonic multi-channel analyzer, integrating sphere and employing U6039-05 PLQY measurement software (Hamamatsu Photonics, Ltd., Shizuoka, Japan). All samples were measured in Suprasil® quartz cuvettes with septa.

Quantum Chemical Calculations: The geometry of the molecular systems investigated (monomer and aggregates) was optimized *via* dispersion-corrected PM6 semiempirical calculations using the *MOPAC* package. The reliability of the optimizations was checked by confirming the absence of negative frequencies in the corresponding predicted vibrational spectra. In all optimized structures non-polar hydrogens were omitted for clarity. Color code: C(grey), O(red), N(blue), H(white).

HPLC: HPLC analysis was performed on an *Agilent Infinity 1260 HPLC* system with a *Daicel Chiralpak AS-H* (0.46 cm * 25 cm) column. Detection was carried out *via* diode array detector (DAD) at 210 nm. *n*-hexane/*i*-propanol (98/2, 0.5 mL/min) was used as eluent.

GPC: Gel permeation chromatography was performed on a *Shimadzu prominence GPC system* decorated with two Tosoh TSKgel columns (G2500H XL; 7.8 mm I.D. x 30 cm, 5 µm; Part. No. 0016135) with CH_2Cl_2 as eluent. The solvent flow was set to be 1 mL/min. Detection was carried out via *Shimadzu prominence SPD-M20A* diode array detector (DAD).

1.2. Synthesis and characterization of (*Z*)-CN-OPE, (*Z*)-CN-OPE* and (*E*)-CN-OPE

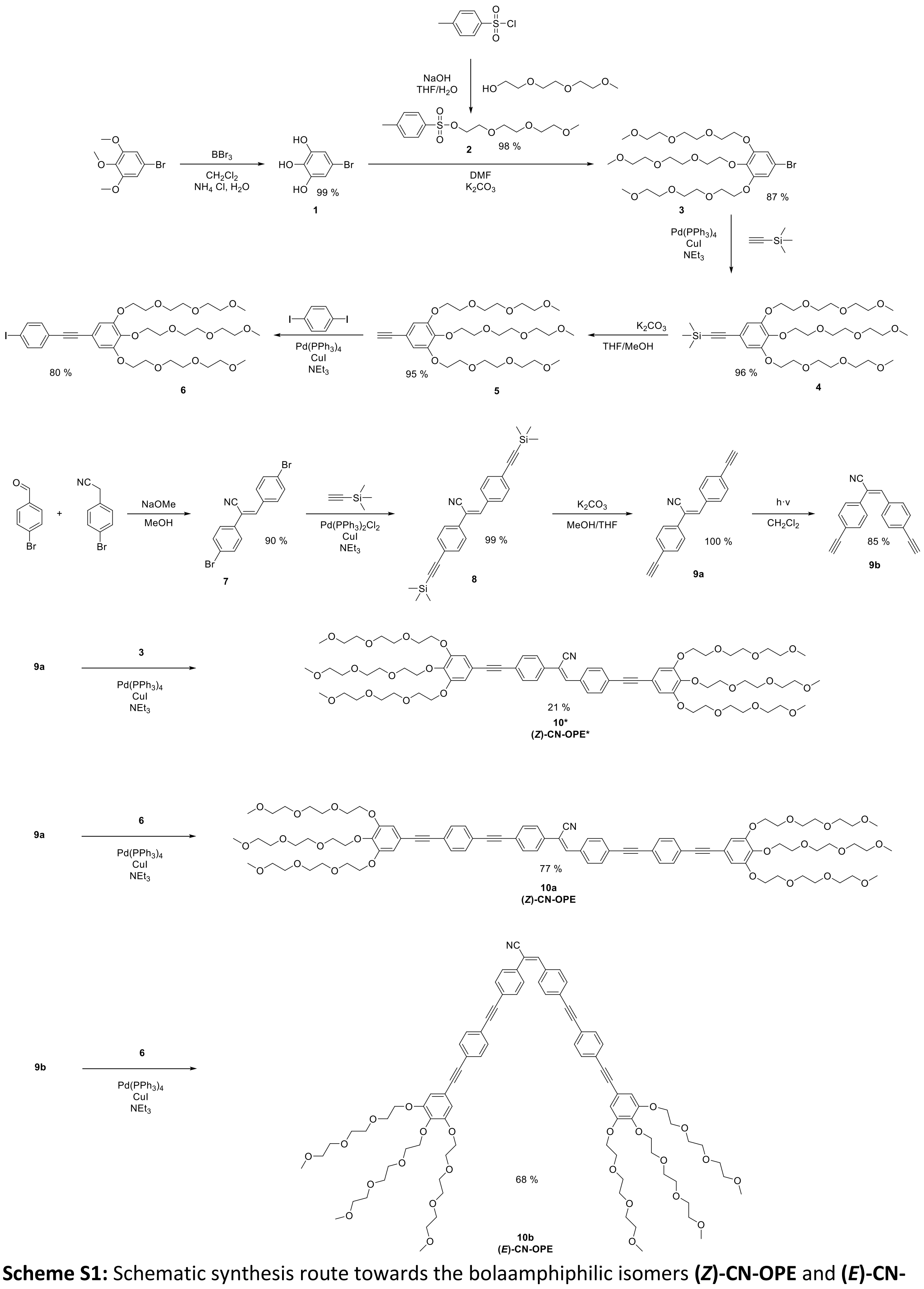

Scheme S1: Schematic synthesis route towards the bolaamphiphilic isomers **(*Z*)-CN-OPE** and **(*E*)-CN-OPE** and **(*Z*)-CN-OPE*.**

1-Bromo-(3,4,5-trihydroxy)benzol (1)

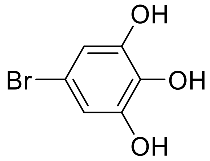

1

$C_6H_5BrO_3$

205,0070 g/mol

According to a modified literature protocol[1], 5-Bromo-1,2,3-trimethoxybenzene (6.17 g; 24.95 mmol; 1.00 eq) was dissolved in freshly distilled DCM (120 mL) and degassed with Argon for 15 min. The solution was cooled to -78 °C and stirred for 30 min. At this temperature BBr_3 (9.47 mL; 99.78 mmol, 4.00 eq) was carefully added dropwise and the reaction mixture was stirred for another 30 min. After slow warming to room temperature the reaction mixture was stirred overnight. A saturated, aqueous solution of NH_4Cl (30 mL) was slowly added to quench the reaction. The phases were separated, the aqueous layer was extracted with EtOAc (3 x 30 mL) and the combined organic layers were washed with water (3 x 100 mL). The organic layer was dried over $MgSO_4$ and all volatile compounds were removed under reduced pressure to afford the product as a grey solid (5.09 g; 24.84 mmol; 99 %). This compound was used without further purification. MS (ESI, MeOH): found 202.9355 $[M-H]^-$, calc. for $C_6H_4O_3Br$: 202.9338; ^1H NMR (DMSO-d_6, 300 MHz, 293 K): δ (ppm) = 9.29 (*s*, br., 2H, -OH), 8.32 (*s*, br., 1H, -OH), 6.40 (*s*, 2H, H_{arom}).

2-(2-(2-methoxyethoxy)ethoxy)ethyl 4-methylbenzenesulfonate (2)

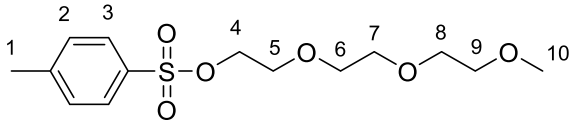

2

$C_{14}H_{22}O_6S$

318,3840 g/mol

Following a modified literature procedure[2], triethyleneglycol monomethylether (8.00 mL; 50.00 mmol; 1.00 eq) and NaOH (7.00 g; 175.00 mmol; 3.50 eq) were dissolved in a 1:1 mixture of THF (35 mL) and water (35 mL) and stirred for 20 min at 0 °C. At this temperature, a solution of p-Toluene sulfonylchloride (11.40 g; 60.00 mmol; 1.20 eq) was added dropwise over a period of 45 min and the reaction mixture was stirred for another 90 min. After slow warming to room temperature the solution was stirred for 17.5 h. The reaction mixture was poured on 5 %-aqueous HCl solution (105 mL) to adjust the pH value to pH = 7. DCM (30 mL) was added, the phases were separated and the organic layer was washed with water (2 x 50 mL). The combined aqueous layers were extracted with DCM (3 x 50 mL). The combined organic layers were dried over $NaSO_4$ and the solvent was removed under reduced pressure. The residue was purified by column chromatography (SiO_2, 2.5 % MeOH/DCM) to afford the desired product as a slightly yellowish oil (15.57 g; 48.94 mmol; 98 %). ^1H NMR ($CDCl_3$, 300 MHz, 293 K): δ (ppm) = 7.80 (*d*; J = 8.3 Hz; 2H; H_2), 7.34 (*d*; J = 8.0 Hz; 2H; H_3), 4.19 – 4.13 (*m*; 2H; H_4), 3.71 – 3.66 (*m*; 2H; H_5), 3.64 – 3.57 (*m*; 6H; $H_6 + H_7 + H_8$), 3.55 – 3.50 (*m*; 2H; H_9), 3.37 (*s*; 3H; H_{10}), 2.45 (*s*; 3H; H_1).

5-bromo-1,2,3-tris(2-(2-(2-methoxyethoxy)ethoxy)ethoxy)benzene (3)

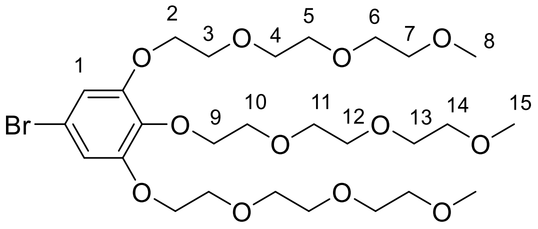

3

$C_{27}H_{47}BrO_{12}$
643,5650 g/mol

Following a modified Literature procedure[1], **1** (1.243 g; 6.07 mmol; 1.00 eq) and **2** (6.75 g; 21.23 mmol; 3.50 eq) were dissolved in freshly distilled DMF (30 mL). K_2CO_3 (4.83 g; 34.90 mmol, 5.75 eq) was added at room temperature and the reaction mixture was heated up to 90 °C and stirred for 39 h. After cooling to room temperature, the mixture was poured on water (60 mL). The aqueous layer was extracted with DCM (60 mL; 50 mL; 40 mL; 30 mL) and the combined organic layers were dried over Na_2SO_4. All volatile compounds were removed under reduced pressure and the residue was purified by column chromatography (SiO_2; 2.5 % MeOH/DCM) to give the product as a brown oil (3.46 g; 5.38 mmol; 87 %). ^{1}H NMR ($CDCl_3$, 300 MHz, 293 K): δ (ppm) = 6.73 (*s*; 2H; H_1), 4.12 (*q*; *J* = 5.2 Hz; 6H; H_2+H_9), 3.90 – 3.51 (*m*; 36H; H_3+H_4+H_5+H_6+H_7+H_{10}+H_{11}+H_{12}+H_{13}+H_{14}), 3.38 (*s*; 9H; H_8+H_{15}).

Trimethyl((3,4,5-tris(2-(2-(2-methoxyethoxy)ethoxy)ethoxy)phenyl)ethynyl)silane (4)

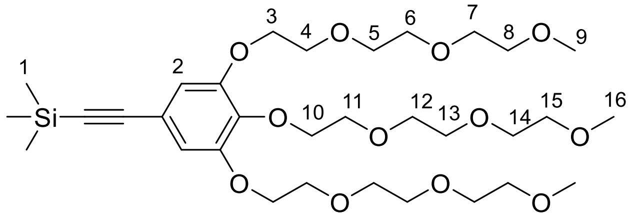

4

$C_{32}H_{56}O_{12}Si$
660,8730 g/mol

According to a modified procedure published in the literature[3], **3** (2.94 g; 4.58 mmol; 1.00 eq), $Pd(PPh_3)_4$ (280.8 mg; 5 mol%), and CuI (76.5 mg; 10 mol%) were dispersed in freshly distilled and degassed NEt_3 (30 mL) and the mixture was stirred for 20 min at room temperature. At this temperature, Trimethylsilylacetylene (792.8 µL; 5.72 mmol; 1.25 eq) was added dropwise and the reaction mixture was heated up to 70 °C and stirred for 16.5 h. After cooling to room temperature, the mixture was diluted with EtOAc, filtered over Celite® and the solvents were removed in vacuo. The residue was purified by column chromatography (SiO_2; 2.5 % MeOH in DCM + 0.4 % NEt_3) to give the product as a brown oil (2.91 g; 4.41 mmol; 96 %). ^{1}H NMR ($CDCl_3$, 300 MHz, 293 K): δ (ppm) = 6.69 (*s*; 2H; H_2), 4.15 – 4.12 (*m*; 6H; H_3+H_{10}), 3.83 (*t*; *J* = 5.0 Hz; 4H; H_4), 3.77 (*t*; *J* = 5.1 Hz; 2H; H_{11}), 3.73 – 3.69 (*m*; 6H; H_5+H_{12}), 3.67 – 3.61 (*m*; 12H; H_6+H_7+H_{13}+H_{14}), 3.56 – 3.52 (*m*; 6H; H_8+H_{15}), 3.37 (*s*; 6H; H_9), 3.37 (*s*; 3H; H_{16}), 0.23 (*s*; 9H; H_1).

5-ethynyl-1,2,3-tris(2-(2-(2-methoxyethoxy)ethoxy)ethoxy)benzene (5)

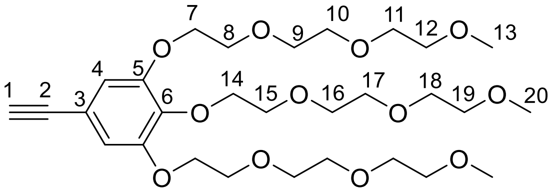

5

$C_{29}H_{48}O_{12}$
588.6910 g/mol

Following a modified literature procedure[4], **4** (2.95 g; 4.46 mmol; 1.00 eq) was dissolved in a 1:1 mixture of MeOH (10 mL) and THF (10 mL). K_2CO_3 (1.54 g; 11.15 mmol; 2.50 eq) was added and the reaction mixture was stirred at room temperature for 1 h. The solution was poured on water (20 mL), the phases were separated, and the organic layer was washed with water (4 x 20 mL). The combined aqueous layers were extracted with DCM (3 x 20 mL) and the combined organic layers were dried over $MgSO_4$. All volatile compounds were removed under reduced pressure and the residue was purified by column chromatography (SiO_2; 2.5 % MeOH in DCM) to give the product as a brown oil (2.49 g; 4.22 mmol; 95 %). HRMS (ESI, Micro Tof, MeOH): *m/z* = found: 611.3042 (100) $[M+Na]^+$, calc. for: $C_{29}H_{48}O_{12}Na^+$ 611.3038; ^{1}H-NMR ($CDCl_3$, 500 MHz, 293 K): δ (ppm) = 6.73 (*s*; 2H; H_4), 4.17 – 4.12 (*m*; 6H; H_7+H_{14}), 3.84 (*t*; *J* = 5.0 Hz; 4H; H_8), 3.78 (*t*; *J* = 5.1 Hz; 2H; H_{15}), 3.74 – 3.69 (*m*; 6H; H_9+H_{16}), 3.67 – 3.61 (*m*; 12H; H_{10}+H_{11}+H_{17}+H_{18}), 3.56 – 3.52 (*m*; 6H; H_{12}+H_{19}), 3.37 (*s*; 6H; H_{13}), 3.37 (*s*; 3H; H_{20}), 2.99 (*s*; 1H; H_1); ^{13}C NMR ($CDCl_3$, 126 MHz, 293 K): δ (ppm) = 152.6 (C_5), 140.0 (C_6), 117.0 (C_3), 112.0 (C_4), 83,7 (C_2), 76,3 (C_1), 72,6 (C_{14}), 72,1 (C_{12}+C_{19}), 71,0 (C_9), 70,9 (C_{10}), 70,8 (C_{17}), 70,7 (C_{11}+C_{18}), 70,7 (C_{15}+C_{16}), 69,8 (C_8), 69,1 (C_7), 59,2 (C_{13}), 59,2 (C_{20}).

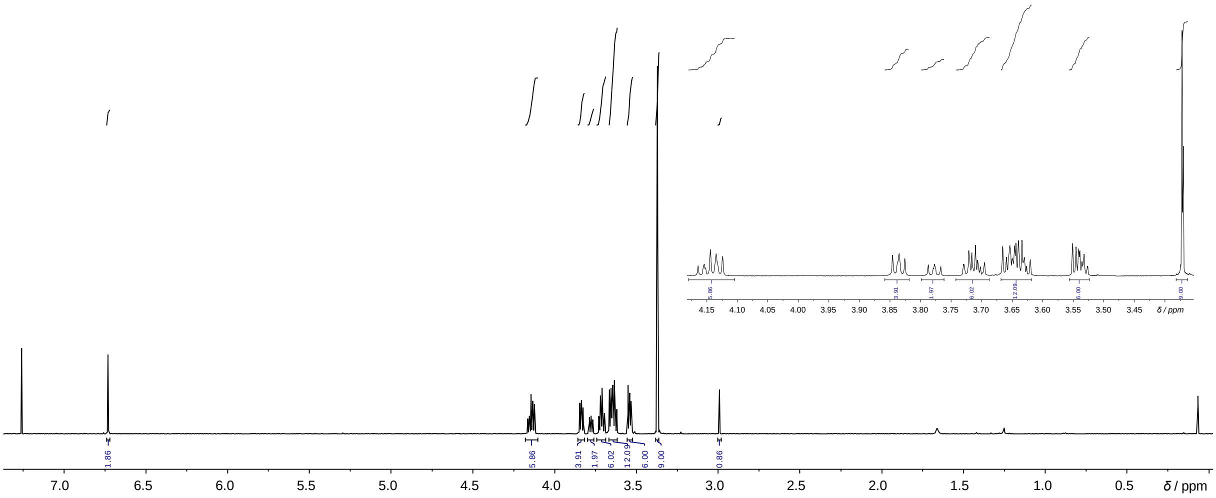

Fig. S1a: ^{1}H NMR ($CDCl_3$, 500 MHz, 299 K) of 5-ethynyl-1,2,3-tris(2-(2-(2-methoxyethoxy)ethoxy)ethoxy)benzene (**5**).

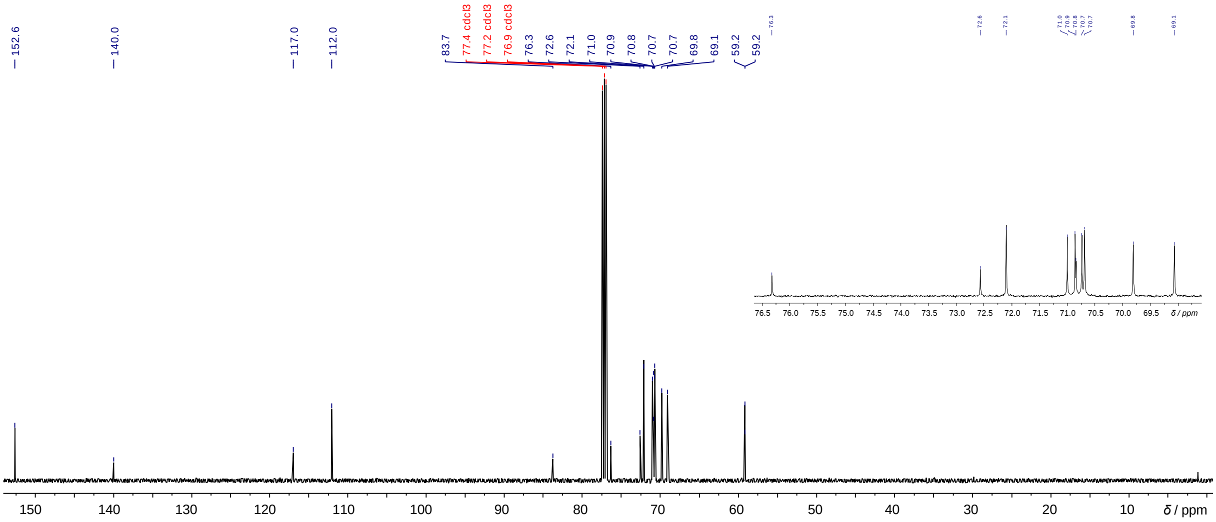

Fig. S1b: ^{13}C NMR ($CDCl_3$, 125 MHz, 299 K) of 5-ethynyl-1,2,3-tris(2-(2-(2-methoxyethoxy)ethoxy)ethoxy)benzene (**5**).

5-((4-iodophenyl)ethynyl)-1,2,3-tris(2-(2-(2-methoxyethoxy)ethoxy)ethoxy)benzene (6)

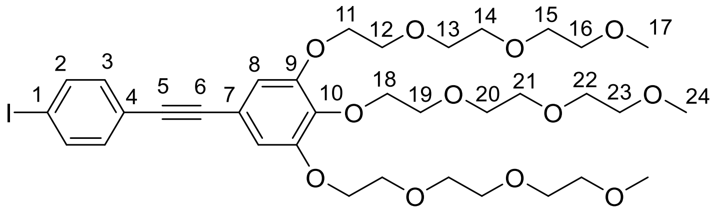

6

$C_{35}H_{51}IO_{12}$
790,2425 g/mol

1,4-Diiodobenzene (4,11 g; 12,44 mmol; 3.00 eq), $Pd(PPh_3)_4$ (239.2 mg; 5 mol%) and CuI (79.0 mg; 10 mol%) were dispersed in freshly distilled and degassed NEt_3 (60 mL) and stirred at room temperature for 20 min. Next, **5** (2.44 g; 4.15 mmol; 1 eq) in freshly distilled and degassed THF (4 mL) was added dropwise and the reaction mixture was heated to 60 °C and stirred for 62.5 h. After cooling to room temperature, the mixture was diluted with EtOAc, filtered over Celite® and the solvents were removed in vacuo. The residue was purified by column chromatography (SiO_2; 1 % to 3 % MeOH in DCM) to give the product as a brownish, highly viscous liquid (2.61 g; 3.30 mmol; 80 %). HRMS (ESI, Micro Tof, MeOH): *m/z* = found: 813.2324 (100) $[M+Na]^+$, calc. for: $C_{35}H_{51}IO_{12}Na^+$ 813.2323; ^{1}H NMR ($CDCl_3$, 600 MHz, 293 K): *δ* (ppm) = 7.68 (*d*; *J* = 8.5 Hz; 2H; H_2), 7.23 (*d*; *J* = 8.5 Hz; 2H; H_3), 6.76 (*s*; 2H; H_8), 4.19 – 4.15 (*m*; 6H; H_{11}+H_{18}), 3.85 (*t*; *J* = 5.0 Hz, 4H, H_{12}), 3.79 (*t*; *J* = 5.0 Hz; 2H; H_{19}), 3.75 – 3.70 (*m*; 6H; H_{13}+H_{20}), 3.68 – 3.62 (*m*; 12H; H_{14}+H_{15}+H_{21}+H_{22}), 3.56 – 3.52 (*m*; 6H; H_{16}+H_{23}), 3.37 (*s*; 3H; H_{24}), 3.37 (*s*; 6H; H_{17}); ^{13}C NMR ($CDCl_3$, 151 MHz, 293K): *δ* (ppm) = 152.7 (C_9), 139.7 (C_{10}), 137.7 (C_2), 133.2 (C_3), 122.9 (C_4), 117.8 (C_7), 111.4 (C_8), 94.2 (C_1), 90.9 (C_6), 87.7 (C_5), 72.6 (C_{18}), 72.1 (C_{23}), 72.1 (C_{16}), 71.0 (C_{13}), 70.9 (C_n), 70.8 (C_{21}), 70.7 (C_{15}+C_{22}), 70.7 (C_{19}), 70.7 (C_{20}), 69.8 (C_{12}), 69.1 (C_{11}), 59.2 (C_{17}), 59,2 (C_{24}).

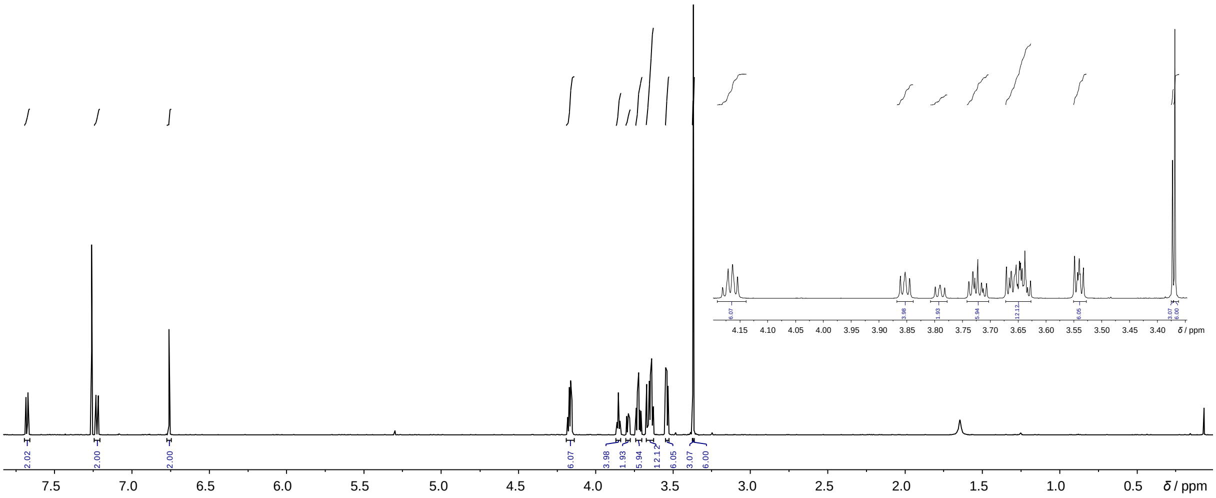

Fig. S2a: ^{1}H NMR ($CDCl_3$, 600 MHz, 299 K) of 5-((4-iodophenyl)ethynyl)-1,2,3-tris(2-(2-(2-methoxyethoxy)ethoxy) ethoxy)benzene (**6**).

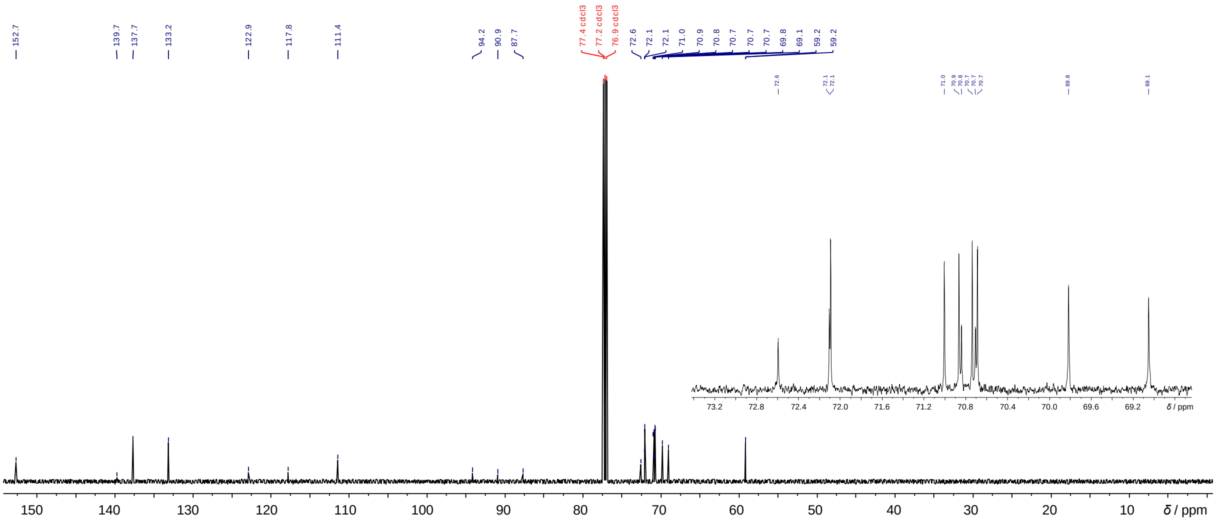

Fig. S2b: ^{13}C NMR ($CDCl_3$, 150 MHz, 299 K) of 5-((4-iodophenyl)ethynyl)-1,2,3-tris(2-(2-(2-methoxyethoxy)ethoxy) ethoxy)benzene (**6**).

(*Z*)-2,3-bis(4-bromophenyl)acrylonitrile (7)

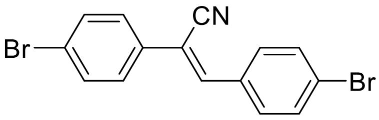

7

$C_{15}H_9Br_2N$

363,0520 g/mol

According to a modified procedure published in the literature[5], 4-Bromophenylacetonitrile (980.2 mg; 5.00 mmol; 1.00 eq) and 4-Bromobenzaldehyde (925.1 mg; 5.00 mmol; 1.00 eq) were dissolved in MeOH (40 mL) and the solution was stirred at room temperature for 15 min. NaOMe (100.0 mg; 1.85 mmol; 0.37 eq) was added with vigorous stirring and the reaction mixture was stirred for 17 h.

The resulting precipitate was filtered off and washed with cold MeOH (10 mL, -10 °C) in order to obtain a white solid (1.29 g). To obtain the remaining product, the solvent of the filtrate was removed under reduced pressure and the residue was purified by column chromatography (SiO_2, 3 % Et_2O/Pentane). The desired product was obtained as a white crystalline solid with an overall yield of 1.64 g (4.51 mmol; 90 %). HRMS (ESI, MicroTof, MeOH): found 385.9876 $[M+Na]^+$, calc. for $C_{15}H_9NBr_2Na^+$: 385.8974; ^1H NMR ($CDCl_3$, 300 MHz, 293 K): δ (ppm) = 7.75 (*d*, $^3J_{H\text{-}H}$ = 8.4 Hz, 2H), 7.63 – 7.50 (*m*, 6H), 7.45 *(s,* 1H).

(*Z*)-2,3-bis(4-((trimethylsilyl)ethynyl)phenyl)acrylonitrile (8)

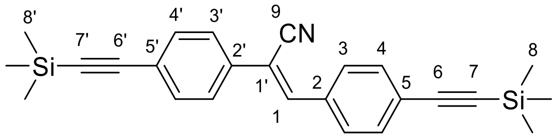

8

$C_{25}H_{27}NSi_2$

397,6680 g/mol

7 (330.4 mg; 0.91 mmol; 1.00 eq), $Pd(PPh_3)_2Cl_2$ (31.6 mg; 5 mol%) and CuI (17.3 mg; 10 mol%) were dispersed in freshly distilled and degassed NEt_3 (3 mL) and the mixture was stirred at room temperature for 20 min. Trimethylsilylacetylene (315 µL; 2.28 mmol; 2.50 eq) was added dropwise, the reaction was heated to 60 °C and stirred for 17 h. After cooling down to room temperature, the reaction mixture was diluted with DCM and filtered over Celite®. All volatile compounds were removed under reduced pressure and the residue was purified by column chromatography (SiO_2, 3% Et_2O in Pentane). The product was obtained as a slightly yellowish powder (357.5 mg; 0.90 mmol; 100 %). ^1H NMR ($CDCl_3$, 500 MHz, 293 K) δ (ppm) = 7.83 (*d*, $^3J_{H\text{-}H}$ = 8.2 Hz, 2H, H_3), 7.61 (*d*, $^3J_{H\text{-}H}$ = 8.7 Hz, 2H, $H_{3'}$), 7.56 – 7.51 (*m*, 4H, H_4+$H_{4'}$), 7.49 (*s*, 1H, H_1), 0.27 (*m*, 18H, H_8+$H_{8'}$). ^{13}C NMR ($CDCl_3$, 126 MHz, 293 K), δ (ppm) = 141.5 (C_1), 134.2 (C_2), 133.5 ($C_{2'}$), 132.7(C_4), 132.6 ($C_{4'}$), 129.3 (C_3), 125.9 ($C_{3'}$), 125.7 (C_5), 124.4 ($C_{5'}$), 117.7 (C_9), 111.6 ($C_{1'}$), 104.5 (C_6), 104.3 ($C_{6'}$), 97.7(C_7), 96.9($C_{7'}$), 0.0 (C_8), 0.0 ($C_{8'}$).

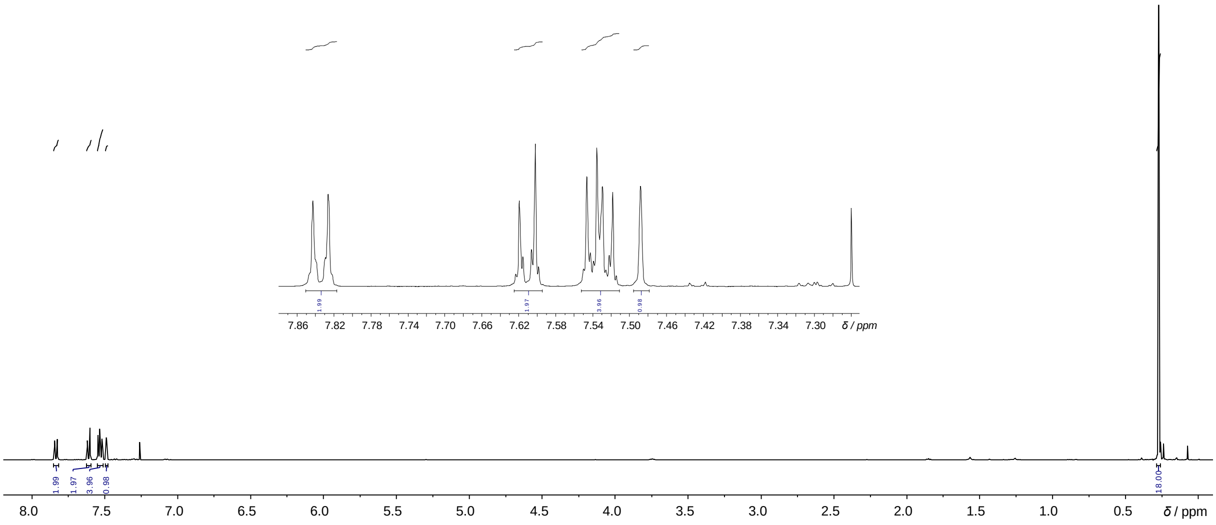

Fig. S3a: ^1H NMR ($CDCl_3$, 500 MHz, 299 K) of (*Z*)-2,3-bis(4-((trimethylsilyl)ethynyl)phenyl)acrylonitrile (**8**).

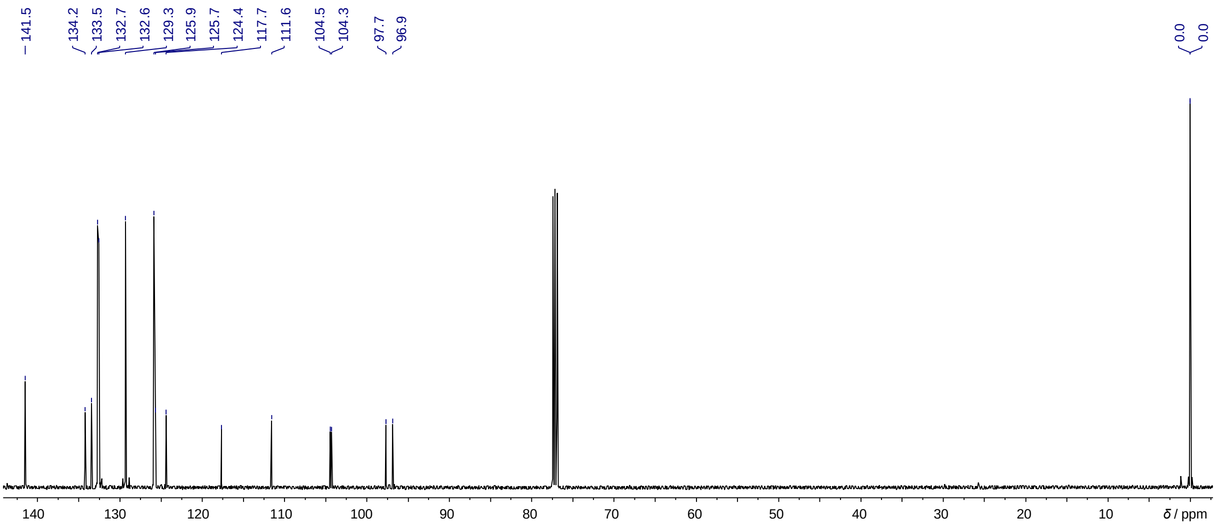

Fig. S3b: ^{13}C NMR (CDCl$_3$, 125 MHz, 299 K) of (*Z*)-2,3-bis(4-((trimethylsilyl)ethynyl)phenyl)acrylonitrile (**8**).

(*Z*)-2,3-bis(4-ethynylphenyl)acrylonitrile (9a)

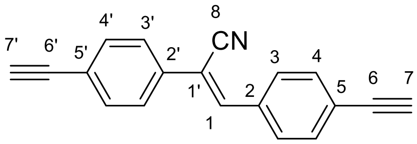

9a

$C_{19}H_{11}N$

253,3040 g/mol

8 (795.3 mg; 2.00 mmol; 1.00 eq) was dissolved in a 1:1 mixture of THF and MeOH (12 mL) and the solution was stirred at room temperature for 30 min. K_2CO_3 (1.106 g; 8.00 mmol; 4.00 eq) was added and the reaction mixture was stirred for 45 min and subsequently poured into water (60 mL). DCM (30 mL) was added, the phases were separated, and the aqueous layer was extracted with DCM (2 x 30 mL). The combined organic layers were washed with water (50 mL), dried over $MgSO_4$ and all volatile compounds were evaporated in vacuo to give the desired product as a slightly yellow solid (521.2 mg; 2.00 mmol; 100 %). HRMS (ESI, Micro Tof, MeOH): *m/z* = found: 276.0783 (100) [M+Na]$^+$; 529.1668 (40) [2M+Na]$^+$, calc. for: $C_{19}H_{11}NNa^+$: 276.0784; $C_{38}H_{22}N_2Na^+$: 529.1675; ^{1}H NMR (CDCl3, 600 MHz, 293 K): *δ* (ppm) = 7.86 (*d*, *J* = 8.3 Hz, 2H, H$_3$), 7.64 (*d*, *J* = 8.5 Hz, 2H, H$_{3'}$), 7.61 – 7.54 (*m*, 4H, H$_4$+H$_{4'}$), 7.51 (*s*, 1H, H$_1$), 3.24 (*s*, 1H, H$_7$), 3.20 (*s*, 1H, H$_{7'}$). ^{13}C NMR (CDCl$_3$, 151 MHz, 293 K) *δ* (ppm) = 141.6 (C$_1$), 134.5 (C$_{2'}$), 133.8 (C$_2$), 132.9 (C$_{4'}$), 132.8 (C$_4$), 129.4 (C$_3$), 126.0 (C$_{3'}$), 124.6 (C$_5$), 123.4 (C$_{5'}$), 117.5 (C$_8$), 111.9 (C$_{1'}$), 83.1 (C$_6$), 83.0 (C$_{6'}$), 80.0 (C$_7$), 79.5 (C$_{7'}$).

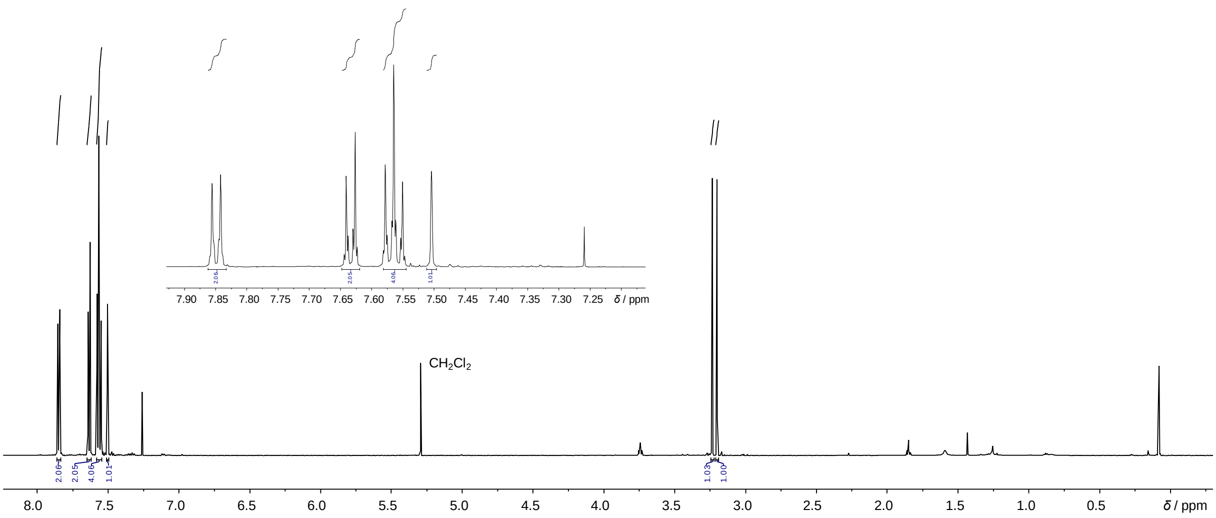

Fig. S4a: ^{1}H NMR ($CDCl_3$, 600 MHz, 299 K) of (*Z*)-2,3-bis(4-ethynylphenyl)acrylonitrile (**9a**).

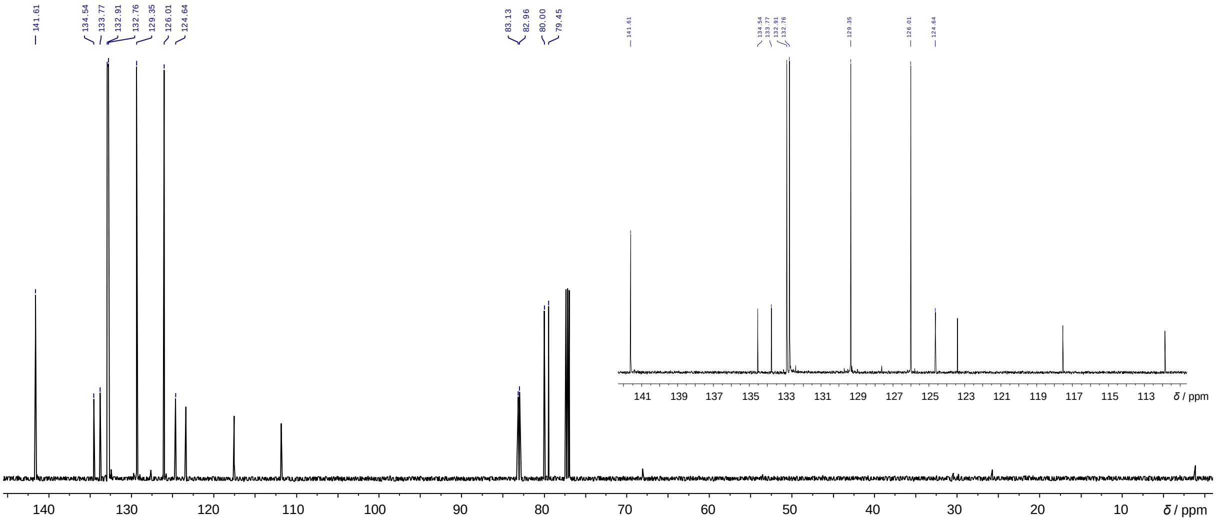

Fig. S4b: ^{13}C NMR ($CDCl_3$, 150 MHz, 299 K) of (*Z*)-2,3-bis(4-ethynylphenyl)acrylonitrile (**9a**)

(*E*)-2,3-bis(4-ethynylphenyl)acrylonitrile (9b)

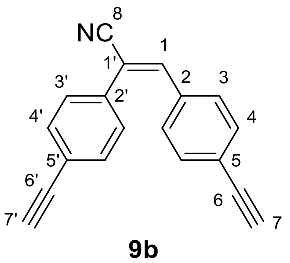

9b

$C_{19}H_{11}N$

253,3040 g/mol

9a (521.2 mg; 2.00 mmol; 1.00 eq) was dissolved in DCM (30 mL) and stirred at room temperature. The reaction mixture was irradiated with UV light (365 nm) for 2 h. The solvent was removed under reduced pressure and the residue was purified by column chromatography (SiO_2, 1 - 5 % Et_2O in Pentane) to give the desired product as a slightly yellowish solid (430.8 mg; 1.70 mmol; 85 %). HRMS (ESI, Micro Tof, MeOH): *m/z* = found: 276.0780 (100) $[M+Na]^+$; 529.1662 (61) $[2M+Na]^+$, calc. for: $C_{19}H_{11}NNa^+$: 276.0784; $C_{38}H_{22}N_2Na^+$: 529.1675; ^{1}H NMR ($CDCl_3$, 500 MHz, 293 K): *δ* (ppm) = 7.47 (*d*, *J* =

8.5 Hz, 2H, $H_{4'}$), 7.36 – 7.31 (*m*, 5H, H_1+$H_{3'}$+H_4), 7.11 (*dd*, *J* = 8.5, 0.6 Hz, 2H, H_3), 3.17 (*s*, 1H, H_7), 3.17 (*s*, 1H, $H_{7'}$). ^{13}C NMR ($CDCl_3$, 126 MHz, 293 K) δ (ppm) = 143.7 (C_1), 133.7 ($C_{2'}$), 132.9 ($C_{4'}$), 132.8 (C_2), 132.4 (C_4), 129.7 (C_3), 129.0 ($C_{3'}$), 123.9 (C_5), 123.6 ($C_{5'}$), 119.5 (C_8), 114.6 ($C_{1'}$), 82.9 (C_6), 82.8 ($C_{6'}$), 79.7 (C_7), 79.2 ($C_{7'}$).

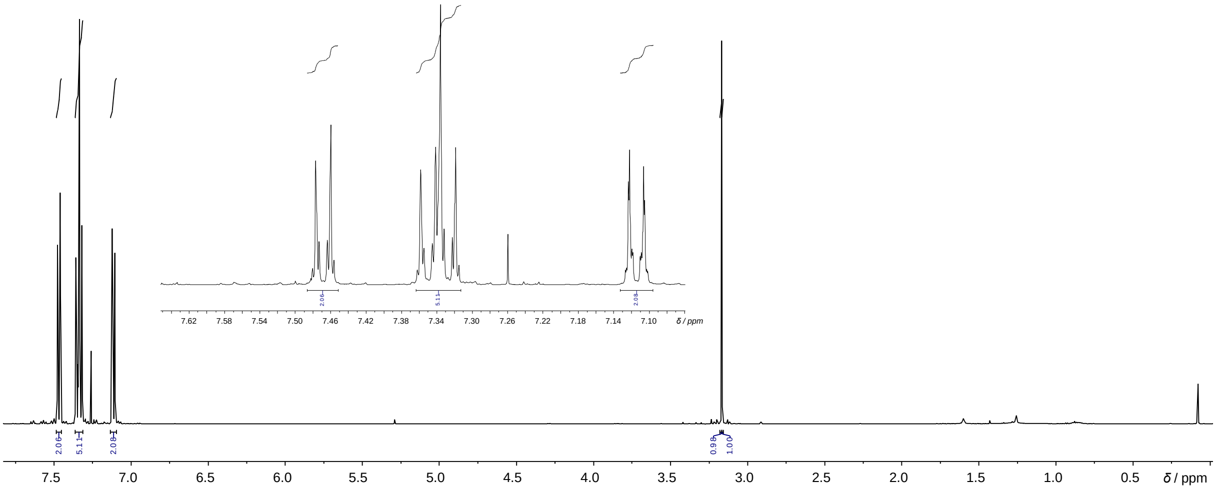

Fig. S5a: ^{1}H NMR ($CDCl_3$, 500 MHz, 299 K) of (*E*)-2,3-bis(4-ethynylphenyl)acrylonitrile (**9b**).

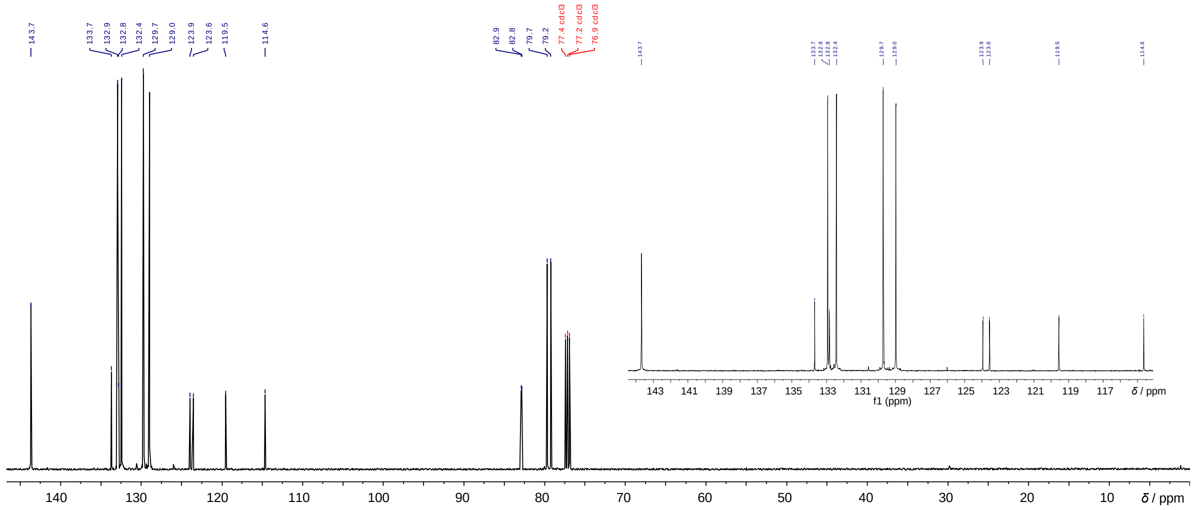

Fig. S5b: ^{13}C NMR ($CDCl_3$, 125 MHz, 299 K) of (*E*)-2,3-bis(4-ethynylphenyl)acrylonitrile (**9b**).

To characterize the double bond geometry of the central C=C-bond of **9a** and **9b**, the C_8-H_1 coupling constant was determined for both isomers respectively. The coupling constants were found to be $^3J_{CN,H}$ = 14.5 Hz for **9a** and $^3J_{CN,H}$ = 9.0 Hz for **9b**, which is in good agreement with corresponding values for CN-substituted stilbenes reported in the literature[6].

(*Z*)-2,3-bis(4-((4-((3,4,5-tris(2-(2-(2-methoxyethoxy)ethoxy)ethoxy)phenyl)ethynyl)phenyl)ethynyl)phenyl)acrylonitrile ((*Z*)-CN-OPE)

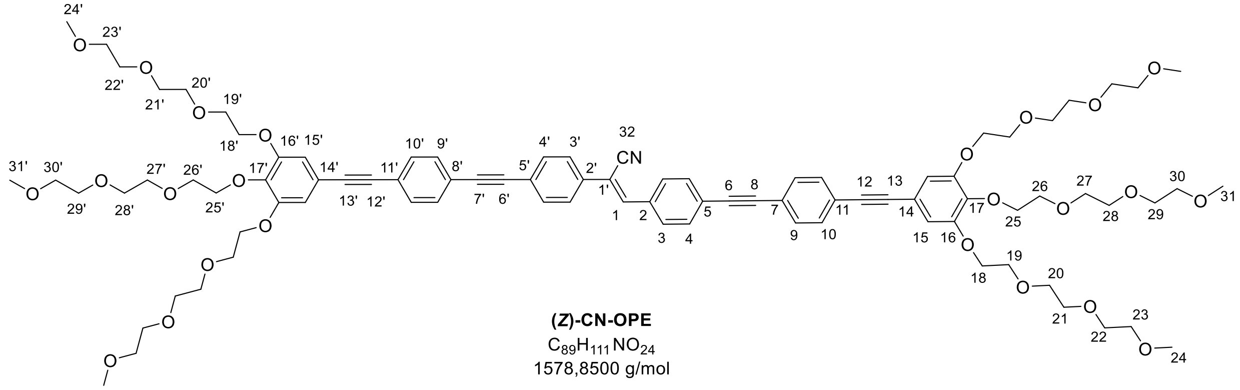

(*Z*)-CN-OPE
$C_{89}H_{111}NO_{24}$
1578,8500 g/mol

6 (948.9 mg; 1.20 mmol; 2.00 eq), $Pd(PPh_3)_4$ (34.7 mg; 5 mol%) and CuI (11.4 mg; 10 mol%) were dispersed in freshly distilled and degassed NEt_3 (7 mL) and the mixture was stirred at room temperature for 20 min. **9a** (153.4 mg; 0.60 mmol; 1.00 eq) in freshly distilled and degassed THF (3 mL) was added dropwise, the solution was heated up to 55 °C and stirred for 83 h. After cooling to room temperature, the mixture was diluted with DCM/EtOAc and filtered over Celite®. All volatile compounds were removed under reduced pressure and the residue was purified by column chromatography (SiO_2, 1-5 % MeOH in DCM) to give the desired product as an orange sticky solid (728.4 mg; 0.46 mmol; 77 %). **HRMS** (ESI, Orbitrap XXL, $CH_3CN/CHCl_3$): *m/z* =809.38686 (40) $[M+Na+NH_4]^{2+}$; 811.86427 (100) $[M+2Na]^{2+}$; 1601.74397 (2) $[2M+2Na]^{+}$, calc. for: $C_{89}H_{111}NO_{24}NaNH_4{}^{2+}$ 809.38633; $C_{89}H_{111}NO_{24}Na_2{}^{2+}$ 811.86402; $(C_{89}H_{111}NO_{24}Na)_2{}^{2+}$ 1601.74214; **^{1}H NMR** (DMSO-d_6, 500 MHz, 293 K) δ (ppm) = 8.17 (*s*, 1H, H_1), 8.02 (*d*, *J* = 8.8 Hz, 2H, H_3), 7.86 (*d*, *J* = 8.5 Hz, 2H, $H_{3'}$), 7.75 – 7.70 (*m*, 4H, H_4+$H_{4'}$), 7.65 – 7.57 (*m*, 8H, H_9+$H_{9'}$+H_{10}+$H_{10'}$), 6.89 (*s*, 4H, H_{15}+$H_{15'}$), 4.14 (*t*, *J* = 4.9 Hz, 8H, H_{18}+$H_{18'}$), 4.07 (*t*, *J* = 4.8 Hz, 4H, H_{25}+$H_{25'}$), 3.75 (*t*, *J* = 4.6 Hz, 8H, H_{19}+$H_{19'}$), 3.68 (*t*, *J* = 4.9 Hz, 4H, H_{26}+$H_{26'}$), 3.63 – 3.59 (*m*, 8H, H_{20}+$H_{20'}$), 3.58 – 3.56 (*m*, 4H, H_{27}+$H_{27'}$), 3.55 – 3.49 (*m*, 24H, H_{21}+$H_{21'}$+H_{22}+$H_{22'}$+H_{28}+$H_{28'}$+H_{29}+$H_{29'}$), 3.44 – 3.40 (*m*, 12H, H_{23}+$H_{23'}$+H_{30}+$H_{30'}$), 3.24 (*s*, 6H, H_{31}+$H_{31'}$), 3.23 (*s*, 12H, H_{24}+$H_{24'}$). **^{13}C NMR** (DMSO-d_6, 126 MHz, 296 K) δ (ppm) = 152.2 (C_{16}+$C_{16'}$), 142.4 (C_1), 138.9 (C_{17}+$C_{17'}$), 133.9 (C_2), 133.9 ($C_{2'}$), 132.2 ($C_{4'}$), 131.9 (C_4), 131.8 (C_9), 131.8 ($C_{9'}$), 131.6 (C_{10}), 131.6 ($C_{10'}$) 129.6 (C_3), 128.7 ($C_{5'}$) 126.2 ($C_{3'}$), 124.2 (C_5), 123.0 (C_8), 122.9 ($C_{8'}$), 122.0 (C_{11}), 121.9 ($C_{11'}$), 117.5 (C_{32}), 116.7 (C_{14}+$C_{14'}$), 110.5 (C_{15}+$C_{15'}$), 110.2 ($C_{1'}$), 92.1 (C_{13}), 92.1 ($C_{13'}$), 91.4 (C_7), 91.0 ($C_{7'}$), 90.9 (C_6), 90.8 ($C_{6'}$), 87.8 (C_{12}+$C_{12'}$), 72.0 (C_{25}+$C_{25'}$), 71.3 (C_{23}+$C_{23'}$+C_{30}+$C_{30'}$), 70.0 (C_{20}+$C_{20'}$), 69.9 (C_{21}+$C_{21'}$+C_{26}+$C_{26'}$), 69.8 (C_{28}+$C_{28'}$), 69.8 (C_{27}+$C_{27'}$), 69.6 (C_{22}+$C_{22'}$), 69.6 (C_{29}+$C_{29'}$), 69.0 (C_{19}+$C_{19'}$), 68.5 (C_{18}+$C_{18'}$), 58.0 (C_{24}+$C_{24'}$+C_{31}+$C_{31'}$).

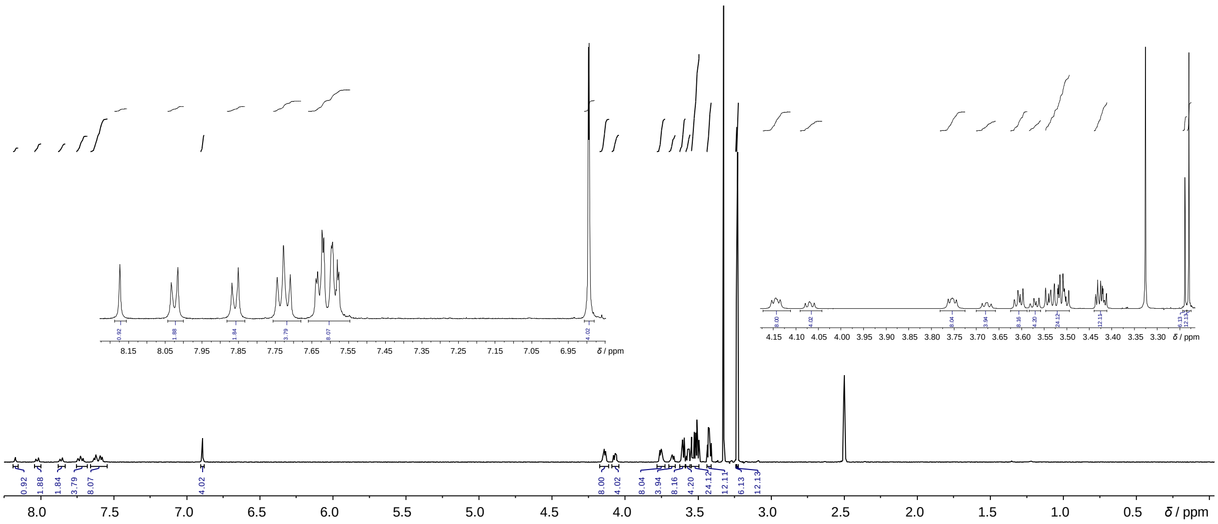

Fig. S6a: ^{1}H NMR (DMSO-d_6, 600 MHz, 299 K) of **(*Z*)-CN-OPE**.

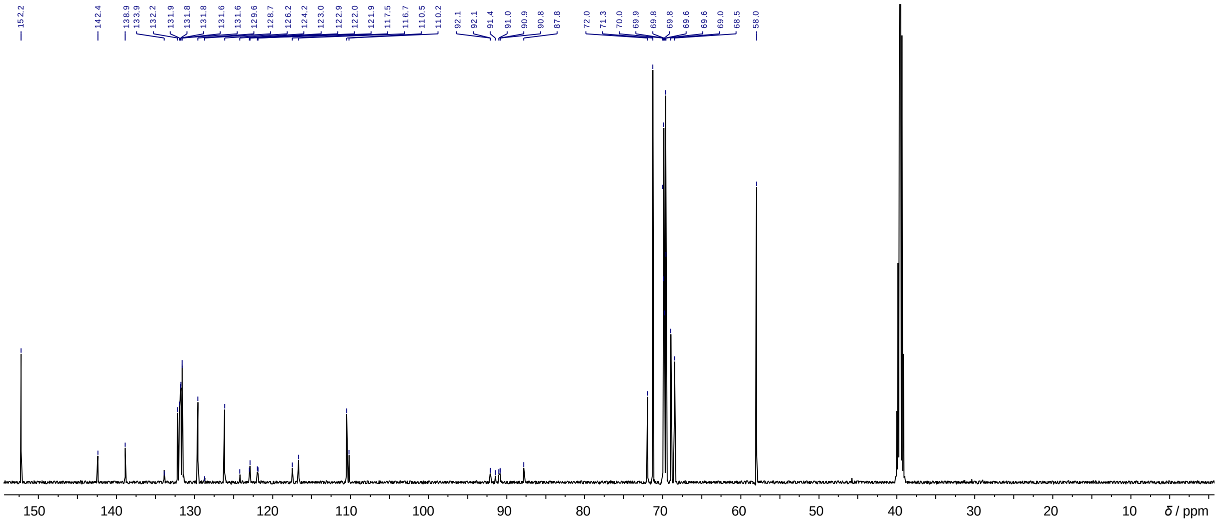

Fig. S6b: ^{13}C NMR (DMSO-d_6, 150 MHz, 299 K) of **(*Z*)-CN-OPE**.

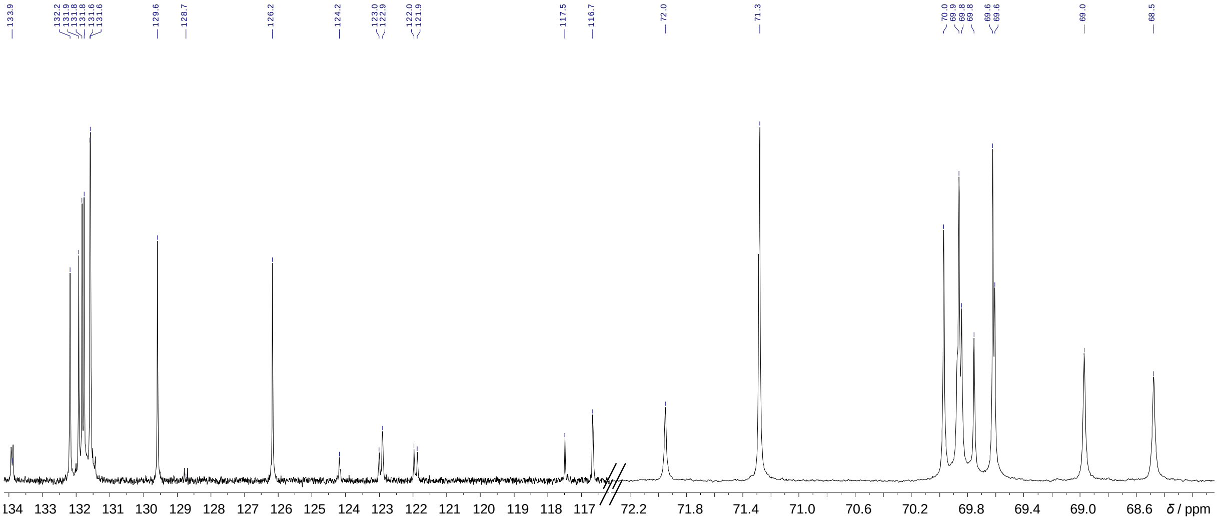

Fig. S6c: Enlargement of the aromatic and aliphatic region of the ^{13}C NMR (DMSO-d_6, 150 MHz, 299 K) of **(*Z*)-CN-OPE**.

(*E*)-2,3-bis(4-((4-((3,4,5-tris(2-(2-(2-methoxyethoxy)ethoxy)ethoxy)phenyl)ethynyl)phenyl) ethynyl)phenyl)acrylonitrile ((*E*)-CN-OPE)

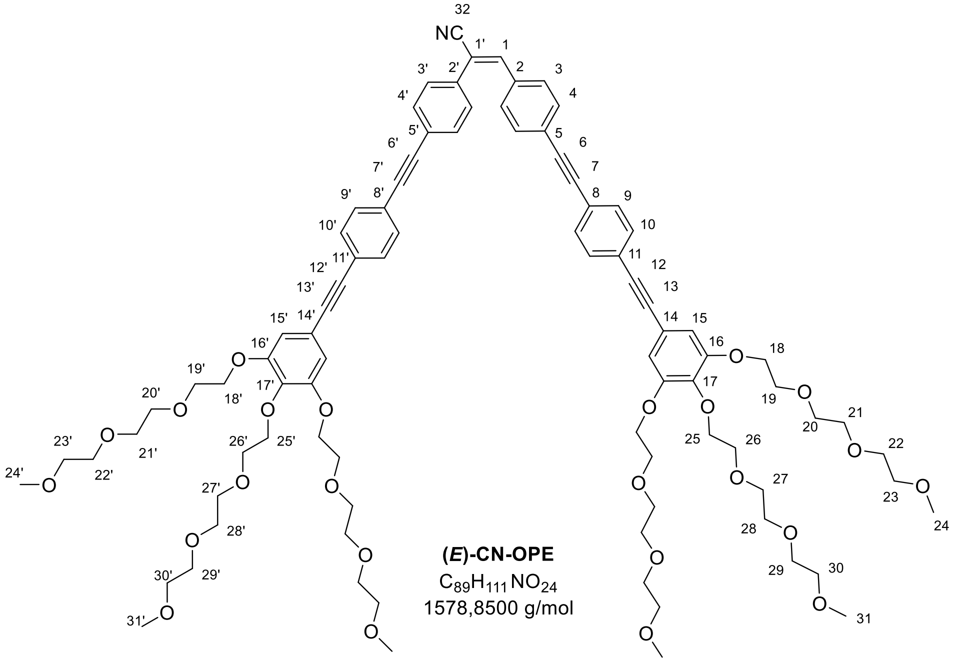

6 (632.5 mg; 0.80 mmol; 2.00 eq), $Pd(PPh_3)_4$ (23.1 mg; 5 mol%) and CuI (7.6 mg; 10 mol%) were dispersed in freshly distilled and degassed NEt_3 (7 mL) and the mixture was stirred at room temperature for 20 min. **9b** (101.3 mg; 0.40 mmol; 1.00 eq) dissolved in freshly distilled and degassed THF (3 mL) was carefully added dropwise, the solution was heated up to 40 °C and stirred for 16 h. After cooling to room temperature, the mixture was diluted with EtOAc and filtered over Celite®. All volatile compounds were removed under reduced pressure and the residue was purified by column chromatography (SiO_2, 0.5-5 % MeOH in DCM) to give the desired product as a brown, highly viscous oil (428.5 mg; 0.27 mmol; 68 %). **HRMS** (ESI, Orbitrap XXL, $CH_3CN/CHCl_3$): *m/z* = 809.38681 (40) $[M+Na+NH_4]^{2+}$; 811.86422 (100) $[M+2Na]^{2+}$; 1601.74353 (2) $[2M+2Na]^{+}$, calc. for: $C_{89}H_{111}NO_{24}NaNH_4^{2+}$ 809.38633; $C_{89}H_{111}NO_{24}Na^{+}$ 811.86402; $C_{89}H_{111}NO_{24}Na^{+}$ 1601.74220; **^{1}H NMR** (DMSO-d_6, 600 MHz, 299 K): δ (ppm) = 7.78 (*s*, 1H, H_1), 7.66 – 7.55 (m, 10H, $H_{4'}+H_9+H_{9'}+H_{10}+H_{10'}$), 7.51 (*d*, *J* = 8.4 Hz, 2H, H_4), 7.45 (*d*, *J* = 8.3 Hz, 2H, $H_{3'}$), 7.28 (*d*, *J* = 86 Hz, 2H, H_3), 6.89 (*s*, 2H, $H_{15'}$), 6.88 (*s*, 2H, H_{15}), 4.17 – 4.11 (*m*, 8H, $H_{18}+H_{18'}$), 4.08 – 4.04 (*m*, 4H, $H_{25}+H_{25'}$), 3.78 – 3.73 (*m*, 8H, $H_{19}+H_{19'}$), 3.69 – 3.66 (*m*, 4H, $H_{26}+H_{26'}$), 3.61 – 3.59 (*m*, 8H, $H_{20}+H_{20'}$), 3.58 – 3.55 (*m*, 4H, $H_{27}+H_{27'}$), 3.55 – 3.49 (*m*, 24H, $H_{21}+H_{21'}+H_{22}+H_{22'}+H_{28}+H_{28'}+H_{29}+H_{29'}$), 3.44 – 3.40 (*m*, 12H, $H_{23}+H_{23'}H_{30}+H_{30'}$), 3.25 – 3.21 (*m*, 18H, $H_{24}+H_{24'}+H_{31}+H_{31'}$). **^{13}C NMR** (DMSO-$d_6$, 126 MHz, 296 K) δ (ppm) = 152.2 ($C_{16}+C_{16'}$), 144.5 (C_1), 138.9 ($C_{17}+C_{17'}$), 133.6 ($C_{2'}$), 132.8 (C_2), 132.3 ($C_{4'}$), 131.8 (C_9), 131.8 ($C_{9'}$), 131.6 (C_4), 131.6 ($C_{10}+C_{10'}$), 130.1 (C_3), 129.1 ($C_{3'}$), 126.2 ($C_{5'}$), 123.5 (C_5), 123.2 (C_8), 123.0 ($C_{8'}$), 121.9 (C_{11}), 121.8 ($C_{11'}$), 119.5 (C_{32}), 116.6 ($C_{14}+C_{14'}$), 113.0 ($C_{1'}$), 110.5 ($C_{15}+C_{15'}$), 92.1 (C_{13}), 92.1 ($C_{13'}$), 91.0 (C_7), 90.8 ($C_{7'}$), 90.6 (C_6), 90.5 ($C_{6'}$), 87.8 ($C_{12}+C_{12'}$), 71.9 ($C_{25}+C_{25'}$), 71.3 ($C_{23}+C_{23'}+C_{30}+C_{30'}$), 70.0 ($C_{20}+C_{20'}$), 69.9 ($C_{21}+C_{21'}+C_{26}+C_{26'}$), 69.8 ($C_{28}+C_{28'}$), 69.7 ($C_{27}+C_{27'}$), 69.6 ($C_{22}+C_{22'}$), 69.6 ($C_{29}+C_{29'}$), 69.0 ($C_{19}+C_{19'}$), 68.5 ($C_{18}+C_{18'}$), 58.0 ($C_{24}+C_{24'}+C_{31}+C_{31'}$).

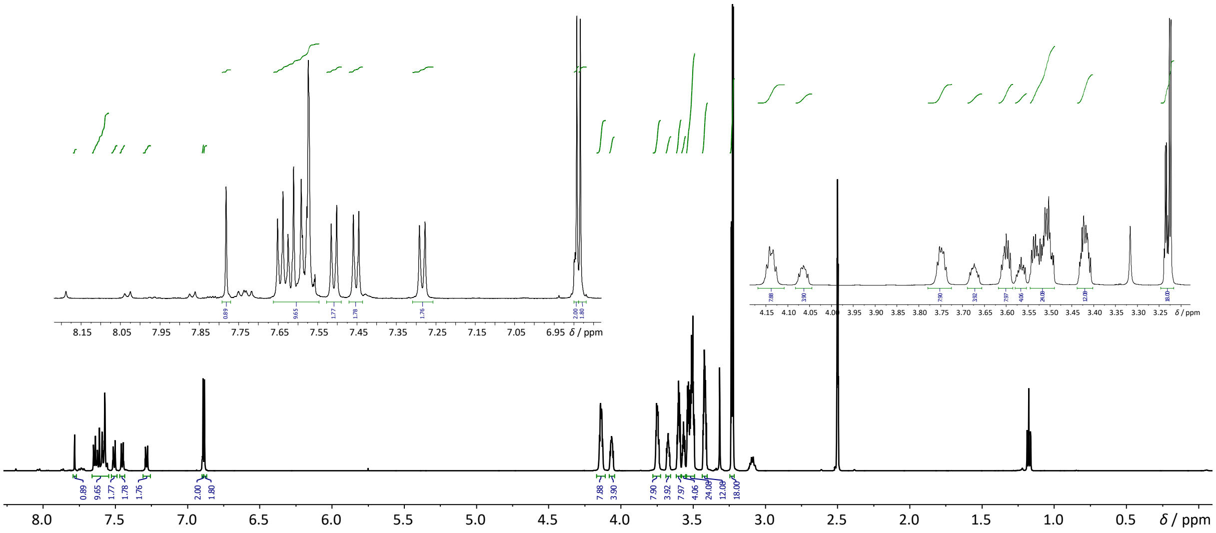

Fig. S7a: ^{1}H NMR (DMSO-d$_6$, 600 MHz, 299 K) of **(*E*)-CN-OPE**.

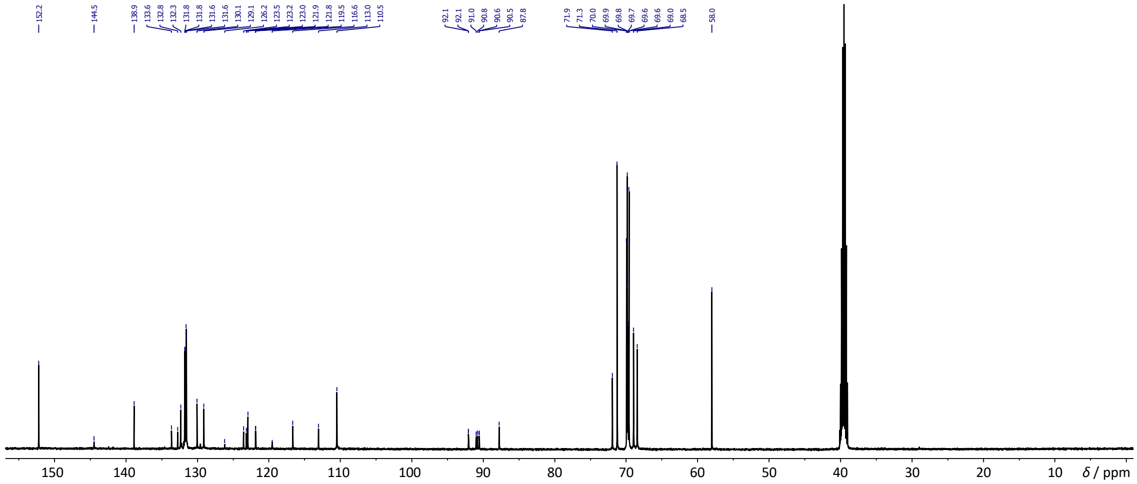

Fig. S7b: ^{13}C NMR (DMSO-d$_6$, 150 MHz, 299 K) of **(*E*)-CN-OPE**.

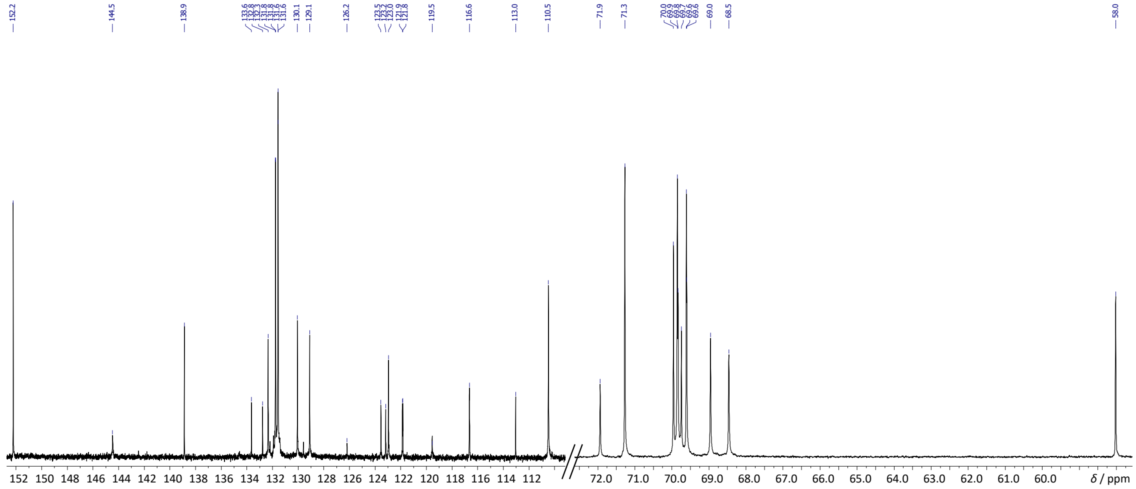

Fig. S7c: Enlargement of the aromatic and aliphatic region of the ^{13}C NMR (DMSO-d$_6$, 150 MHz, 299 K) of **(*E*)-CN-OPE**.

To characterize the double bond geometry of the central C=C-bond of **(*Z*)-CN-OPE** and **(*E*)-CN-OPE**, the C_8-H_1 coupling constant was determined for both isomers respectively. The coupling constants were found to be $^3J_{CN,H}$ = 15.6 Hz for **(*Z*)-CN-OPE** and $^3J_{CN,H}$ = 8.7 Hz for **(*E*)-CN-OPE**, which is in good agreement with corresponding values for CN-substituted stilbenes reported in the literature[6].

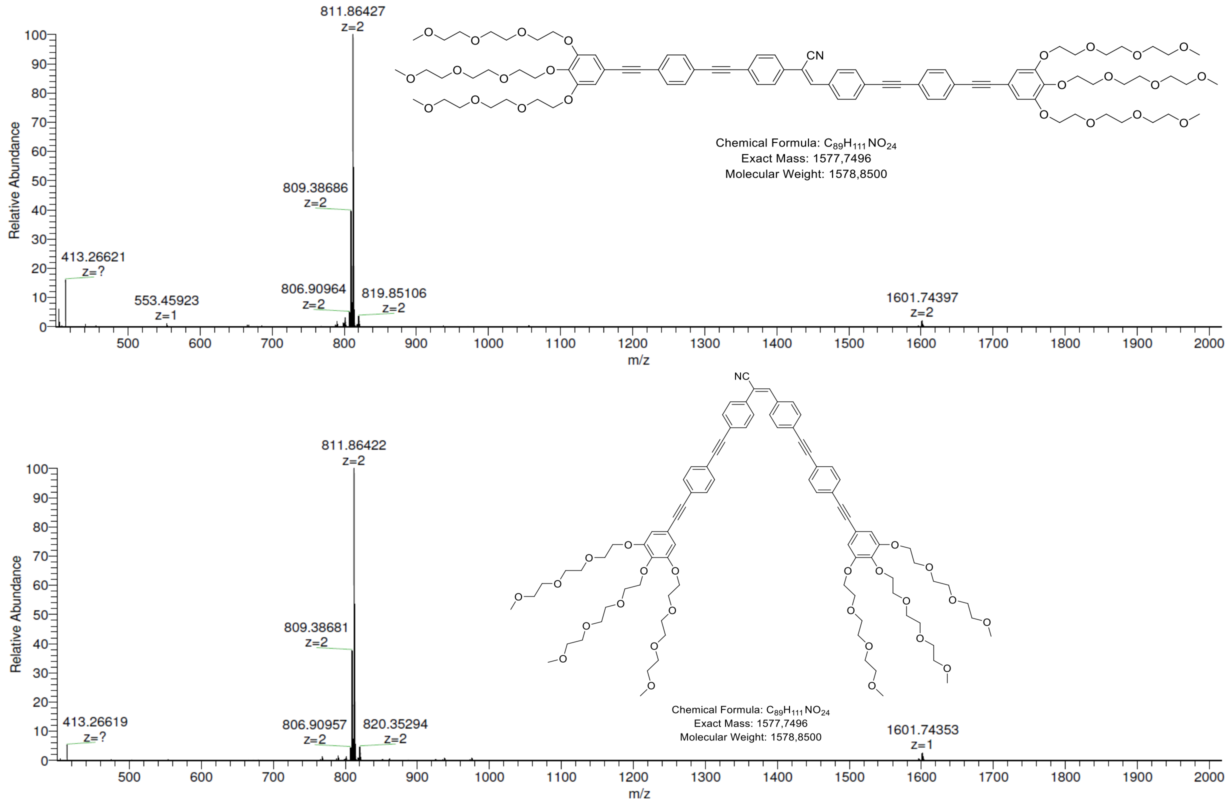

Figure S8: High-resolution mass spectrometry (HRMS, $CHCl_3$/CH_3CN, Orbitrap XL) of **(*Z*)-CN-OPE** (top) and **(*E*)-CN-OPE** (bottom).

(Z)-2,3-bis(4-((3,4,5-tris(2-(2-(2-methoxyethoxy)ethoxy)ethoxy)phenyl)ethynyl)phenyl)acrylonitrile ((*Z*)-CN-OPE*)

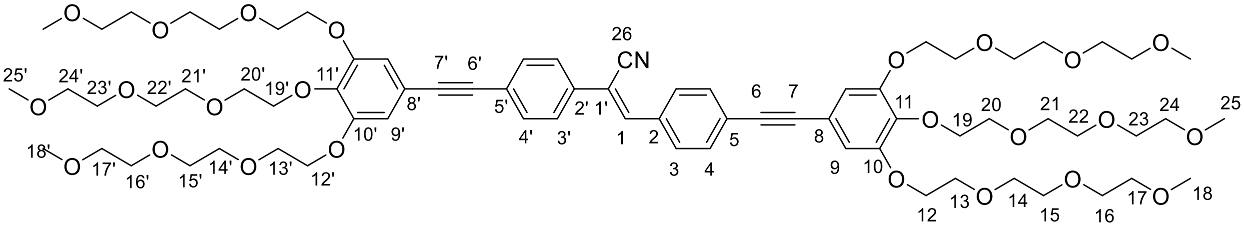

(*Z*)-CN-OPE*
$C_{73}H_{103}NO_{24}$
1378.6100 g/mol

3 (446.6 mg; 0.69 mmol; 2.00 eq), $Pd(PPh_3)_4$ (40.1 mg; 10 mol%) and CuI (13.4 mg; 20 mol%) were dispersed in freshly distilled and degassed NEt_3 (12 mL) and the mixture was stirred at room temperature for 20 min. **9a** (88.0 mg; 0.35 mmol; 1.00 eq) in freshly distilled and degassed THF (2 mL) was added dropwise, the solution was heated up to 70 °C and stirred for 63 h. After cooling to room temperature, the mixture was diluted with DCM and filtered over Celite®. All volatile compounds were removed under reduced pressure and the residue was purified by column chromatography (SiO_2, 1-5 % MeOH in DCM) to give the desired product as an orange highly viscous oil (102.9 mg; $7.4\cdot10^{-5}$ mol; 21 %). **HRMS** (ESI, Orbitrap XXL, MeOH): *m/z* =711.83258 (100) $[M+2Na]^{2+}$; 1400.67592 (20) $[M+Na]^{+}$, calc. for: $C_{73}H_{103}NO_{24}Na_2^{2+}$ 711.83272; $C_{73}H_{103}NO_{24}Na^{+}$ 1400.67732; **^{1}H NMR** ($CDCl_3$, 600 MHz, 293 K) δ (ppm) = 7.89 (*d*, J = 8.5 Hz, 2H, H_3), 7.67 (*d*, J = 8.4 Hz, 2H, $H_{3'}$), 7.58 (*m*, 4H, $H_4+H_{4'}$), 7.54 (*s*, 1H, H_1), 6.80 (*s*, 2H, H_9), 6.79 (*s*, 2H, $H_{9'}$), 4.20 – 4.16 (*m*, 12H, $H_{12}+H_{12'}+H_{19}+H_{19'}$), 3.86 (*t*, J = 5.0 Hz, 8H, $H_{13}+H_{13'}$), 3.79 (*t*, J = 5.0 Hz, 4H, $H_{20}+H_{20'}$), 3.75 – 3.70 (*m*, 12H, $H_{14}+H_{14'}+H_{21}+H_{21'}$), 3.68 – 3.62 (*m*, 24H, $H_{15}+H_{15'}+H_{22}+H_{22'}+H_{16}+H_{16'}+H_{23}+H_{23'}$), 3.55 – 3.53 (*m*, 12H, $H_{17}+H_{17'}+H_{24}+H_{24'}$), 3.38 – 3.36 (*m*, 18H, $H_{18}+H_{18'}+H_{25}+H_{25'}$). **^{13}C NMR** ($CDCl_3$, 151 MHz, 296 K) δ (ppm) = 152.7($C_{10}+C_{10'}$), 141.4 (C_1), 139.9 (C_{11}), 139.8 ($C_{11'}$), 134.0 (C_2), 133.2 ($C_{2'}$), 132.3 ($C_{4'}$), 132.1 (C_4), 129.5 (C_3), 126.0 ($C_{3'}$), 125.8 (C_5), 124.5 ($C_{5'}$), 117.8 (C_{26}), 117.7 (C_8), 117.7 ($C_{8'}$), 111.5 (C_9), 111.5 ($C_{9'}$), 111.4 (C_1), 92.5 (C_7), 91.7($C_{7'}$), 88.2 (C_6), 88.0 ($C_{6'}$), 72.6 ($C_{19}+C_{19'}$), 72.1 ($C_{24}+C_{24'}$), 72.1 ($C_{17}+C_{17'}$), 71.0 ($C_{14}+C_{14'}$), 70.8 ($C_{15}+C_{15'}+C_{20}+C_{20'}$), 70.8 ($C_{22}+C_{22'}$), 70.7 ($C_{16}+C_{16'}$), 70.7 ($C_{23}+C_{23'}$), 70.7 ($C_{21}+C_{21'}$), 69.8 ($C_{13}+C_{13'}$), 69.0 ($C_{12}+C_{12'}$), 59.2 ($C_{18}+C_{18'}$), 59.2 ($C_{25}+C_{25'}$).

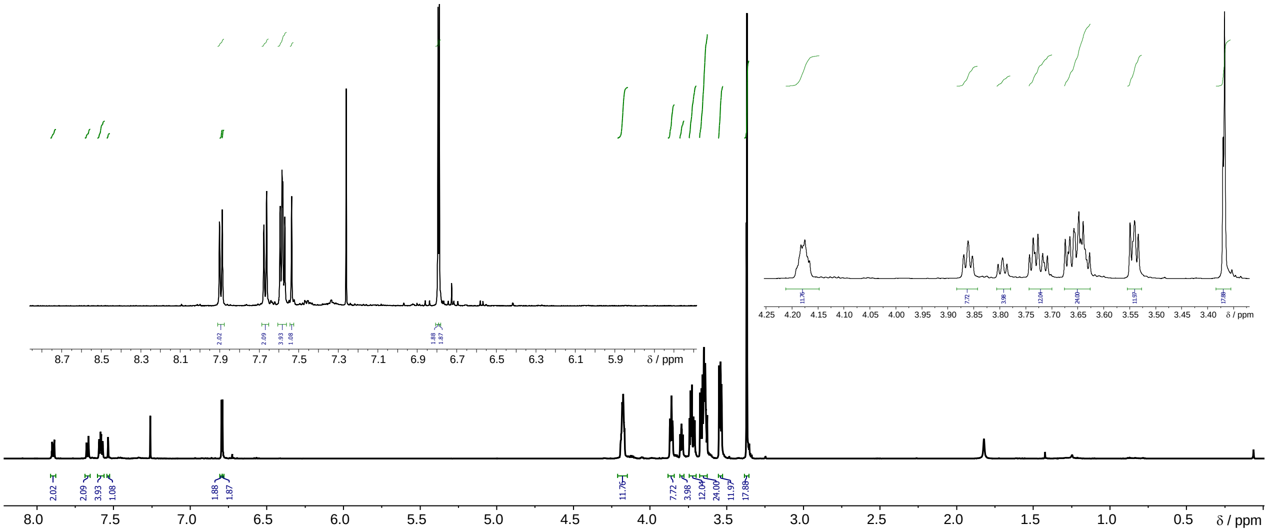

Figure S9a: ^{1}H NMR ($CDCl_3$, 600 MHz, 299 K) of **(Z)-CN-OPE***.

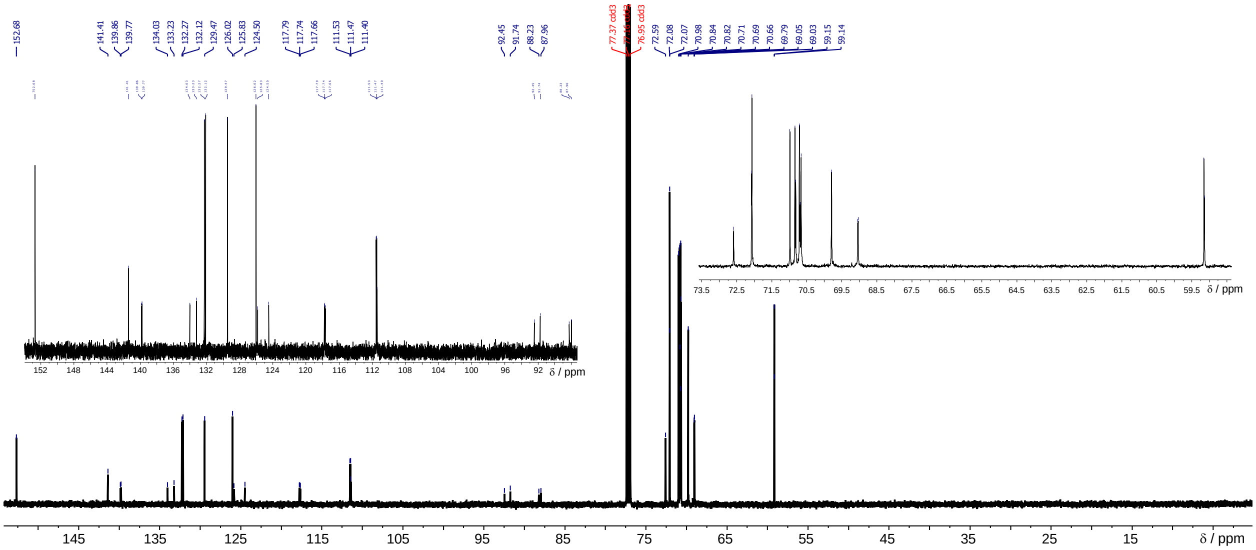

Figure S9b: ^{13}C NMR (CDCl$_3$, 150 MHz, 299 K) of ***(Z)*-CN-OPE***.

Cyc-CN-OPE

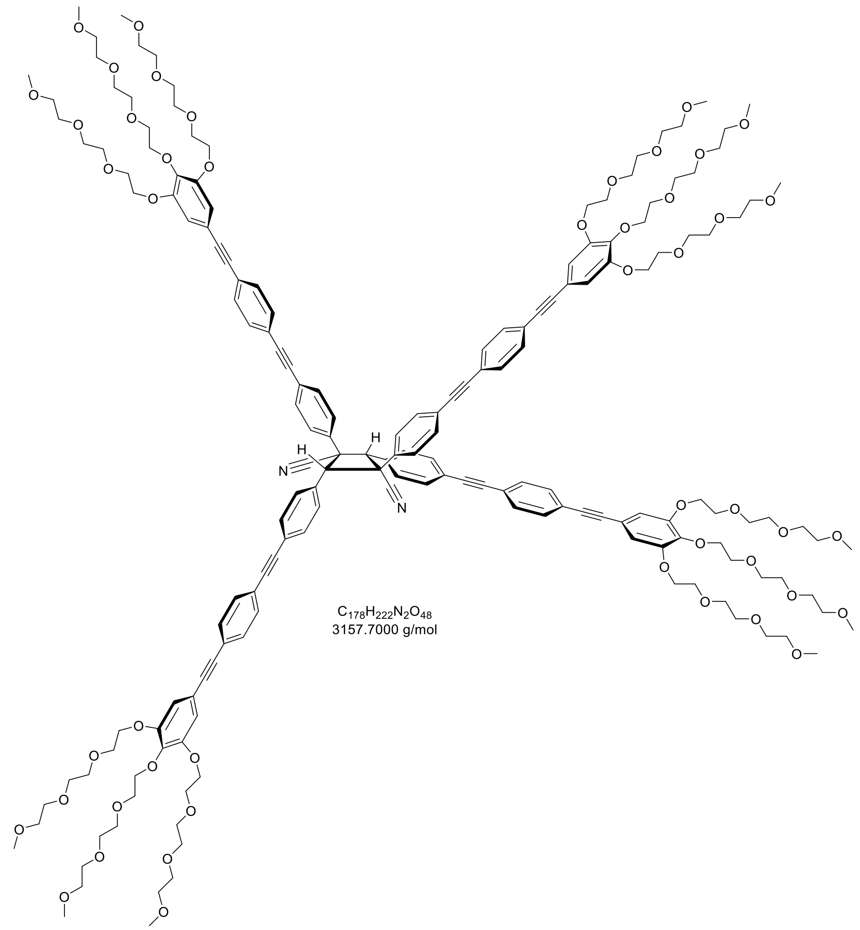

(*Z*)-CN-OPE (35.8 mg; 2.267·10^{-2} mmol; 1.00 eq) was dissolved in freshly distilled THF (5 mL) and the solution was added dropwise into vigorously stirred water (500 mL). The solution was stirred in the dark at room temperature for 20 min and afterwards irradiated with light (λ = 465 nm) for 80 min until no further reaction was observable (monitored by UV-Vis spectroscopy). The reaction mixture was extracted with DCM (8 x 200 mL) and the solvent of the combined organic layers was removed under reduced pressure. The residue was dried in vacuo to yield in a yellowish paste (34.51 mg; 1.093·10^{-2} mmol; 96 %). HRMS (ESI, Orbitrap XXL, $CH_3OH/CHCl_3$ + HCOOH): *m/z* = 1070.53690 (20) $[M+3NH_3]^{3+}$; 1070.18860 (80) $[M+Na+2NH_4]^{3+}$; 1070.84036 (100) $[M+2Na+NH_4]^{3+}$; 1075.49206 (50) $[M+3Na]^{3+}$; 1596.78769 (14) $[M+2NH_4]^{2+}$; 1598.76399 (20) $[M+Na+NH_4]^{2+}$; 1601.74349 (16) $[M+2Na]^{2+}$, calc. for: $C_{178}H_{222}N_2O_{48}(NH_4)_3{}^{3+}$ 1070.535752; $C_{178}H_{222}N_2O_{48}(NH_4)_2Na^{3+}$ 1072.18756; $C_{178}H_{222}N_2O_{48}NH_4Na_2{}^{3+}$ 1073.83936; $C_{178}H_{222}N_2O_{48}Na_3{}^{3+}$ 1075.491168; $C_{178}H_{222}N_2O_{48}(NH_4)_2{}^{2+}$ 1596.78672; $C_{178}H_{222}N_2O_{48}NH_4Na^{2+}$ 1598.762810; $C_{178}H_{222}N_2O_{48}Na_2{}^{2+}$ 1601.74214;^{1}H NMR ($CDCl_3$, 500 MHz, 299 K): *δ* (ppm) = 7.57 – 7.39 (*m*, 24H), 7.27 (*dd*, *J* = 20.8, 8.2 Hz, 8H), 6.82 – 6.73 (*m*, 8H), 5.22 (*s*, 2H), 4.19 – 4.13 (*m*, 24H), 3.84 (*t*, *J* = 4.9 Hz, 16H), 3.78 (*t*, *J* = 5.0 Hz, 8H), 3.74 – 3.69 (*m*, 24H), 3.67 – 3.61 (*m*, 48H), 3.55 – 3.51 (*m*, 24H), 3.37 – 3.35 (*m*, 36H). ^{13}C NMR ($CDCl_3$, 126 MHz, 296 K) *δ* (ppm) = 152.6, 139.7, 134.4, 132.7, 132.3, 132.0, 131.7, 131.7, 131.6, 129.6, 128.0, 124.1, 123.6, 123.5, 122.6, 122.5, 121.0, 117.8, 111.4, 91.6, 91.6, 91.0, 90.9, 90.4, 90.1, 88.2, 77.4, 77.2, 76.9, 72.5, 72.0, 72.0, 70.9, 70.8, 70.8, 70.7, 70.7, 70.6, 69.8, 69.0, 59.1, 59.1, 55.9, 47.8.

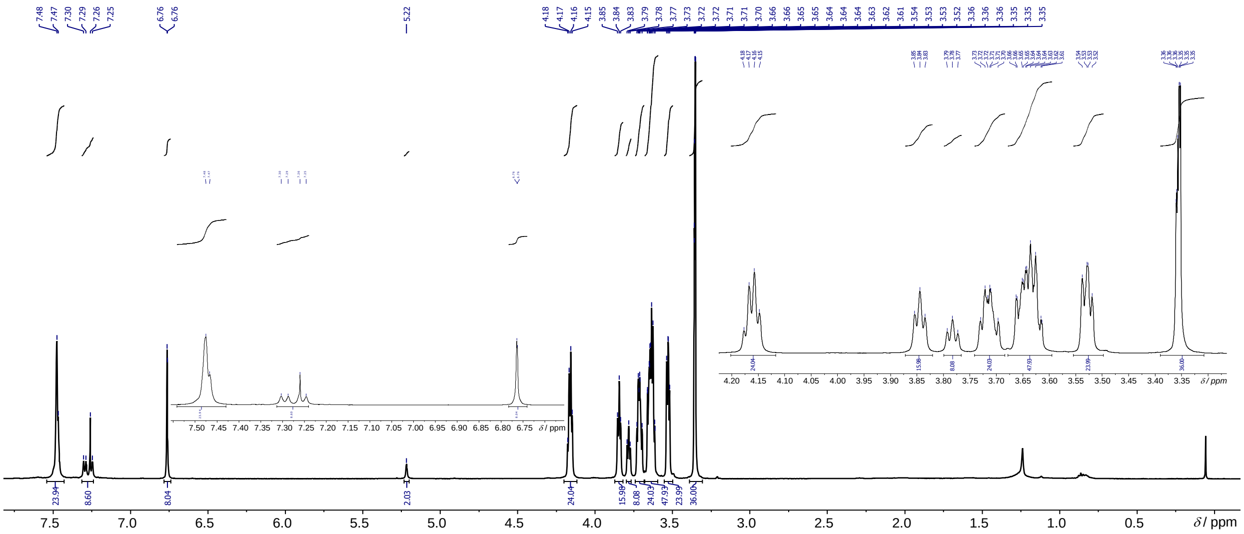

Figure S10a: ^{1}H NMR ($CDCl_3$, 500 MHz, 299 K) of **cyc-CN-OPE**.

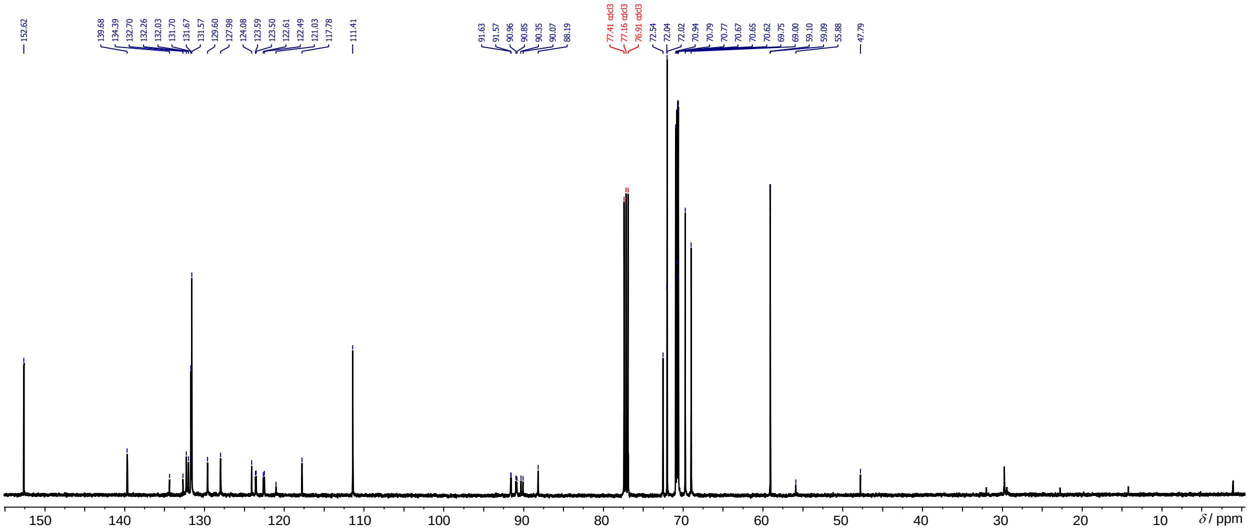

Figure S10b: ^{13}C NMR ($CDCl_3$, 126 MHz, 299 K) of **cyc-CN-OPE**.

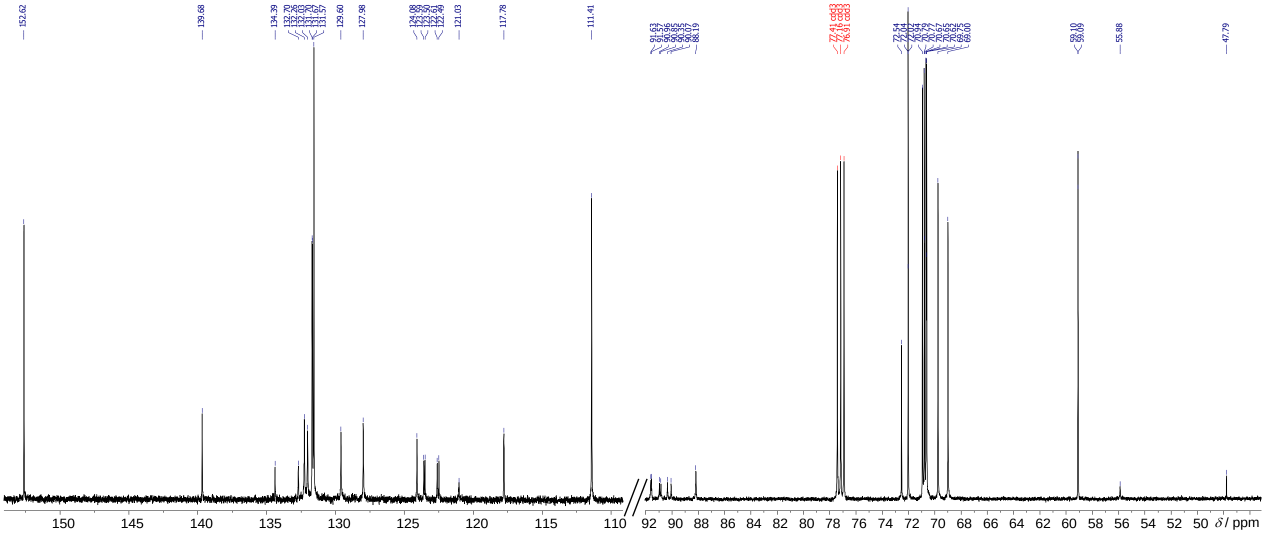

Figure S10c: Enlargement of the aromatic and aliphatic region of the ^{13}C NMR ($CDCl_3$, 126 MHz, 299 K) of **cyc-CN-OPE**.

cyc-CN-OPE*

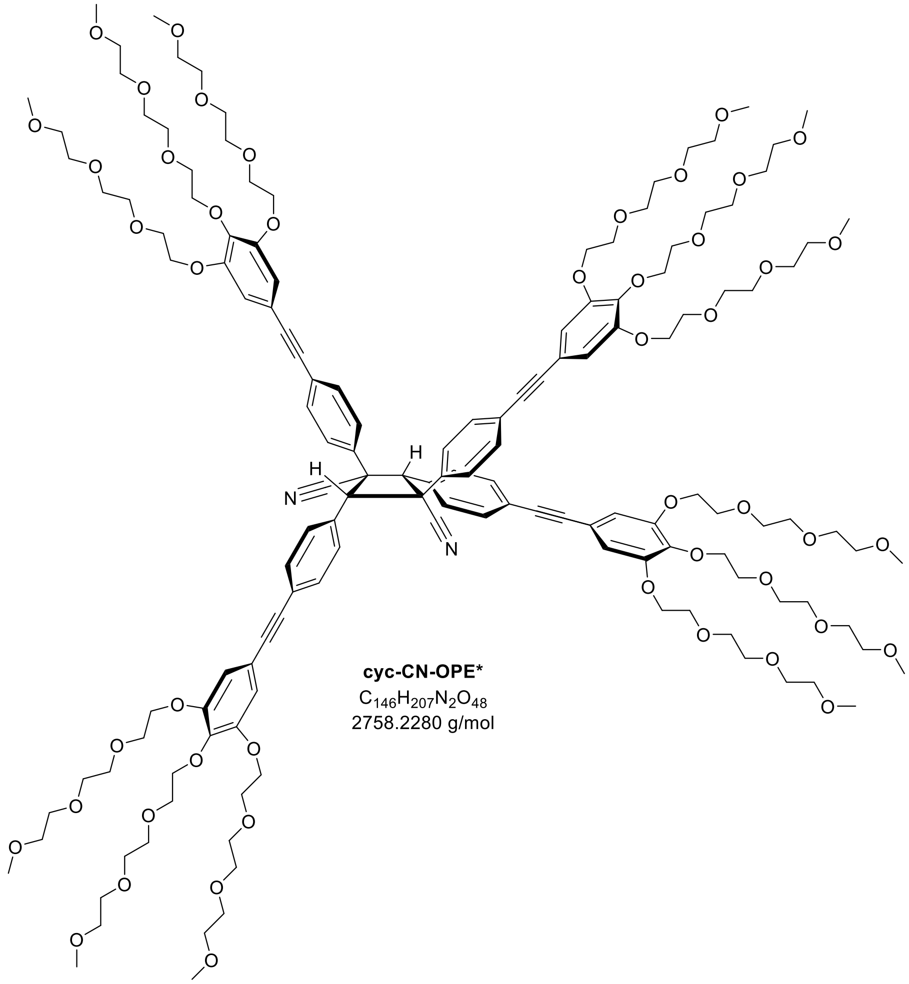

cyc-CN-OPE*
$C_{146}H_{207}N_2O_{48}$
2758.2280 g/mol

(*Z*)-CN-OPE* (31.2 mg; $2.263 \cdot 10^{-5}$ mmol; 1.00 eq) was dissolved in water (250 mL). The solution was stirred in the dark at room temperature for 20 min and afterwards irradiated with light (λ = 465 nm) for 65 min until no further reaction was observable (monitored by UV-Vis spectroscopy). The reaction mixture was extracted with DCM (6 x 150 mL), the combined organic layers were dried over $MgSO_4$ and the solvent was removed under reduced pressure to yield in a yellowish oil (28.0 mg; $1.015 \cdot 10^{-5}$ mmol; 90 %). HRMS (ESI, Nanospray, H_2O/CH_3CN): *m/z* = found: 1413.65614 (100) $[M+2Cl]^{2-}$; 2792.35400 (25) $[M+Cl]^{-}$; calc. for: $C_{146}H_{206}N_2O_{48}Cl_2^{2-}$ 1413.65821; $C_{146}H_{206}N_2O_{48}Cl^{-}$ 2792.34823; **^{1}H NMR** ($CDCl_3$, 500 MHz, 299 K): *δ* (ppm) = 7.44 (*d*, *J* = 8.3 Hz, 8H), 7.27 (*d*, *J* = , 8.6 Hz, 4H), 7.24 (*d*, *J* = 8.5 Hz, 4H), 6.78 – 6.73 (*m*, 8H), 5.20 (*s*, 2H), 4.19 – 4.13 (*m*, 24H), 3.84 (*t*, *J* = 5.3 Hz, 16H), 3.78 (*t*, *J* = 4.8 Hz, 8H), 3.74 – 3.70 (*m*, 24H), 3.67 – 3.61 (*m*, 48H), 3.55 – 3.51 (*m*, 24H), 3.37 – 3.34 (*m*, 36H). ^{13}C NMR ($CDCl_3$, 126 MHz, 296 K) *δ* (ppm) = 152.66, 152.65, 139.81, 139.75, 134.21, 132.52, 132.26, 132.20, 132.18, 132.12, 131.95, 131.76, 129.84, 129.57, 129.04, 128.68, 128.58, 127.97, 125.14, 124.28, 124.26, 121.13, 117.68, 117.56, 111.58, 111.46, 111.43, 91.31, 91.18, 87.67, 87.42, 77.41, 77.16, 76.91, 72.58, 72.44, 72.07, 72.06, 70.97, 70.82, 70.81, 70.75, 70.69, 70.68, 70.65, 69.90, 69.78, 69.69, 69.23, 69.04, 59.13, 59.12.

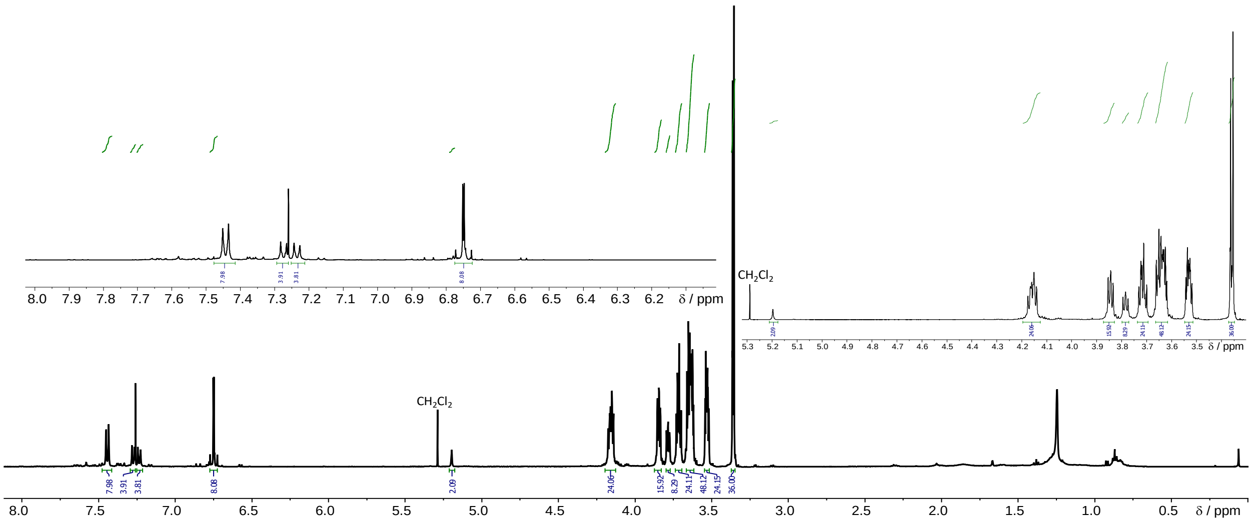

Figure S11a: ^{1}H NMR (CDCl$_3$, 500 MHz, 299 K) of **cyc-CN-OPE***.

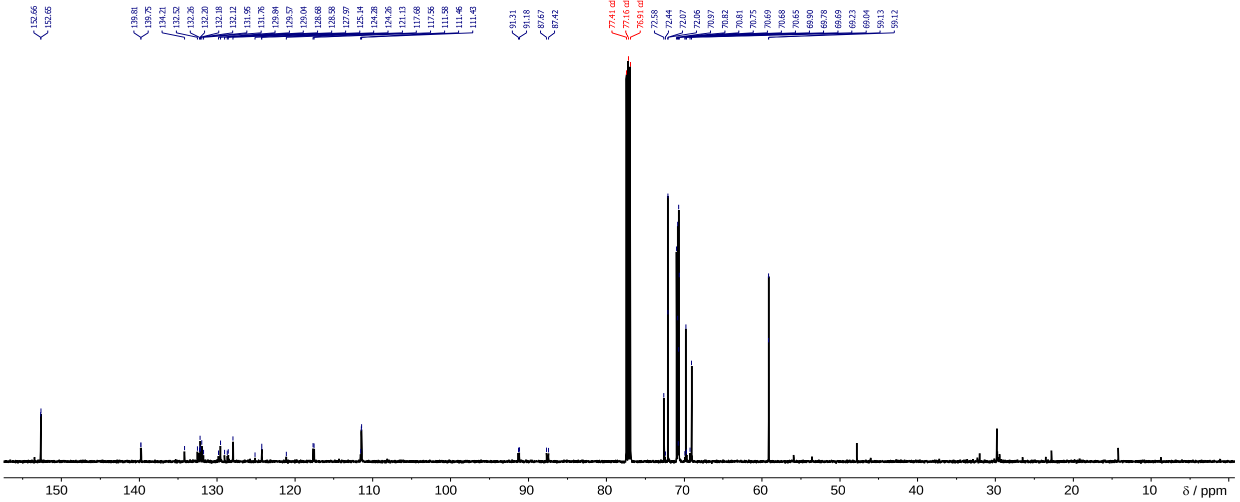

Figure S11b: ^{13}C NMR (CDCl$_3$, 126 MHz, 299 K) of **cyc-CN-OPE***.

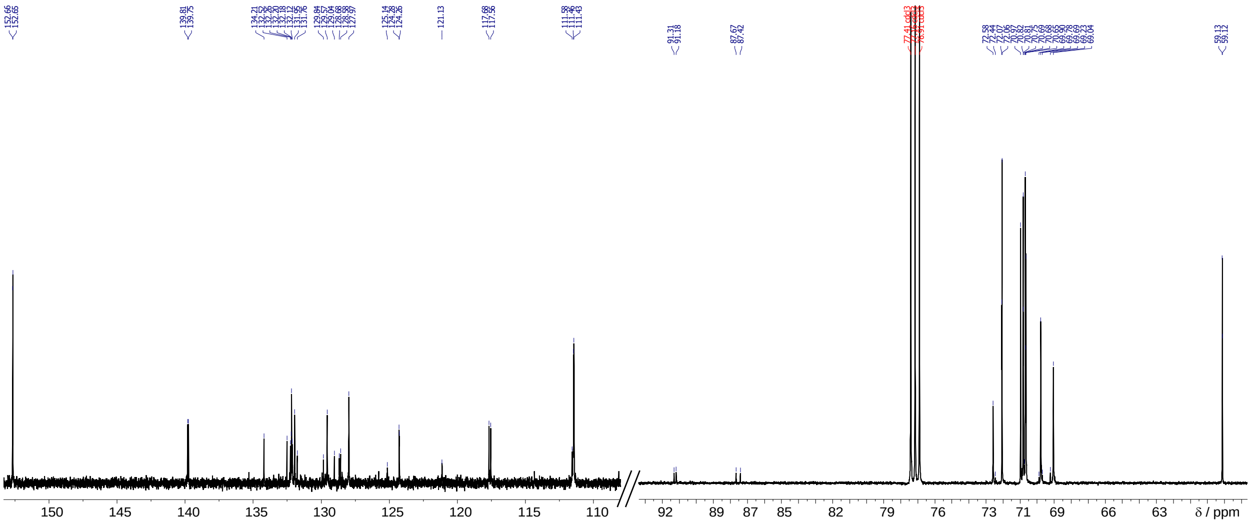

Figure S11c: Enlargement of the aromatic and aliphatic region of the ^{13}C NMR (CDCl$_3$, 126 MHz, 299 K) of **cyc-CN-OPE***.

2. Nucleation-Elongation model for Cooperative Supramolecular Polymerizations

The equilibrium between the monomeric and supramolecular species can be described in a cooperative process with the *Nucleation-Elongation model* which is developed by Ten Eikelder, Markvoort and Meijer.[7,8] This model is used to describe the aggregation of **(*Z*)-CN-OPE** which exhibits a non-sigmoidal cooling curve as shown in fluorescence and UV-Vis temperature-dependent experiments. The model extends nucleation-elongation based equilibrium models for growth of supramolecular homopolymers to the case of two monomer and aggregate types and can be applied to symmetric supramolecular copolymerizations, as well as to the more general case of nonsymmetric supramolecular copolymerizations.

In a cooperative process, the polymerization occurs by a nucleation step, to a nucleus size assumed of B, and a following elongation step. The values T_e, ΔH°_{nucl}, ΔH° and ΔS° can be determined by a non-linear least-square analysis of the experimental melting curves. The equilibrium constants associated with the nucleation and elongation phases can be calculated using equations **1** and **2**:

$$\text{Nucleation step: } K_n = e^{\left(\frac{-(\Delta H^o - \Delta H^o_{nucl}) - T\Delta S^o}{RT}\right)} \qquad (\mathbf{1})$$

$$\text{Elongation step: } K = e^{\left(\frac{-(\Delta H^o - T\Delta S^o)}{RT}\right)} \qquad (\mathbf{2})$$

And the cooperativity factor (σ) is given by:

$$\sigma = \frac{K_n}{K_e} = e^{\left(\frac{\Delta H^o_{nucl}}{RT}\right)} \qquad (\mathbf{3})$$

3. Supplementary Images

3.1. Aggregation Studies

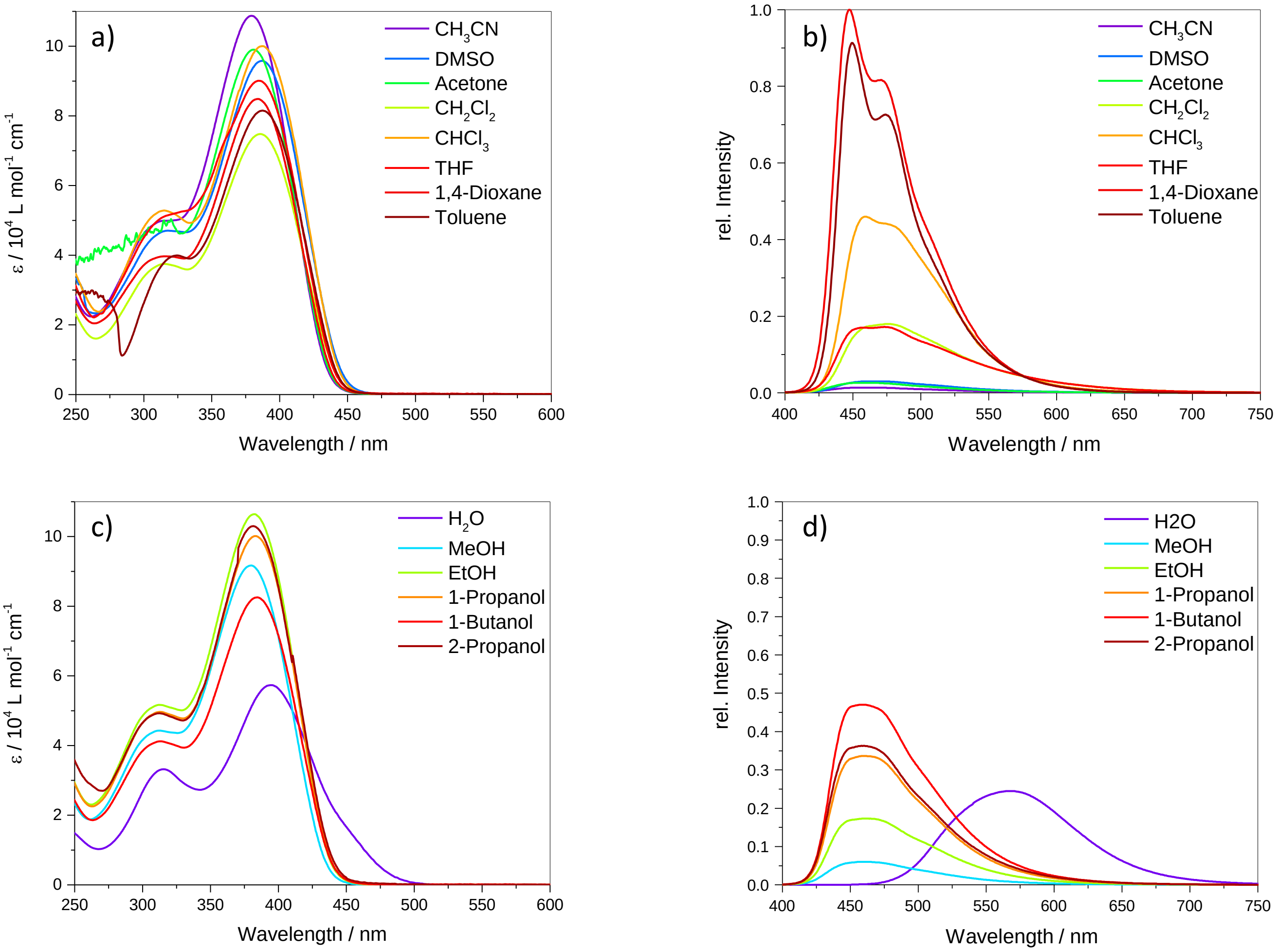

Figure S12: a) UV-Vis spectra of **(*Z*)-CN-OPE** in different non-protic solvents at *c* = 10^{-5} M and 298 K. b) Emission spectra of **(*Z*)-CN-OPE** in different non-protic solvents at *c* = 10^{-5} M and 298 K. c) UV-vis spectra of **(*Z*)-CN-OPE** in different protic solvents at *c* = 10^{-5} M and 298 K. d) Emission spectra of **(*Z*)-CN-OPE** in different protic solvents at *c* = 10^{-5} M and 298 K.

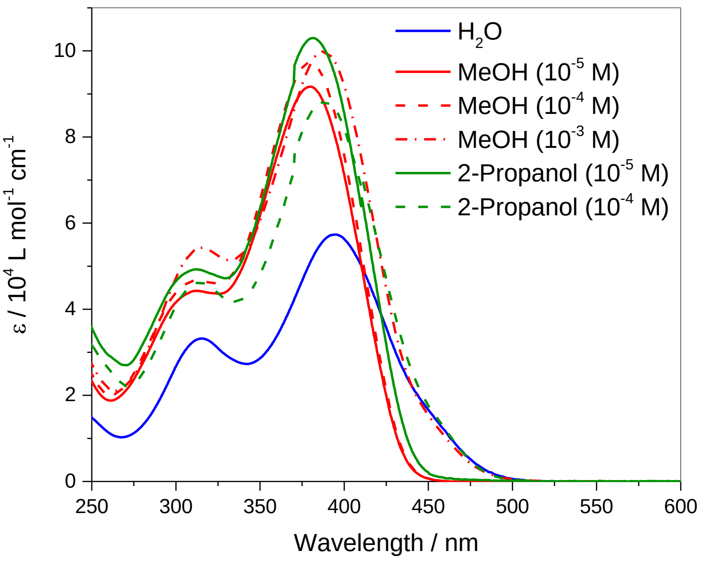

Figure S13: UV-Vis spectra of **(*Z*)-CN-OPE** in water, methanol and *i*-PrOH at different concentrations at 298 K.

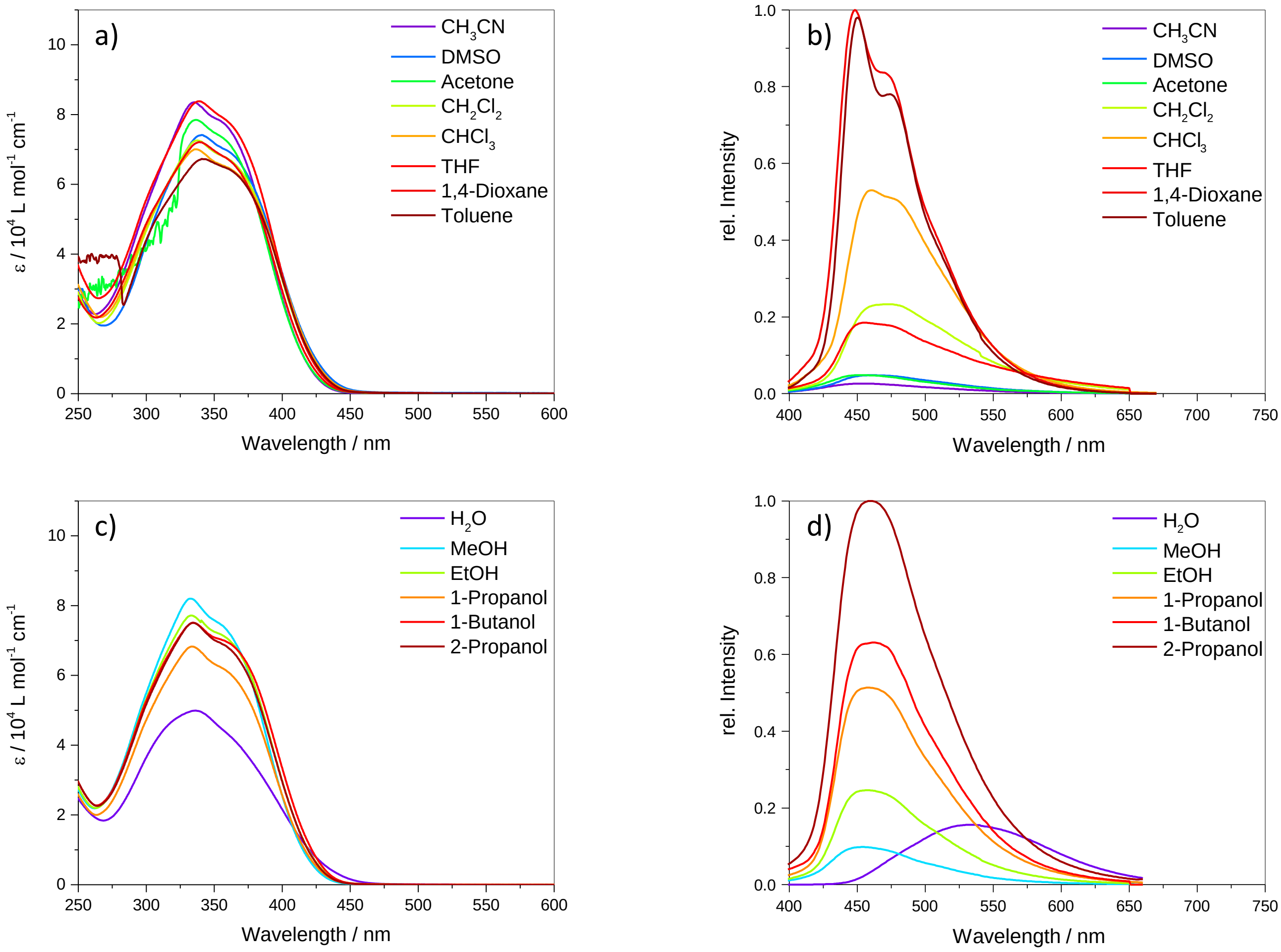

Figure S14: a) UV-Vis spectra of **(*E*)-CN-OPE** in different non-protic solvents with *c* = 10^{-5} M at 298 K. b) Emission spectra of **(*E*)-CN-OPE** in different non-protic solvents with *c* = 10^{-5} M at 298 K. c) UV-vis spectra of **(*E*)-CN-OPE** in different protic solvents with *c* = 10^{-5} M at 298 K. d) Emission spectra of **(*E*)-CN-OPE** in different protic solvents with *c* = 10^{-5} M at 298 K.

Table S1: Summary of the spectroscopic characteristics of **(*Z*)-CN-OPE** and **(*E*)-CN-OPE** in different solvents ($c = 10^{-5}$ M) at 298 K.

Entry	Solvent	$E_T(30)$ /kcal·mol^{-1}	$\lambda_{max}(Z)$ / nm	$\lambda_{max}(E)$ / nm	$\lambda_{em}(Z)^a$ / nm	$\lambda_{em}(E)^a$ / nm	$\Delta\lambda_{ST}{}^b(Z)$ / nm (eV)	$\Delta\lambda_{ST}{}^b(E)$ / nm (eV)
1	H_2O	63.1	395	336	567^c	534^c	172 (0.952)	198 (1.368)
2	MeOH	55.4	381	333	460^c	454^c	79 (0.559)	121 (0.992)
3	EtOH	51.9	380	333	462^c	457^c	82 (0.579)	124 (1.010)
4	1-Propanol	50.7	388	333	459^c	458^c	71 (0.494)	125 (1.016)
5	1-Butanol	49.7	383	334	457^c	462^c	74 (0.524)	128 (1.028)
6	2-Propanol	48.4	384	335	459^c	460^c	75 (0.528)	125 (1.006)
7	CH_3CN	45.6	379	335	458^c	453^c	79 (0.564)	118 (0.964)
8	DMSO	45.1	387	341	468^c	461^c	81 (0.555)	120 (0.947)
9	Acetone	42.2	381	337	459^c	452^c	78 (0.553)	115 (0.936)
10	CH_2Cl_2	40.7	386	338	461	472	75 (0.523)	134 (1.041)
11	$CHCl_3$	39.1	388	337	459	460	71 (0.494)	123 (0.984)
12	THF	37.4	387	339	458	455	71 (0.497)	116 (0.932)
13	1,4-Dioxane	36.4	384	339	448	448	64 (0.461)	109 (0.889
14	Toluene	33.9	387	341	450	450	63 (0.449)	109 (0.931)

[a] The emission was detected by excitation at λ_{max} of the corresponding UV-vis-spectrum. [b] The stokes shift was calculated according to $\Delta\lambda_{ST} = \lambda_{em} - \lambda_{max}$. [c] broad signal.

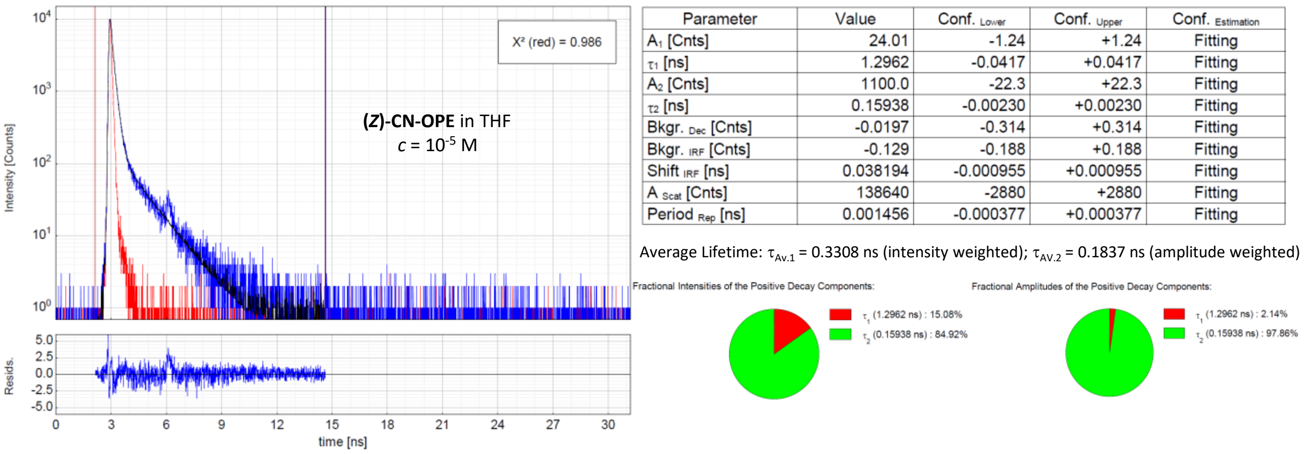

Parameter	Value	Conf. Lower	Conf. Upper	Conf. Estimation
A_1 [Cnts]	24.01	-1.24	+1.24	Fitting
τ_1 [ns]	1.2962	-0.0417	+0.0417	Fitting
A_2 [Cnts]	1100.0	-22.3	+22.3	Fitting
τ_2 [ns]	0.15938	-0.00230	+0.00230	Fitting
Bkgr. $_{Dec}$ [Cnts]	-0.0197	-0.314	+0.314	Fitting
Bkgr. $_{IRF}$ [Cnts]	-0.129	-0.188	+0.188	Fitting
Shift $_{IRF}$ [ns]	0.038194	-0.000955	+0.000955	Fitting
A $_{Scat}$ [Cnts]	138640	-2880	+2880	Fitting
Period $_{Rep}$ [ns]	0.001456	-0.000377	+0.000377	Fitting

Average Lifetime: $\tau_{Av.1}$ = 0.3308 ns (intensity weighted); $\tau_{AV.2}$ = 0.1837 ns (amplitude weighted)

Figure S15a: Left: Time-resolved luminescence decay of **(*Z*)-CN-OPE** in THF at 298 K (c = 10^{-5} M), including the residuals (λ_{exc} = 375 nm, λ_{em} = 450 nm). Right: Fitting parameters including pre-exponential factors and confidence limits.

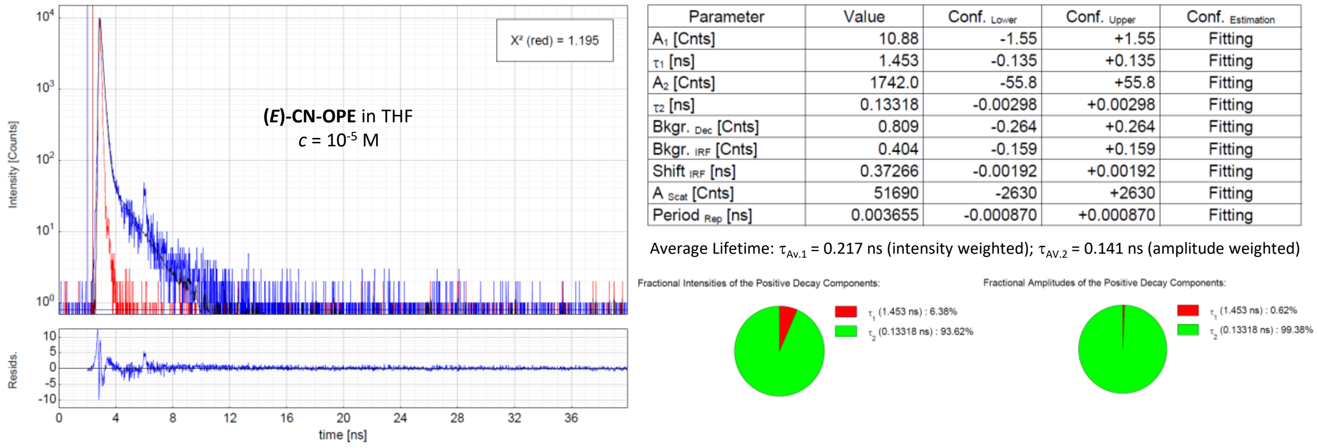

Parameter	Value	Conf. Lower	Conf. Upper	Conf. Estimation
A_1 [Cnts]	10.88	-1.55	+1.55	Fitting
τ_1 [ns]	1.453	-0.135	+0.135	Fitting
A_2 [Cnts]	1742.0	-55.8	+55.8	Fitting
τ_2 [ns]	0.13318	-0.00298	+0.00298	Fitting
Bkgr. $_{Dec}$ [Cnts]	0.809	-0.264	+0.264	Fitting
Bkgr. $_{IRF}$ [Cnts]	0.404	-0.159	+0.159	Fitting
Shift $_{IRF}$ [ns]	0.37266	-0.00192	+0.00192	Fitting
A $_{Scat}$ [Cnts]	51690	-2630	+2630	Fitting
Period $_{Rep}$ [ns]	0.003655	-0.000870	+0.000870	Fitting

Average Lifetime: $\tau_{Av.1}$ = 0.217 ns (intensity weighted); $\tau_{AV.2}$ = 0.141 ns (amplitude weighted)

Figure S15b: Left: Time-resolved luminescence decay of **(*E*)-CN-OPE** in THF at 298 K (c = 10^{-5} M), including the residuals (λ_{exc} = 375 nm, λ_{em} = 450 nm). Right: Fitting parameters including pre-exponential factors and confidence limits.

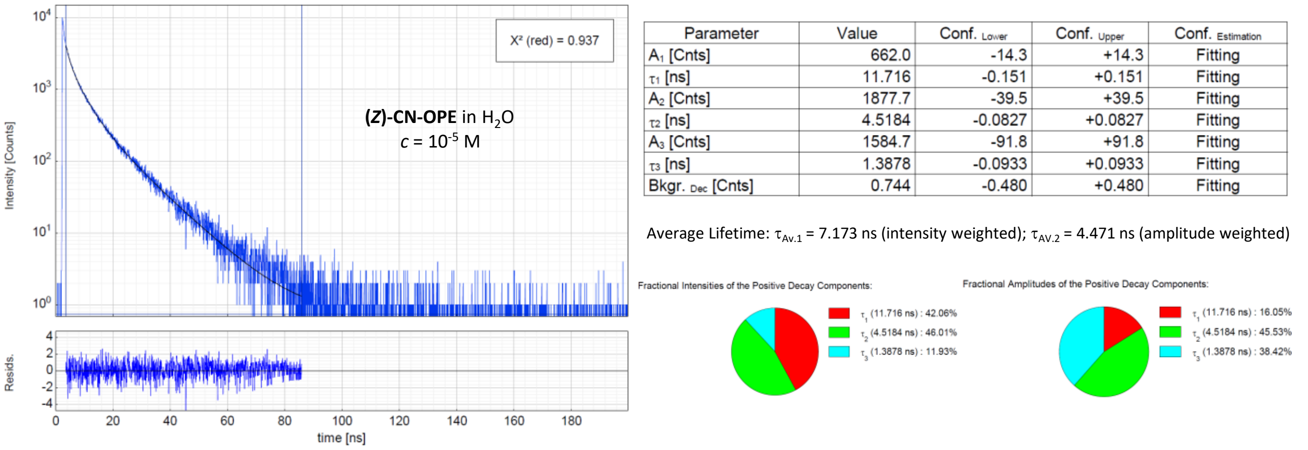

Parameter	Value	Conf. Lower	Conf. Upper	Conf. Estimation
A_1 [Cnts]	662.0	-14.3	+14.3	Fitting
τ_1 [ns]	11.716	-0.151	+0.151	Fitting
A_2 [Cnts]	1877.7	-39.5	+39.5	Fitting
τ_2 [ns]	4.5184	-0.0827	+0.0827	Fitting
A_3 [Cnts]	1584.7	-91.8	+91.8	Fitting
τ_3 [ns]	1.3878	-0.0933	+0.0933	Fitting
Bkgr. $_{Dec}$ [Cnts]	0.744	-0.480	+0.480	Fitting

Average Lifetime: $\tau_{Av.1}$ = 7.173 ns (intensity weighted); $\tau_{AV.2}$ = 4.471 ns (amplitude weighted)

Figure S15c: Left: Time-resolved luminescence decay of **(*Z*)-CN-OPE** in H_2O at 298 K (c = 10^{-5} M), including the residuals (λ_{exc} = 375 nm, λ_{em} = 580 nm). Right: Fitting parameters including pre-exponential factors and confidence limits.

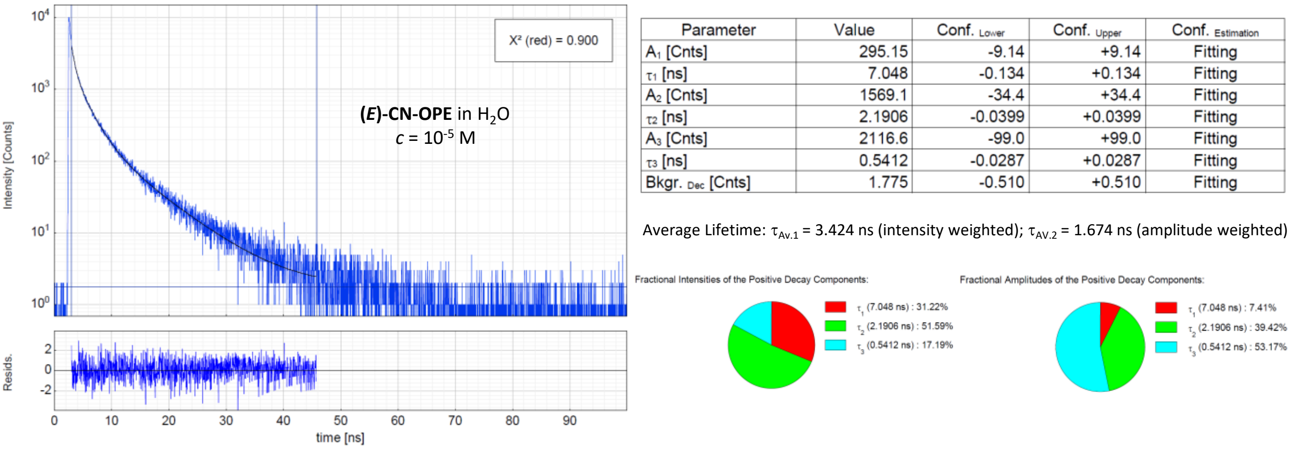

Parameter	Value	Conf. Lower	Conf. Upper	Conf. Estimation
A$_1$ [Cnts]	295.15	-9.14	+9.14	Fitting
τ$_1$ [ns]	7.048	-0.134	+0.134	Fitting
A$_2$ [Cnts]	1569.1	-34.4	+34.4	Fitting
τ$_2$ [ns]	2.1906	-0.0399	+0.0399	Fitting
A$_3$ [Cnts]	2116.6	-99.0	+99.0	Fitting
τ$_3$ [ns]	0.5412	-0.0287	+0.0287	Fitting
Bkgr. Dec [Cnts]	1.775	-0.510	+0.510	Fitting

Average Lifetime: $\tau_{AV.1}$ = 3.424 ns (intensity weighted); $\tau_{AV.2}$ = 1.674 ns (amplitude weighted)

Figure S15d: Left: Time-resolved luminescence decay of **(*E*)-CN-OPE** in H_2O at 298 K (c = 10^{-5} M), including the residuals (λ_{exc} = 375 nm, λ_{em} = 580 nm). Right: Fitting parameters including pre-exponential factors and confidence limits.

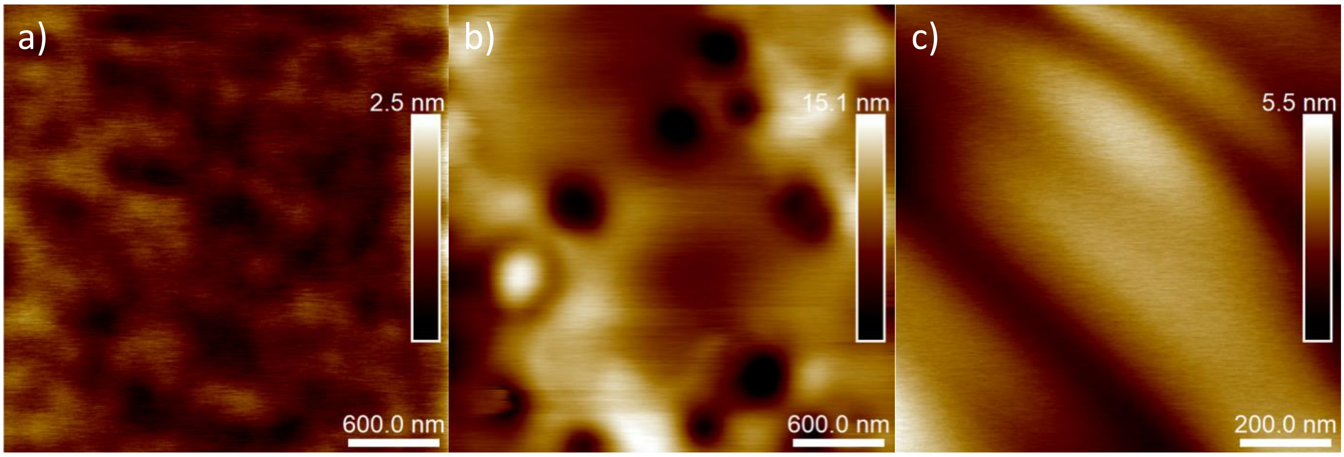

Figure S16: a) AFM images of aqueous solutions of **(*E*)-CN-OPE** onto MICA according to the following sample preparations procedures: a) 20 µL (10^{-4} M) dropcasted on surface, letting rest for 20 min, then spin coated for 20 min (1000 rpm); b) 50 µL (10^{-5} M) dropcasted on surface and letting dry overnight; c) 25 µL (10^{-5} M) dropcasted on surface and letting dry over night;

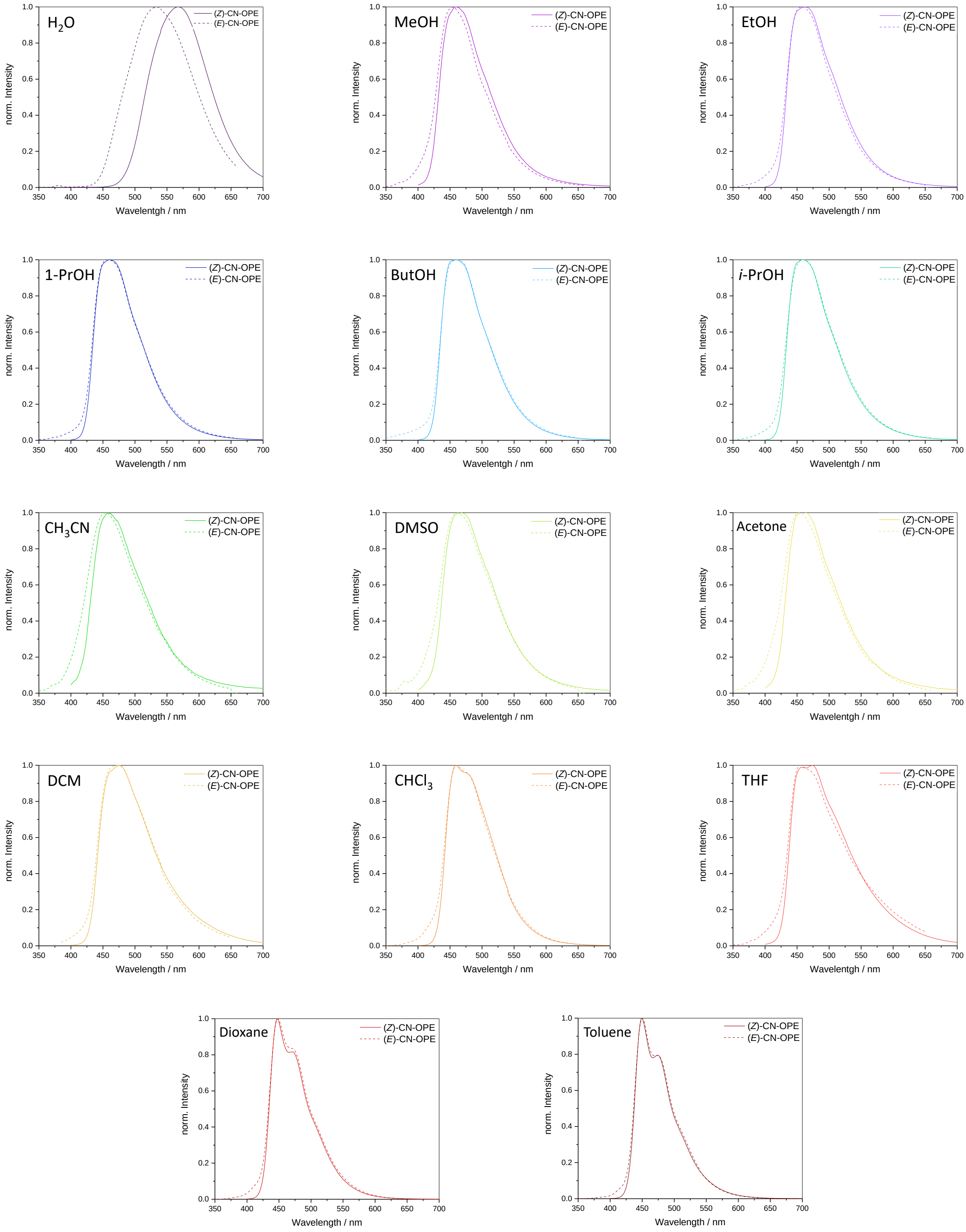

Figure S17: Direct comparison of the emission spectra of the *E*- and *Z*-isomers in different solvents ($c = 10^{-5}$ M) at 298 K by overlaying the respective spectra.

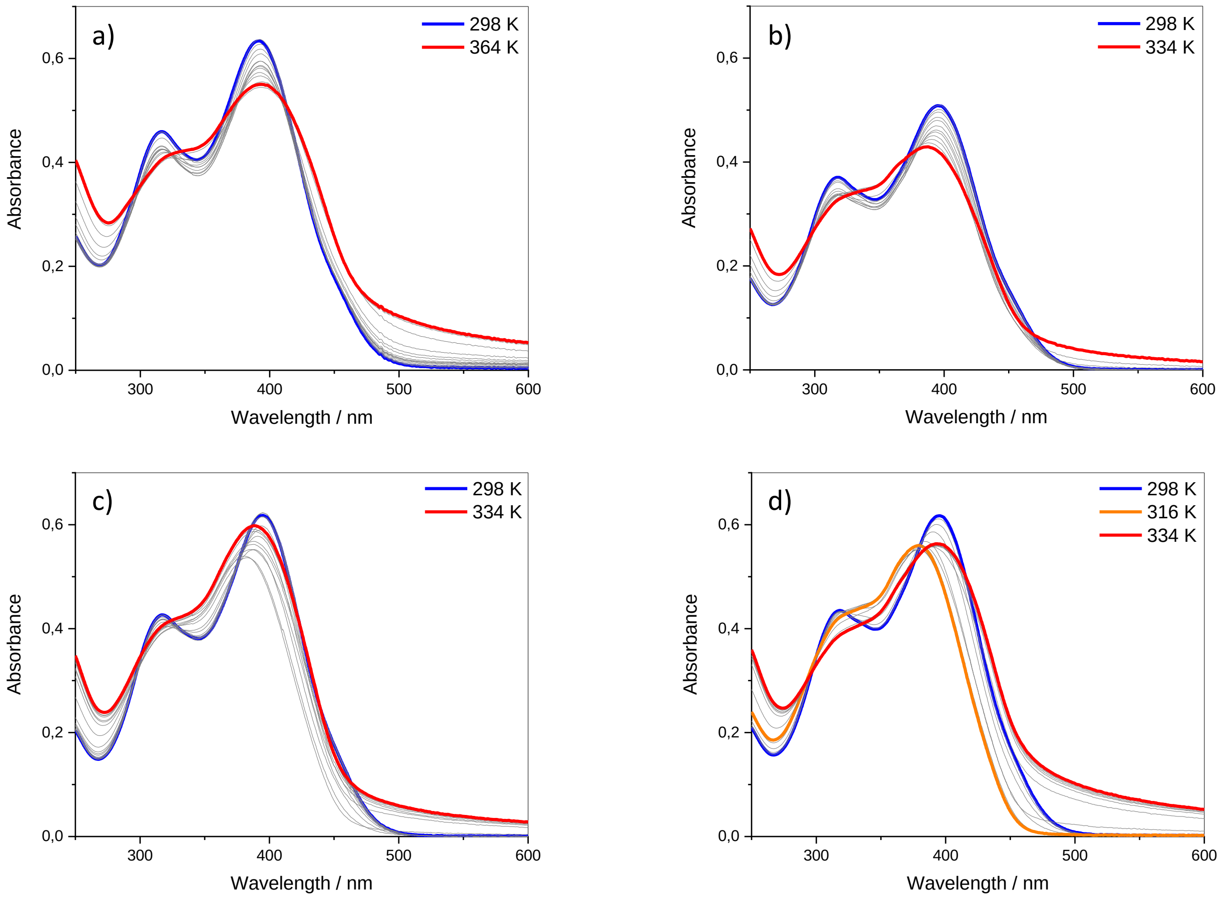

Figure S18: Temperature-dependent UV-Vis spectra of **(*Z*)-CN-OPE** in THF/ water mixtures consisting of: a) 100 % Water; b) 90% water/ 10 % THF; c) 85 % Water/ 15 % THF; d) 80 % water/ 20 % THF ($c = 10^{-5}$ M). The increase in absorbance (scattering) observed in the region above 500 nm is due to the dehydration of the glycol chains under these conditions upon heating (LCST behavior).

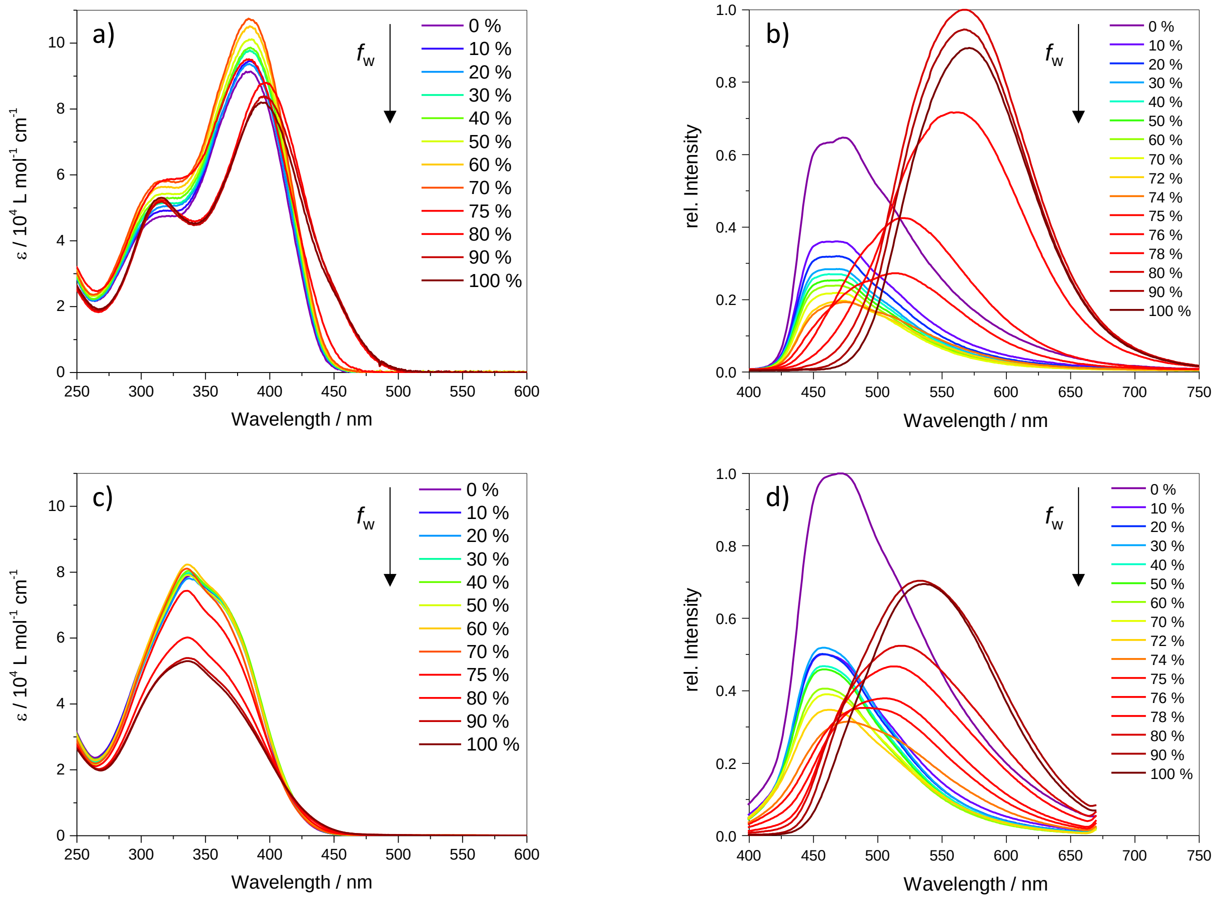

Figure S19: UV-Vis spectra (a) and corresponding fluorescence spectra (b) of **(*Z*)-CN-OPE** in different THF/H_2O mixtures upon increasing volume fraction f_w of water at $c = 10^{-5}$ M. UV-Vis-spectra (c) and fluorescence spectra (d) of **(*E*)-CN-OPE** in different THF/H_2O mixtures upon increasing volume fraction f_w of water at 10^{-5} M.

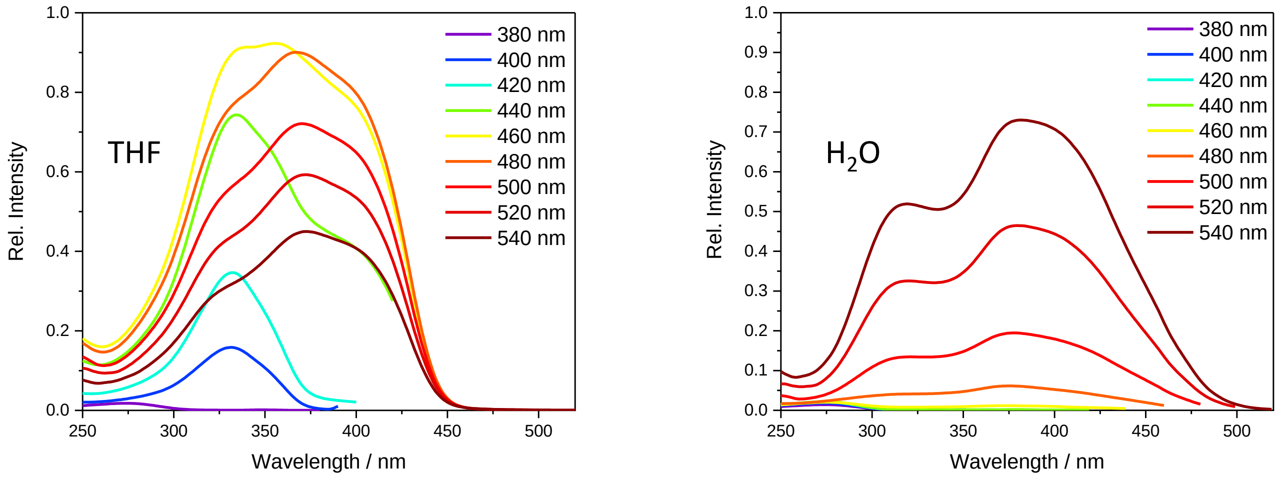

Figure S20: Excitation spectra of **(*Z*)-CN-OPE** at $c = 10^{-5}$ M and 298 K in THF (monomer, left) and H_2O (aggregate, right).

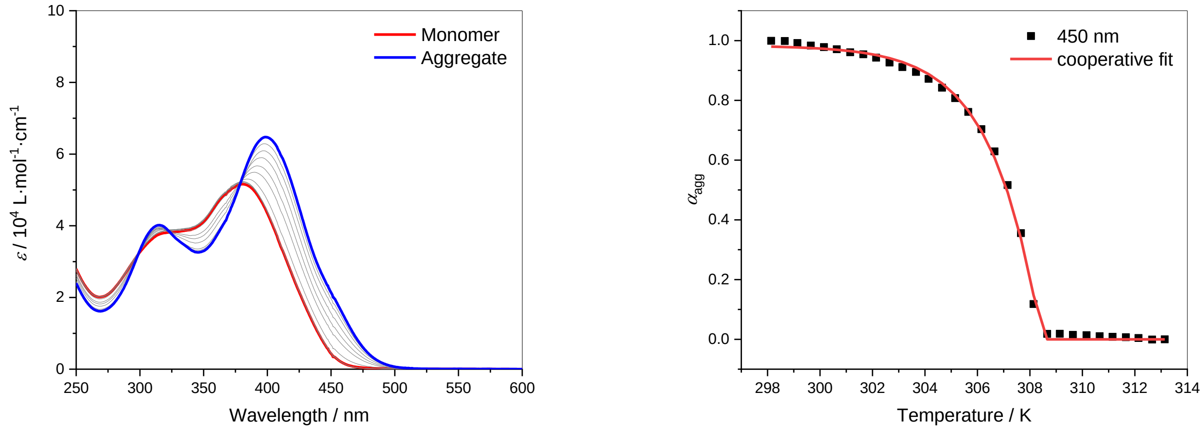

Figure S21a: Left: VT UV-Vis spectra of **(*Z*)-CN-OPE** in a 20:80 mixture of THF and H_2O at 10^{-5} M between 313 K and 298 K. Right: Corresponding degree of aggregation α_{agg} (monitored at $\lambda = 450$ nm) plotted against the temperature and fit to the cooperative nucleation-elongation model[7].

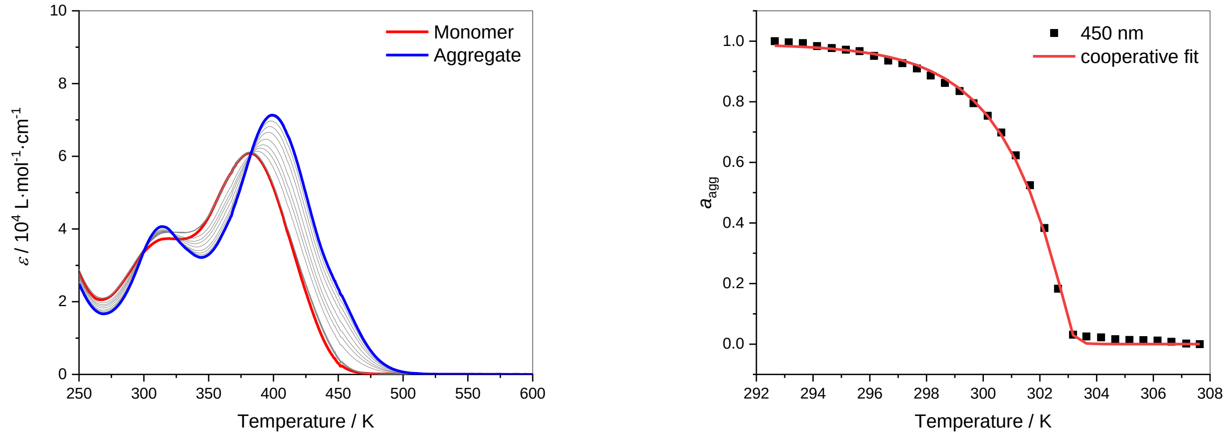

Figure S21b: Left: VT UV-Vis spectra of **(*Z*)-CN-OPE** in a 22.5:77.5 mixture of THF and H_2O at 10^{-5} M between 313 K and 298 K. Right: Corresponding degree of aggregation α_{agg} (monitored at $\lambda = 450$ nm) plotted against the temperature and fit to the cooperative nucleation-elongation model[7].

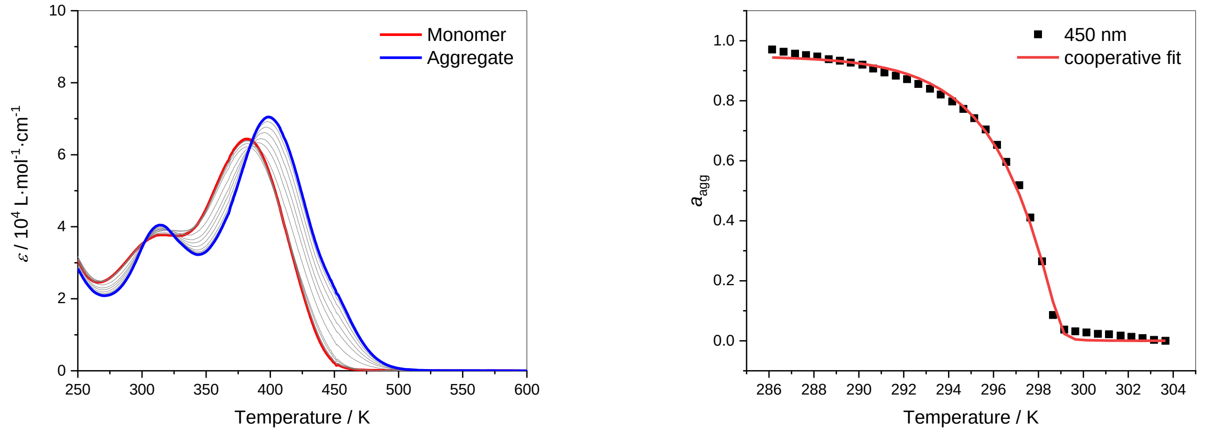

Figure S21c: Left: VT UV-Vis spectra of **(*Z*)-CN-OPE** in a 25.0:75.0 mixture of THF and H_2O at 10^{-5} M between 313 K and 298 K. Right: Corresponding degree of aggregation α_{agg} (monitored at $\lambda = 450$ nm) plotted against the temperature and fit to the cooperative nucleation-elongation model[7].

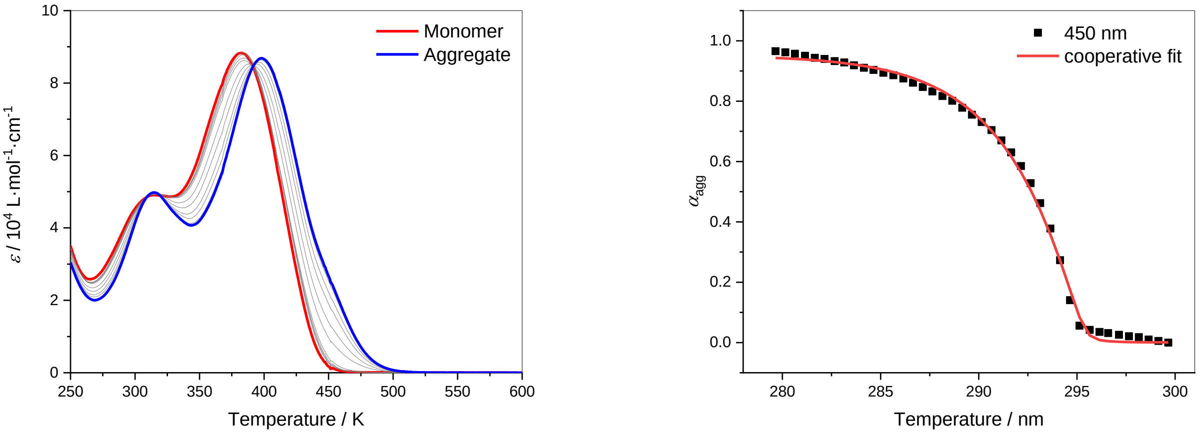

Figure S21d: Left: VT UV-Vis spectra of ***(Z)*-CN-OPE** in a 27.5:72.5 mixture of THF and H_2O at 10^{-5} M between 313 K and 298 K. Right: Corresponding degree of aggregation α_{agg} (monitored at $\lambda = 450$ nm) plotted against the temperature and fit to the cooperative nucleation-elongation model[7].

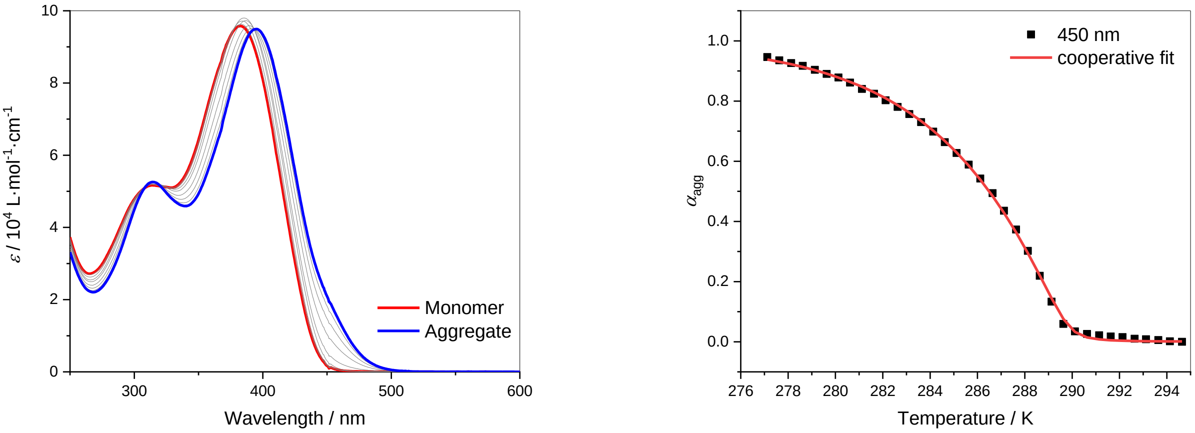

Figure S21e: Left: VT UV-Vis spectra of ***(Z)*-CN-OPE** in a 30.0:70.0 mixture of THF and H_2O at 10^{-5} M between 313 K and 298 K. Right: Corresponding degree of aggregation α_{agg} (monitored at $\lambda = 450$ nm) plotted against the temperature and fit to the cooperative nucleation-elongation model[7].

Table S2: Thermodynamic parameters associated with the self-assembly of **(*Z*)-CN-OPE** in aqueous solutions with varying solvent ratio of THF/H_2O at *c* = 10^{-5} M until stated otherwise.

f_w / %	ΔH^0 / kJ·mol^{-1}	ΔH^0nucl / kJ·mol^{-1}	ΔS^0 /kJ·mol^{-1}·K^{-1}	T_e / K	K_{nucl} / L·mol^{-1}	K_{el} / L·mol^{-1}	σ / 10^{-4}
100.0[a]	-442.104±20.75	-17.164±1.46	-1.1790±0.0603	345.7±0.1	424.95	166785,93	2.548
77.5	-365.34±14.61	-22.83±4.16	-1.1096±0.0484	303.2±0.1	11.65	100073.621	1.164
75.0	-297.53±14.55	-19.74±3.79	-0.8997±0.0489	298.9±0.1	35.56	100065.903	3.554
72.5	-209.04±9.22	-18.26±2.61	-0.6125±0.0315	295.2±0.1	58.76	100066.829	5.872
70.0	-151.96±4.25	-17.31±0.96	-0.4291±0.0148	289.5±0.1	75.45	100070.456	7.539

[a] at *c* = 6 x 10^{-6} M.

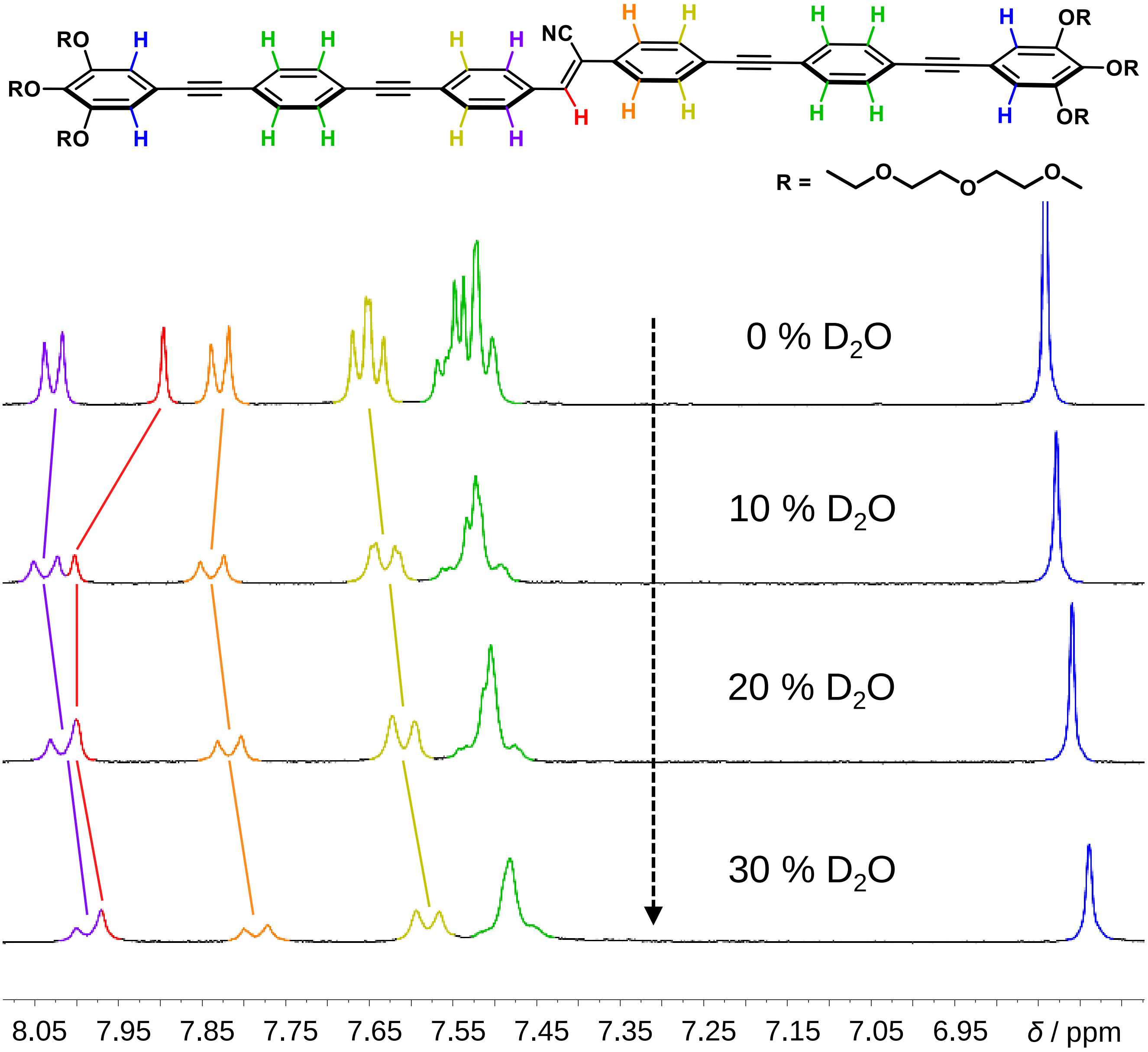

Figure S22: Partial ^{1}H NMR (THF-d$_8$/D$_2$O; 300 MHz; 298 K) of **(*Z*)-CN-OPE** under subsequent addition of D$_2$O at c = 3.96 x 10^{-3} M.

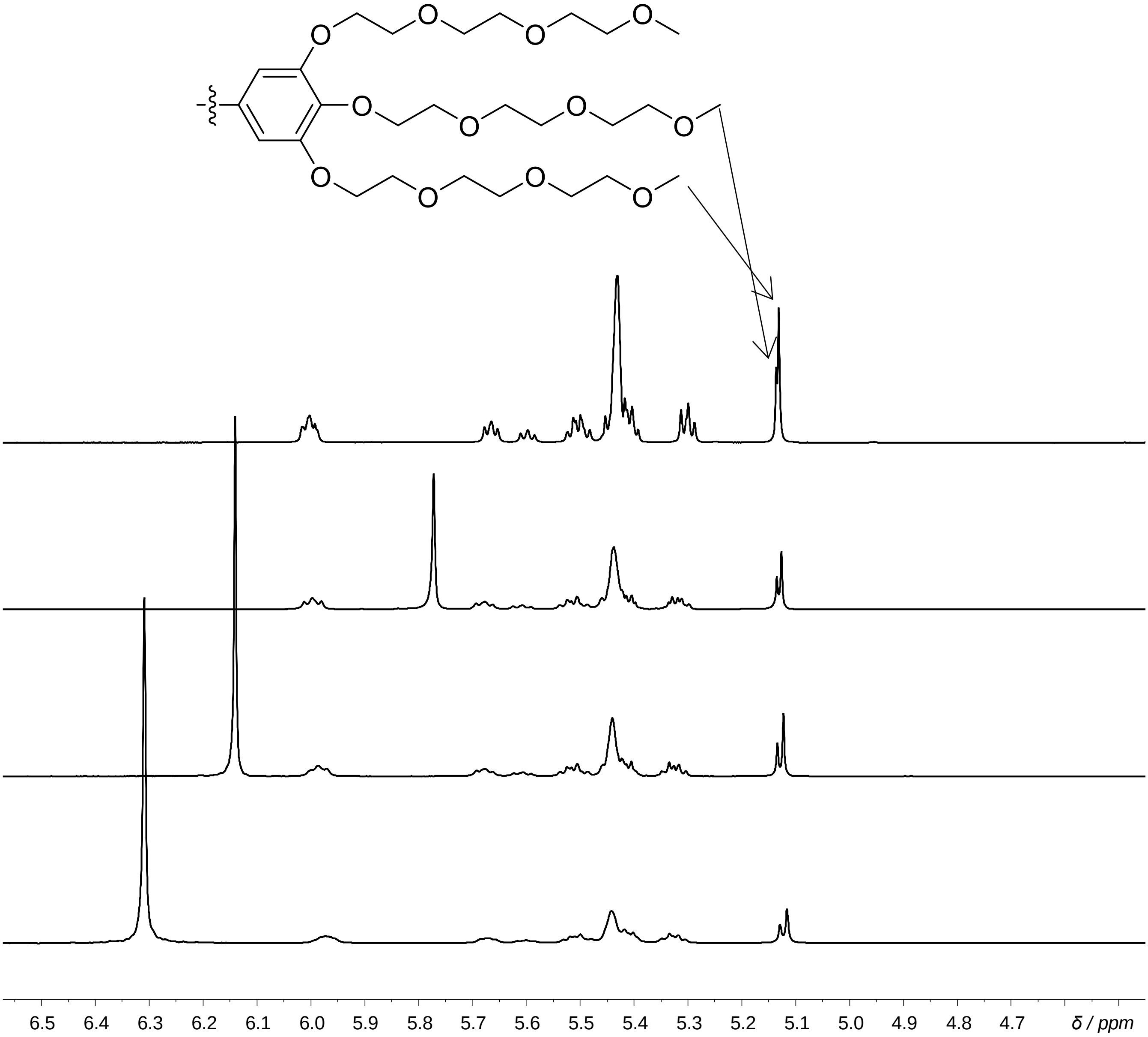

Figure S23: Details of the aliphatic region in the ^{1}H NMR spectrum of **(*Z*)-CN-OPE** in THF-d_8 upon addition of D_2O at *c* = 3.96 x 10^{-3} M.

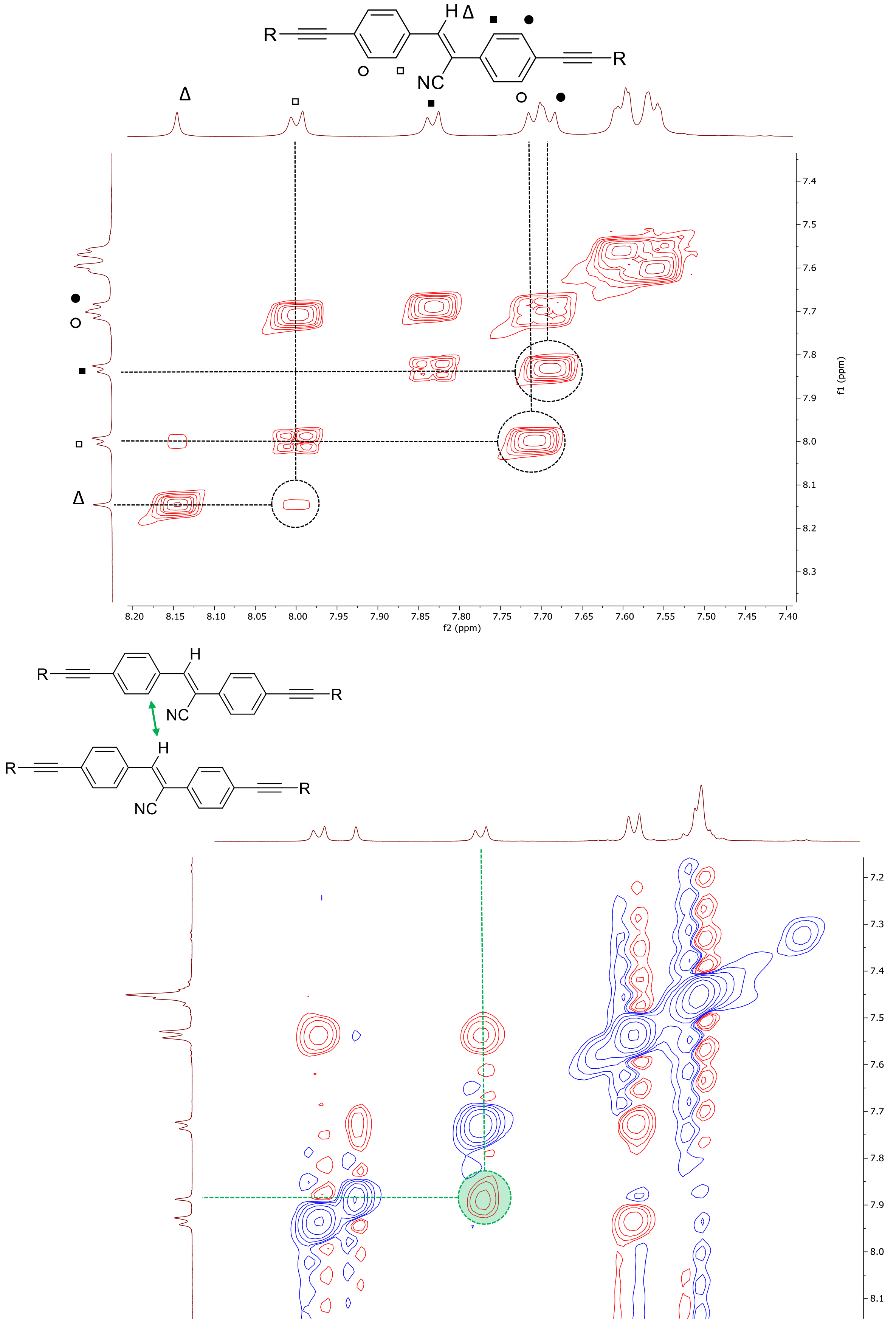

Figure S24: Top: *H,H*-COSY NMR of **(*Z*)-CN-OPE** (600 MHz, DMSO-d_6, 299 K) with highlighted intramolecular interactions. Bottom: ROESY NMR of **(*Z*)-CN-OPE** (600 MHz, 299 K) in 50 % THF-d_8/ 50 % D_2O at $4{\cdot}10^{-3}$ M with highlighted intermolecular interaction.

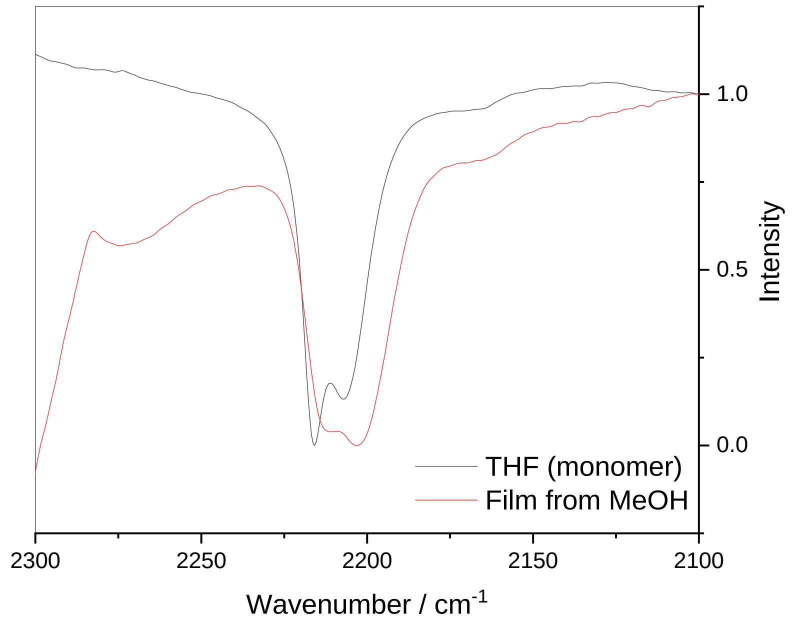

Figure S25: FTIR C≡N-stretching band of ***(Z)*-CN-OPE** in the monomeric state ($4\cdot10^{-3}$ M in THF, black line) and in an aggregated state (casted from a MeOH solution at $4\cdot10^{-3}$ M, red line).

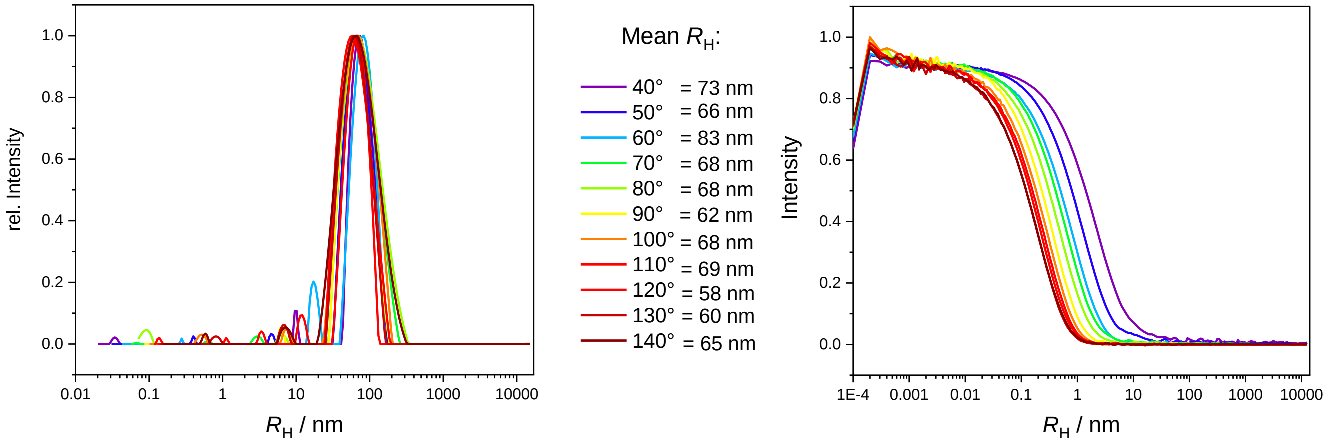

Figure S26: Left: Unweighted size distributions derived from angular dependent DLS measurements of ***(Z)*-CN-OPE** in H_2O ($c = 10^{-5}$ M) at T = 293 K. Middle: Average hydrodynamic radii. Right: Corresponding correlation functions.

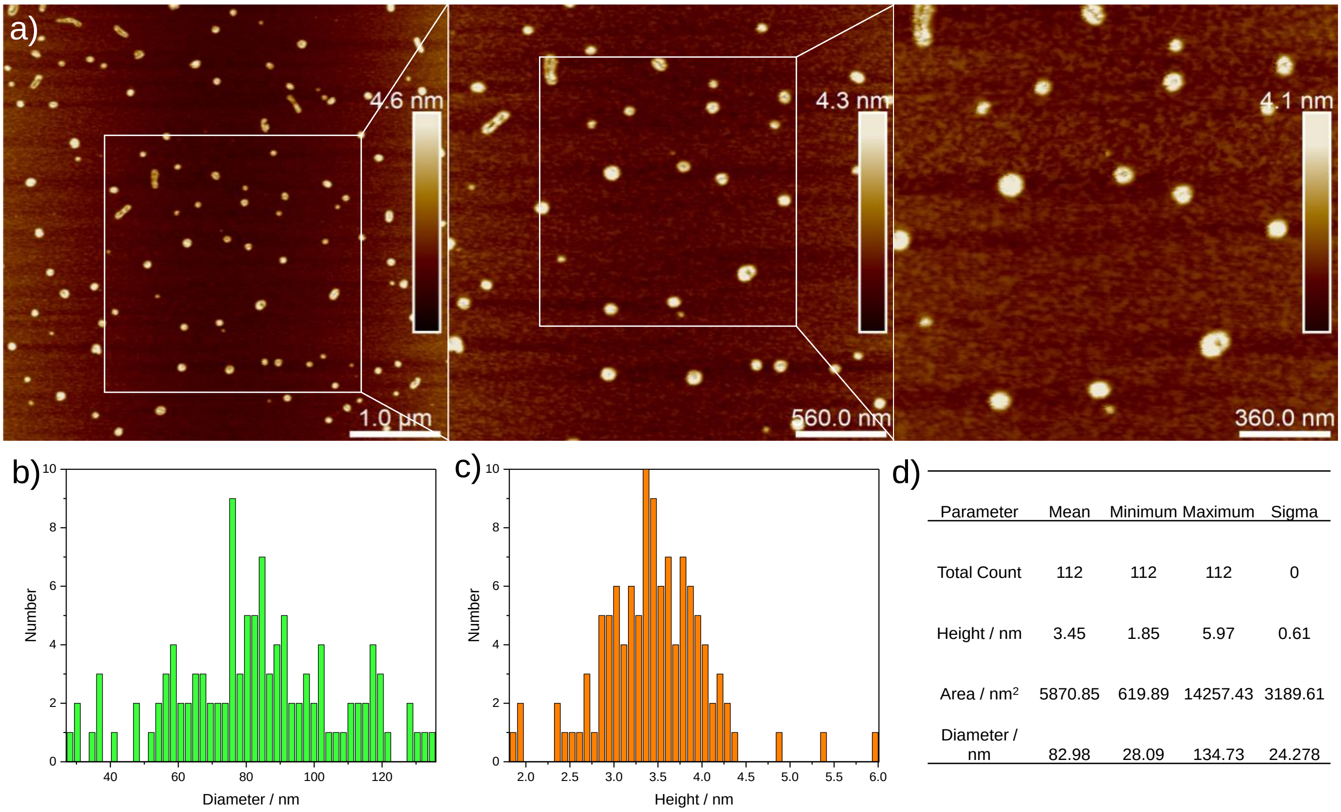

Parameter	Mean	Minimum	Maximum	Sigma
Total Count	112	112	112	0
Height / nm	3.45	1.85	5.97	0.61
Area / nm²	5870.85	619.89	14257.43	3189.61
Diameter / nm	82.98	28.09	134.73	24.278

Figure S27a: a) AFM images of **(*Z*)-CN-OPE** in aqueous solutions at *c* = 10^{-5} M 100 % H_2O on MICA in different magnifications. The sample was prepared by drop-casting a defined volume (10 µL) onto MICA, let it rest for 10 min and removal of the solvent by spinning (4000 rpm for 10 min). This procedure was repeated three times. b) Diameter distribution c) Height distribution and d) summary of the applied particle analysis.

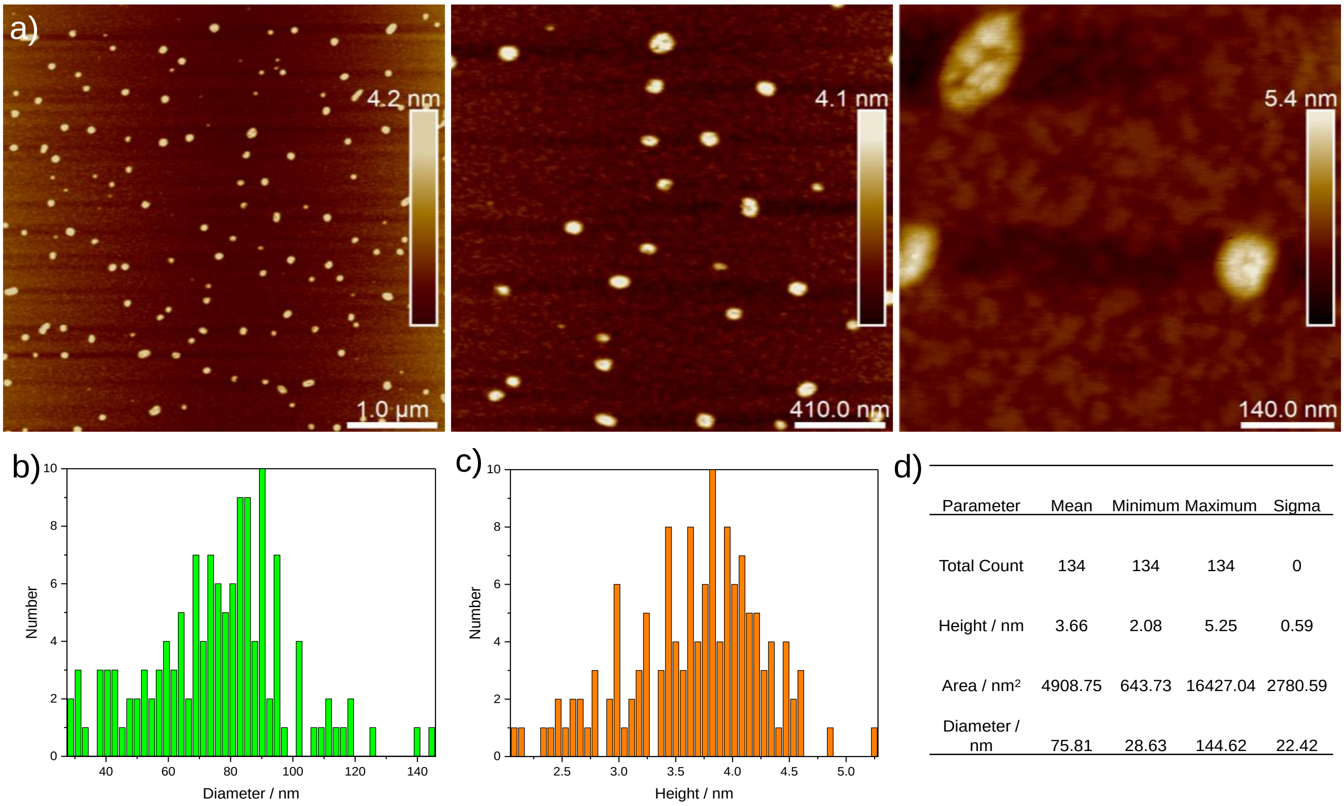

Parameter	Mean	Minimum	Maximum	Sigma
Total Count	134	134	134	0
Height / nm	3.66	2.08	5.25	0.59
Area / nm²	4908.75	643.73	16427.04	2780.59
Diameter / nm	75.81	28.63	144.62	22.42

Figure S27b: a) AFM images of **(*Z*)-CN-OPE** in aqueous solutions at *c* = 10^{-5} M 100 % H_2O on MICA in different magnifications. The sample was prepared by drop-casting a defined volume (10 µL) onto MICA, let it rest for 10 min and removal of the solvent by spinning (4000 rpm for 10 min). This procedure was repeated three times. b) Diameter distribution c) Height distribution and d) summary of the applied particle analysis.

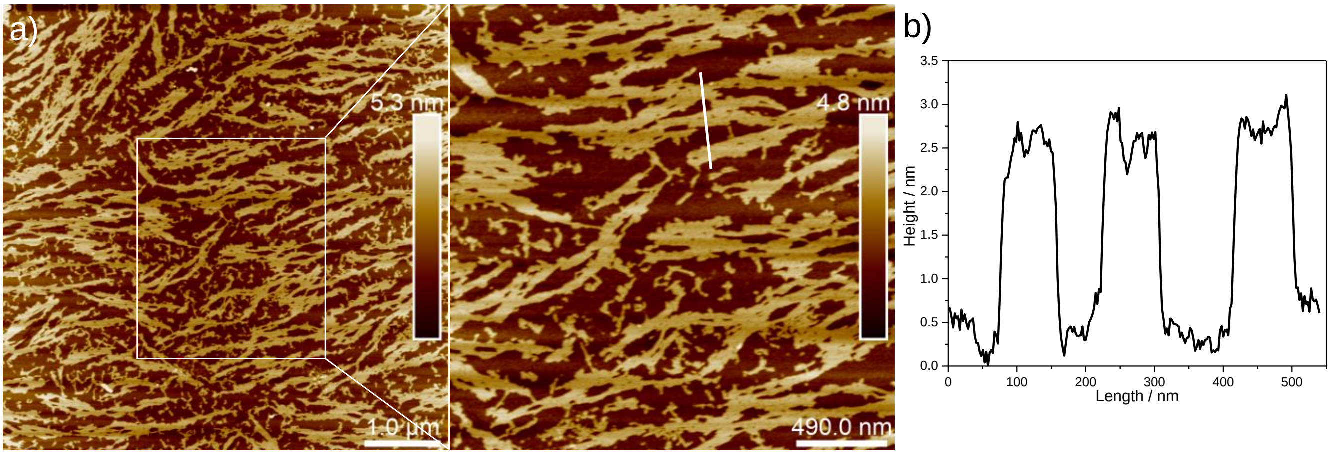

Figure S27c: a) AFM images of **(*Z*)-CN-OPE** in aqueous solutions at c = 10^{-5} M 100 % H_2O on MICA in different magnifications. The sample was prepared by drop-casting a defined volume (30 µL) onto MICA, let it rest for 2.5 h and removal of the solvent by spinning (4000 rpm for 45 min). b) Height profile of a selected cross section.

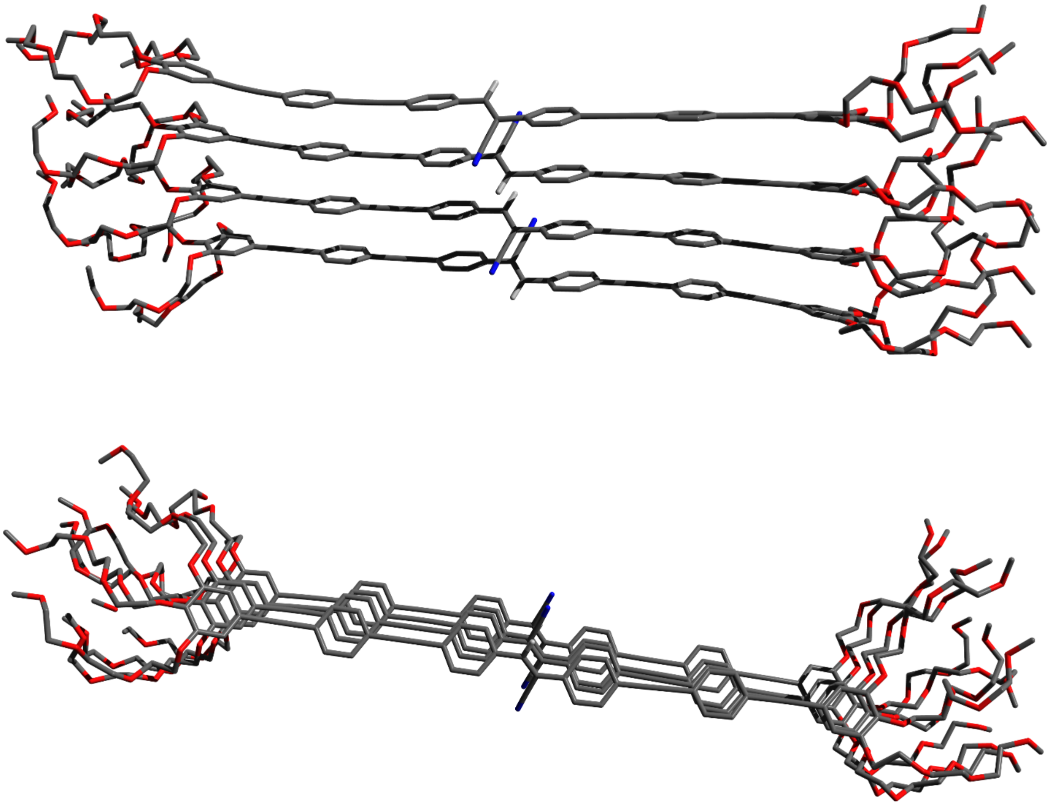

Figure S28: Proposed tetramer stacks of **(*Z*)-CN-OPE** derived from Quantum mechanical calculations at the semiempirical dispersion-corrected PM6 level.

3.2. Photoisomerization studies

Because photoreactions can be influenced by concentration, which will decrease the penetration depth of the irradiated light[9], diluted solutions at $c = 10^{-5}$ mol L^{-1} were used and the occurring photoinduced process was followed by UV-Vis spectroscopy. While the applied concentration range is far too low for quantification via ^1H NMR spectroscopy, another method to determine the present *E* to *Z* ratio was employed as follows:

1. A solution of **(*Z*)-CN-OPE** was irradiated with λ_{irr} = 465 nm and subsequently analyzed by UV-Vis. It was possible to extract an isosbestic point during the transition (e.g. 361 nm for DCM), indicative for the transition between two distinct species.
2. Calibration spectra containing different isomer ratios between 0 % and 100 % in ~10 % steps at a constant concentration of $c = 10^{-5}$ mol L^{-1} were recorded (Figures S24a-g, a).
3. Applying a linear regression of ε (at λ_{max} (*Z*)) in dependence of the ratio of **(*Z*)-CN-OPE** resulted in a calibration function, which is used to determine the further ratio values (Figures S24a-g, b).
4. To investigate the photoequilibrium state at λ_{irr} = 465 nm, pure solutions of **(*Z*)-CN-OPE** and **(*E*)-CN-OPE** were exposed to light of this wavelength, respectively. Full UV-Vis spectra were recorded after and before defined exposure times (1 s, 2 s, 3 s, 4 s, 5 s, 10 s, 20 s, 30 s, 60 s, 120 s, 180 s, 300 s and 600 s). By using the calculated calibration function the evolution of the *E*/*Z*-ratio over time could be followed (See figures S24a-g, c).
5. To investigate the full window of the photoswitchable states, additionally a pure solution of **(*E*)-CN-OPE** was irradiated with λ_{irr} = 365 nm and the evolution over time was followed as explained before (See figures S24a-g, d).

All samples presented in the following figures (S24a-g) were irradiated using a LED-light source in a quartz cuvette (1 x 1 x 3 cm, QS) with a distance of 7 cm between the sample and the light source.

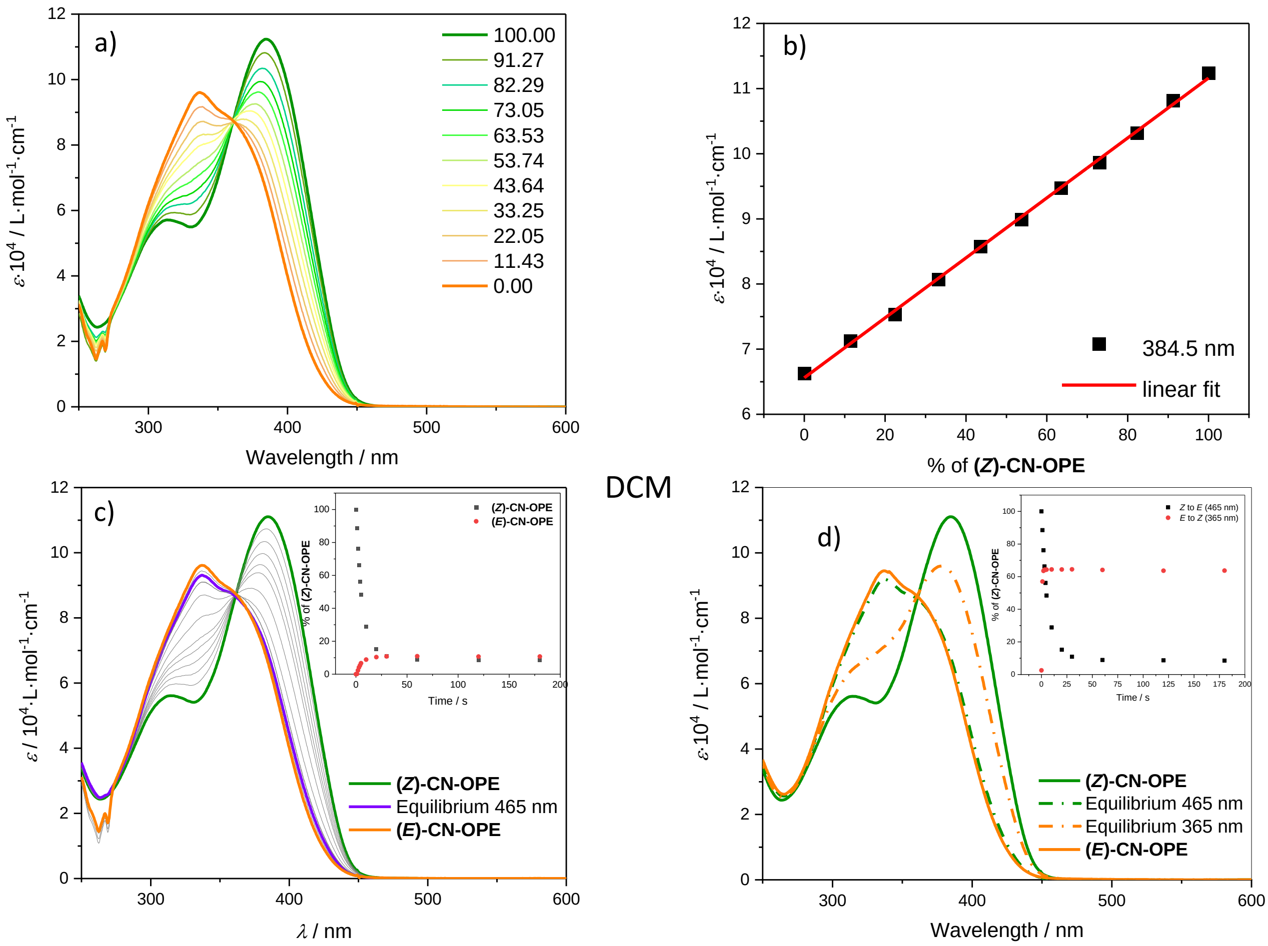

Figure S29a: a) UV-Vis spectra of mixtures of *E*/*Z* isomers in DCM in ~10 % ratio steps at $c = 10^{-5}$ M. b) Equilibration function of the evolution of absorbance at $\lambda = 384.5$ nm. c) UV-Vis spectra of **(*Z*)-CN-OPE** (green) and **(*E*)-CN-OPE** (orange) at $c = 10^{-5}$ M in DCM upon irradiation with $\lambda_{irr} = 465$ nm until the photoequilibrium (purple) is reached. Inset: Determination of the *E* to *Z* ratio as a function of irradiation time. d) UV-Vis spectra of **(*Z*)-CN-OPE** (green) and **(*E*)-CN-OPE** (orange) at $c = 10^{-5}$ M in DCM upon irradiation with $\lambda_{irr} = 465$ nm (*Z*→*E*) and $\lambda_{irr} = 365$ nm (*E*→*Z*). Inset: Determination of the *E* to *Z* ratio as a function of irradiation time.

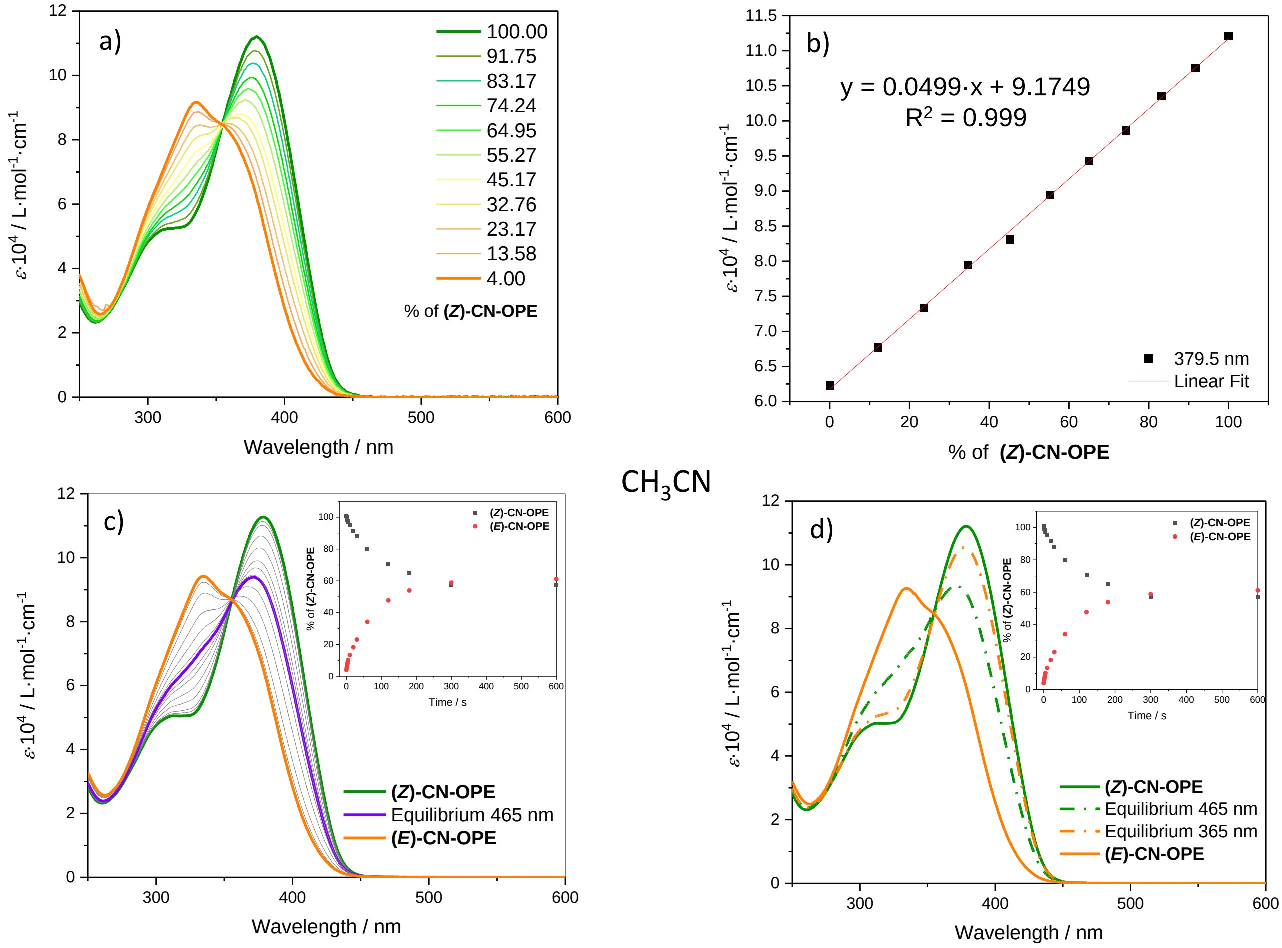

Figure S29b: a) UV-vis spectra of *E*/*Z*-mixtures in CH_3CN in ~10 % ratio steps at $c = 10^{-5}$ M. b) Equilibration function of the evolution of absorbance at $\lambda = 378.0$ nm. c) UV-Vis spectra of **(*Z*)-CN-OPE** (green) and **(*E*)-CN-OPE** (orange) at $c = 10^{-5}$ M in CH_3CN upon irradiation with $\lambda_{irr} = 465$ nm until the photoequilibrium (purple) is reached. Inset: Determination of the *E* to *Z* ratio as a function of irradiation time. d) UV-Vis spectra of **(*Z*)-CN-OPE** (green) and **(*E*)-CN-OPE** (orange) at $c = 10^{-5}$ M in CH_3CN upon irradiation with $\lambda_{irr} = 465$ nm (*Z*→*E*) and $\lambda_{irr} = 365$ nm (*E*→*Z*). Inset: Determination of the *E* to *Z* ratio as a function of irradiation time.

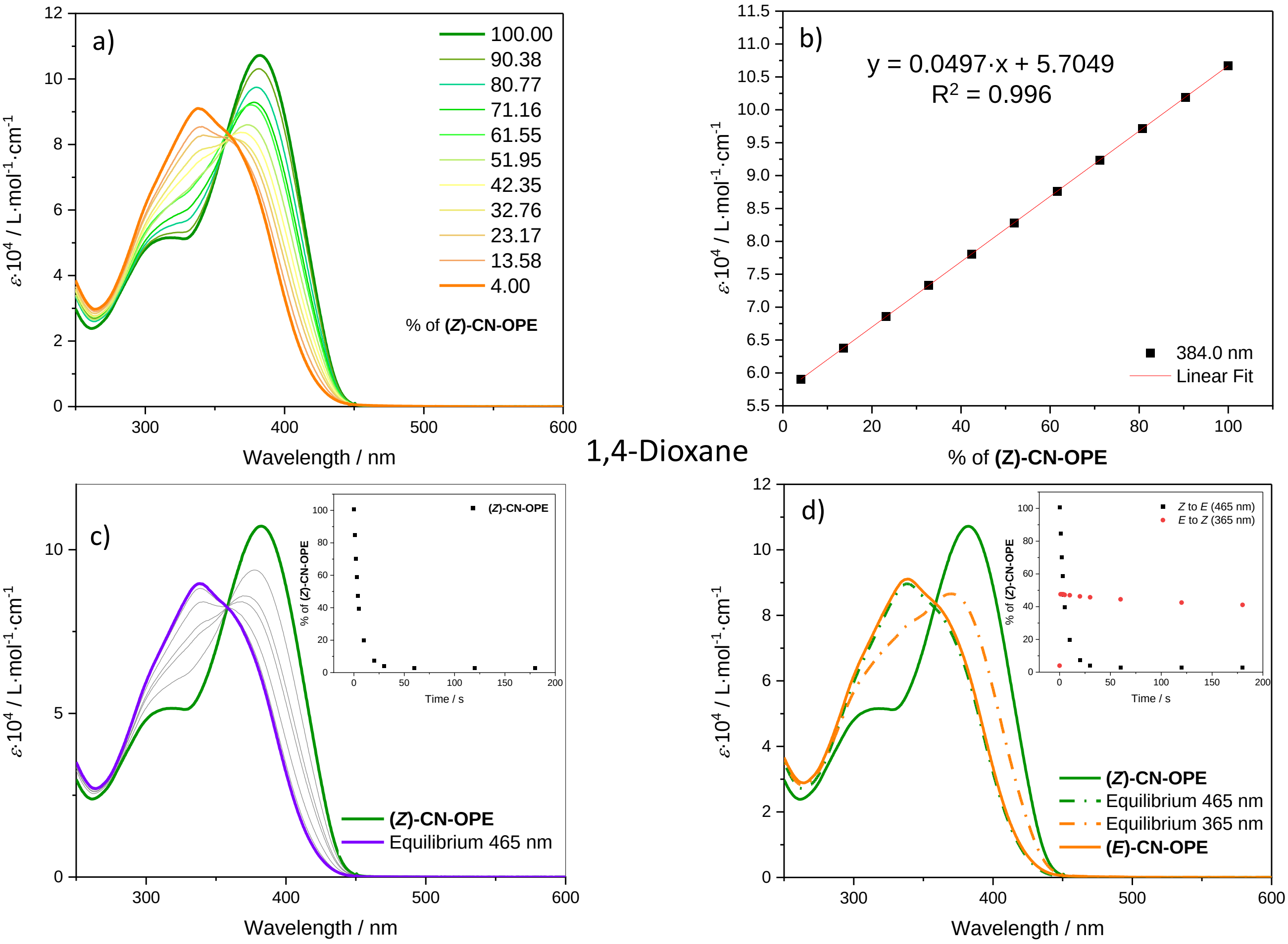

Figure S29c: a) UV-Vis spectra of *E*/*Z*-mixtures in 1,4-Dioxane in ~10 % ratio steps at $c = 10^{-5}$ M. b) Equilibration function of the evolution of absorbance at $\lambda = 384.0$ nm. c) UV-Vis spectra of **(*Z*)-CN-OPE** (green) and **(*E*)-CN-OPE** (orange) at $c = 10^{-5}$ M in 1,4-Dioxane upon irradiation with $\lambda_{irr} = 465$ nm until the photoequilibrium (purple) is reached. Inset: Determination of the *E* to *Z* ratio as a function of irradiation time. d) UV-Vis spectra of **(*Z*)-CN-OPE** (green) and **(*E*)-CN-OPE** (orange) at $c = 10^{-5}$ M in 1,4-Dioxane upon irradiation with $\lambda_{irr} = 465$ nm (*Z*→*E*) and $\lambda_{irr} = 365$ nm (*E*→*Z*). Inset: Determination of the *E* to *Z* ratio as a function of irradiation time.

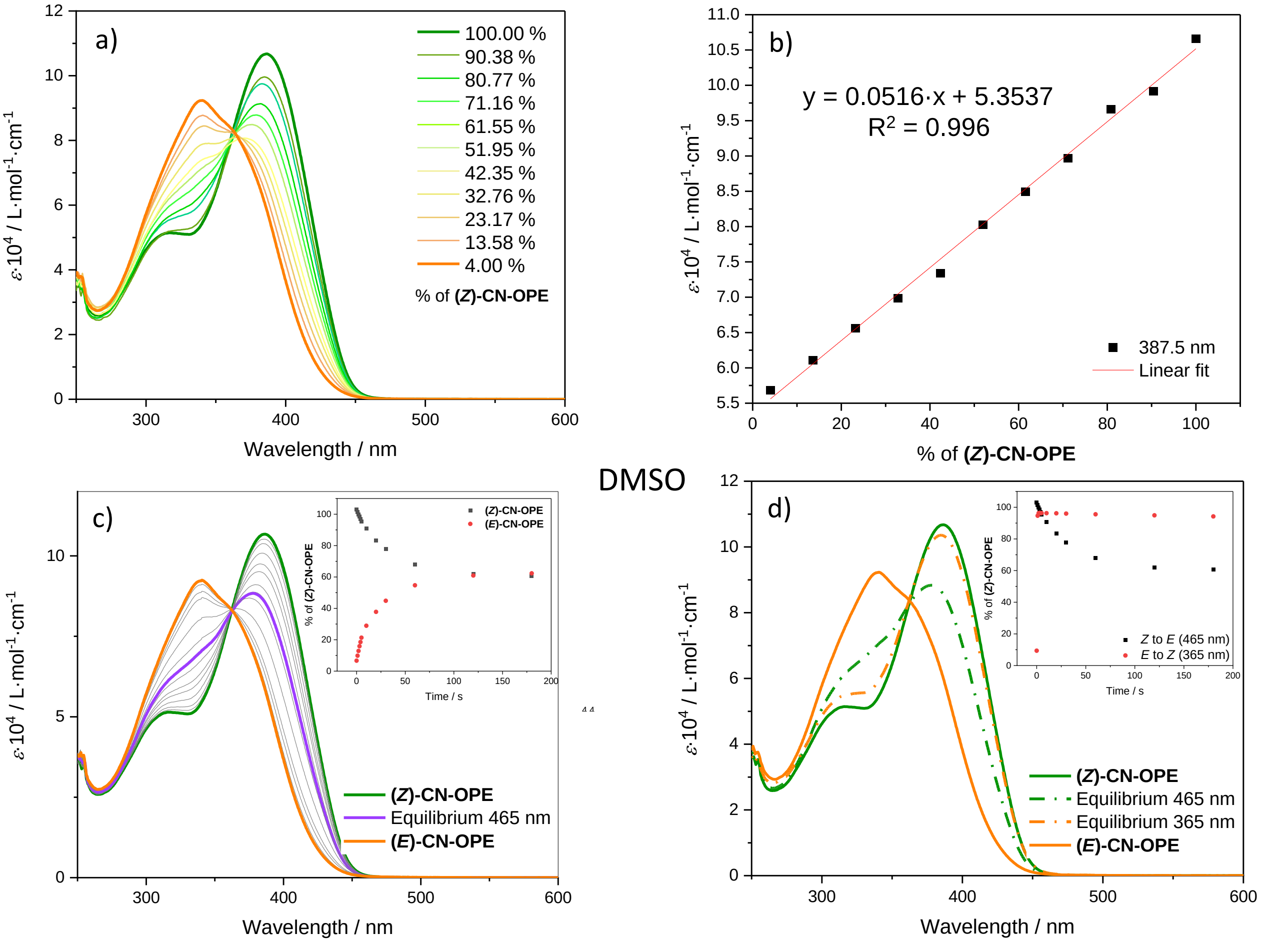

Figure S29d: a) UV-Vis spectra of E/Z-mixtures in DMSO in ~10 % ratio steps at $c = 10^{-5}$ M. b) Equilibration function of the evolution of absorbance at λ = 379 nm. c) UV-Vis spectra of **(*Z*)-CN-OPE** (green) and **(*E*)-CN-OPE** (orange) at $c = 10^{-5}$ M in DMSO upon irradiation with λ_{irr} = 465 nm until the photoequilibrium (purple) is reached. Inset: Determination of the E to Z ratio as a function of irradiation time. d) UV-Vis spectra of **(*Z*)-CN-OPE** (green) and **(*E*)-CN-OPE** (orange) at $c = 10^{-5}$ M in DMSO upon irradiation with λ_{irr} = 465 nm ($Z \rightarrow E$) and λ_{irr} = 365 nm ($E \rightarrow Z$). Inset: Determination of the E to Z ratio as a function of irradiation time.

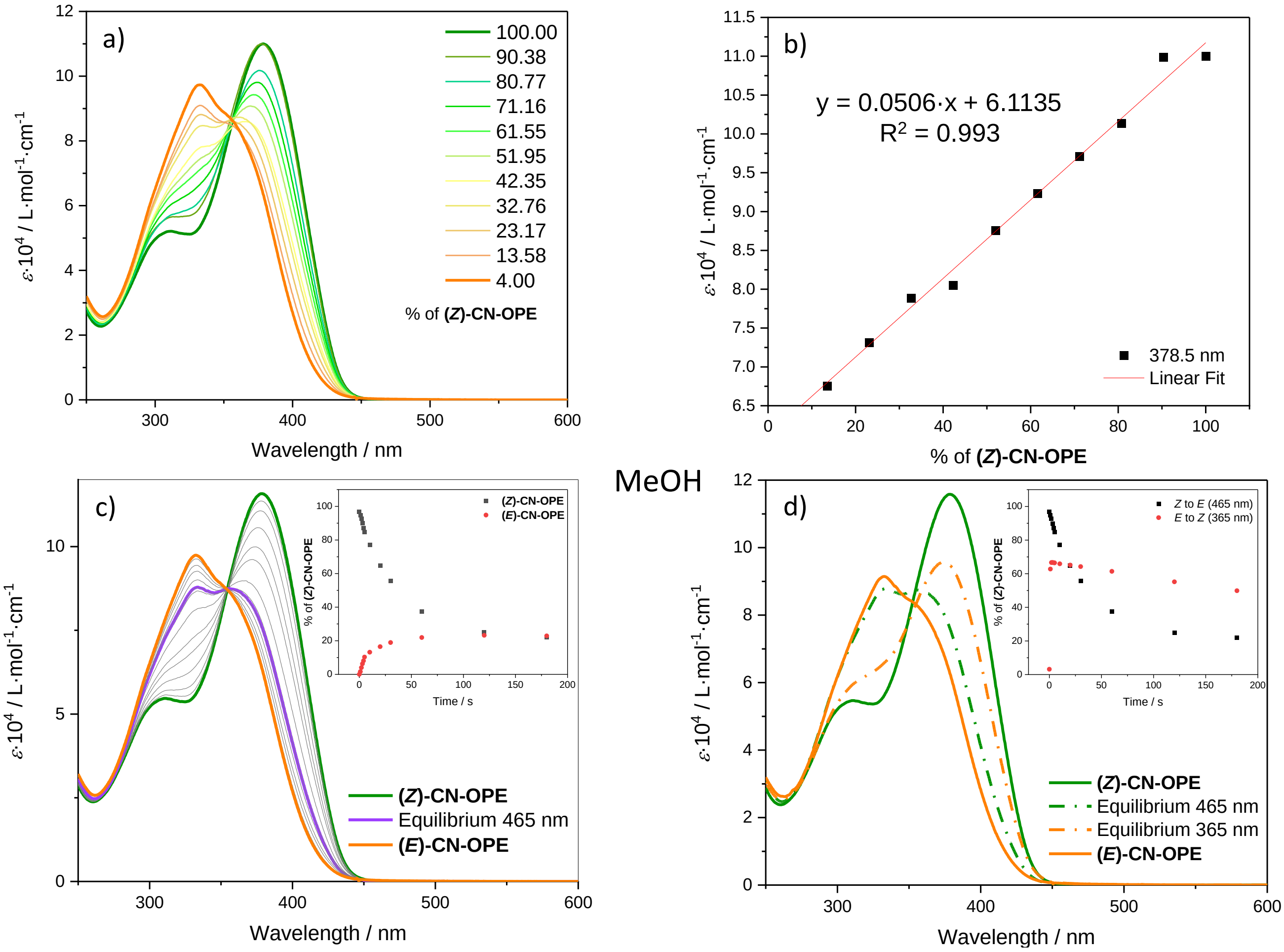

Figure S29e: a) UV-Vis spectra of *E*/*Z*-mixtures in MeOH in ~10 % ratio steps at *c* = 10^{-5} M. b) Equilibration function of the evolution of absorbance at λ = 378.5 nm. c) UV-Vis spectra of **(*Z*)-CN-OPE** (green) and **(*E*)-CN-OPE** (orange) at *c* = 10^{-5} M in MeOH upon irradiation with λ_{irr} = 465 nm until the photoequilibrium (purple) is reached. Inset: Determination of the *E* to *Z* ratio as a function of irradiation time. d) UV-Vis spectra of **(*Z*)-CN-OPE** (green) and **(*E*)-CN-OPE** (orange) at *c* = 10^{-5} M in MeOH upon irradiation with λ_{irr} = 465 nm (*Z*→*E*) and λ_{irr} = 365 nm (*E*→*Z*). Inset: Determination of the *E* to *Z* ratio as a function of irradiation time.

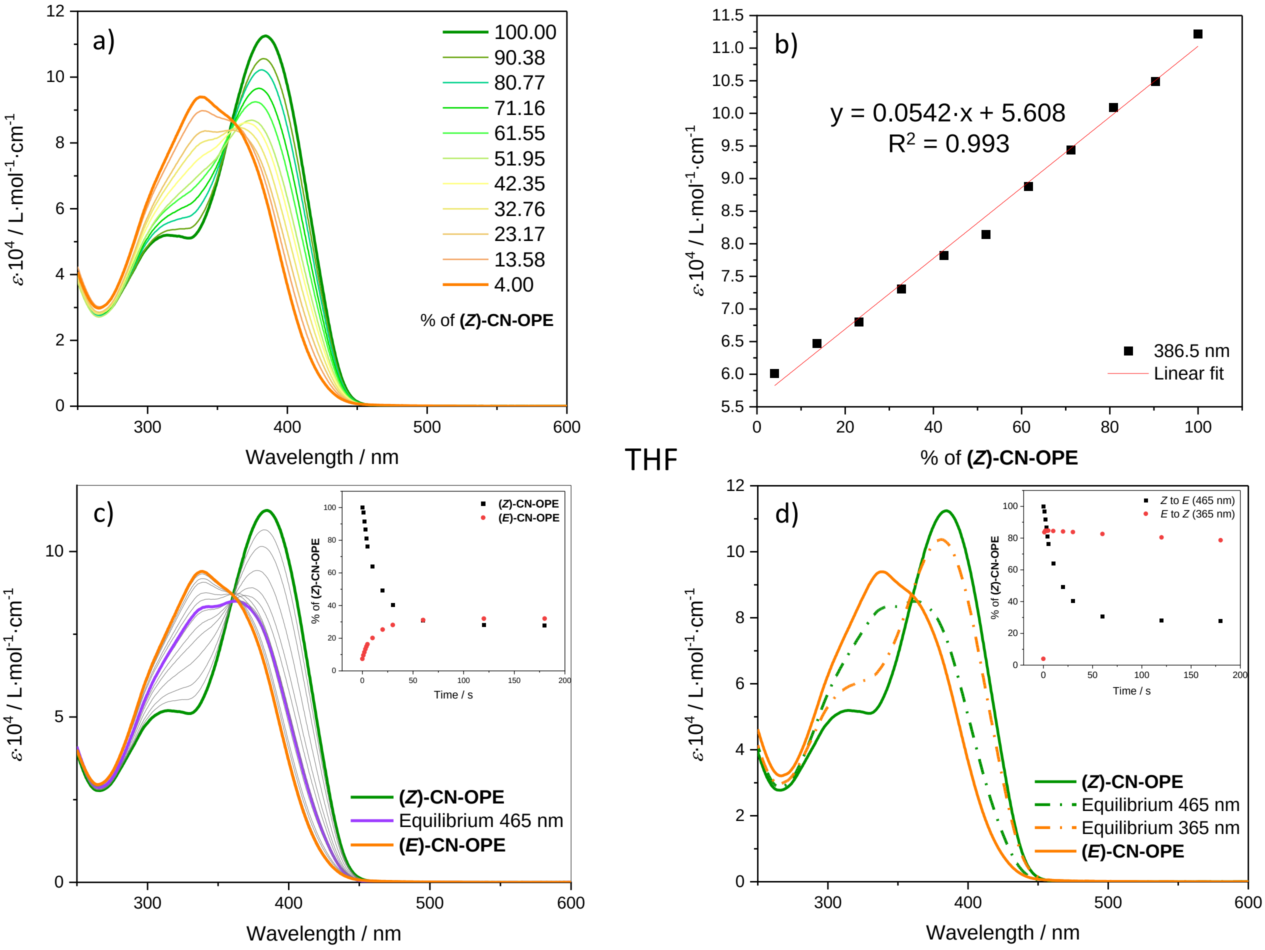

Figure S29f: a) UV-Vis spectra of *E*/*Z*-mixtures in THF in ~10 % ratio steps at *c* = 10^{-5} M. b) Equilibration function of the evolution of absorbance at λ = 378.5 nm. c) UV-Vis spectra of **(*Z*)-CN-OPE** (green) and **(*E*)-CN-OPE** (orange) at *c* = 10^{-5} M in THF upon irradiation with λ_{irr} = 465 nm until the photoequilibrium (purple) is reached. Inset: Determination of the *E* to *Z* ratio as a function of irradiation time. d) UV-vis-spectra of **(*Z*)-CN-OPE** (green) **and (*E*)-CN-OPE** (orange) at *c* = 10^{-5} M in THF upon irradiation with λ_{irr} = 465 nm (*Z*→*E*) and λ_{irr} = 365 nm (*E*→*Z*). Inset: Determination of the *E* to *Z* ratio as a function of irradiation time.

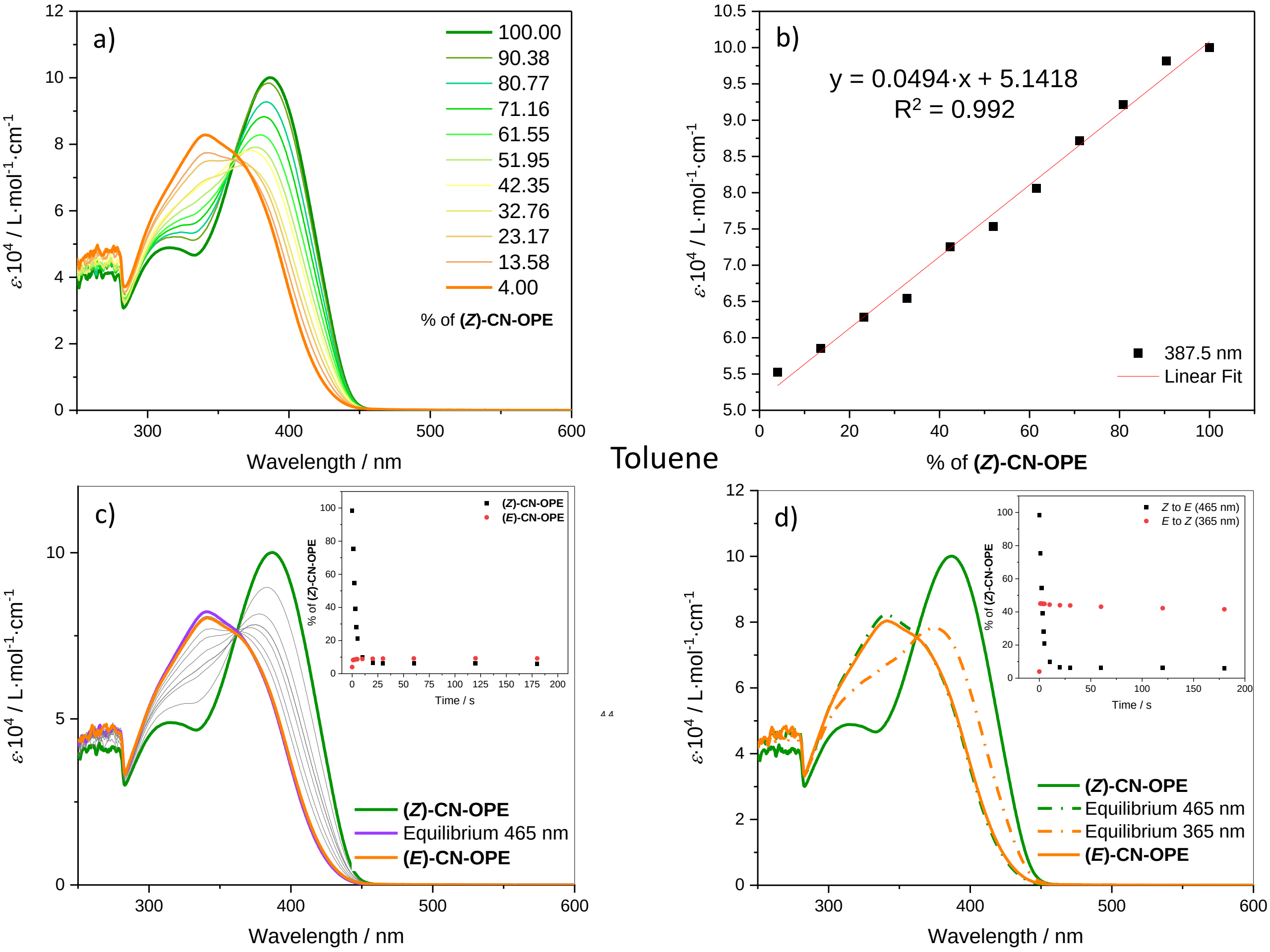

Figure S29g: a) UV-Vis spectra of *E*/*Z*-mixtures in Toluene in ~10 % ratio steps at *c* = 10^{-5} M. b) Equilibration function of the evolution of absorbance at λ = 387.5 nm. c) UV-Vis spectra of **(*Z*)-CN-OPE** (green) and **(*E*)-CN-OPE** (orange) at *c* = 10^{-5} M in Toluene upon irradiation with λ_{irr} = 465 nm until the photoequilibrium (purple) is reached. Inset: Determination of the *E* to *Z* ratio as a function of irradiation time. d) UV-Vis spectra of **(*Z*)-CN-OPE** (green) and **(*E*)-CN-OPE** (orange) at *c* = 10^{-5} M in Toluene upon irradiation with λ_{irr} = 465 nm (*Z*→*E*) and λ_{irr} = 365 nm (*E*→*Z*). Inset: Determination of the *E* to *Z* ratio as a function of irradiation time.

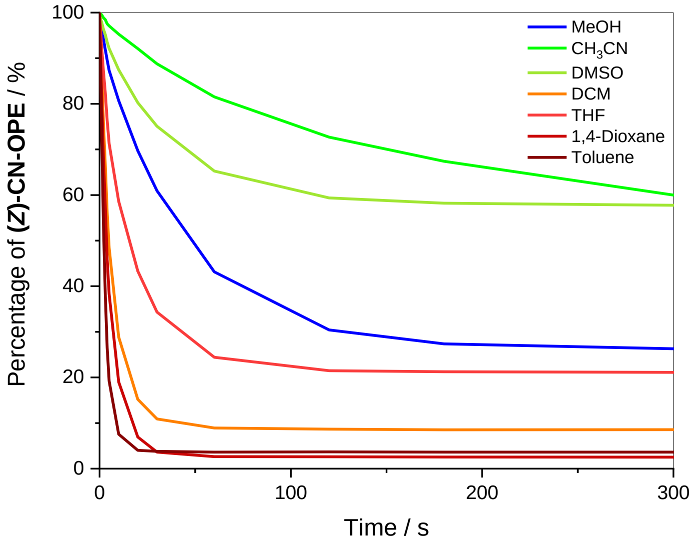

Figure S30: Evolution of *Z* to *E* ratio under the influence of light with λ_{irr} = 465 nm over time in different solvents (*c* = 10^{-5} M) at T = 298 K.

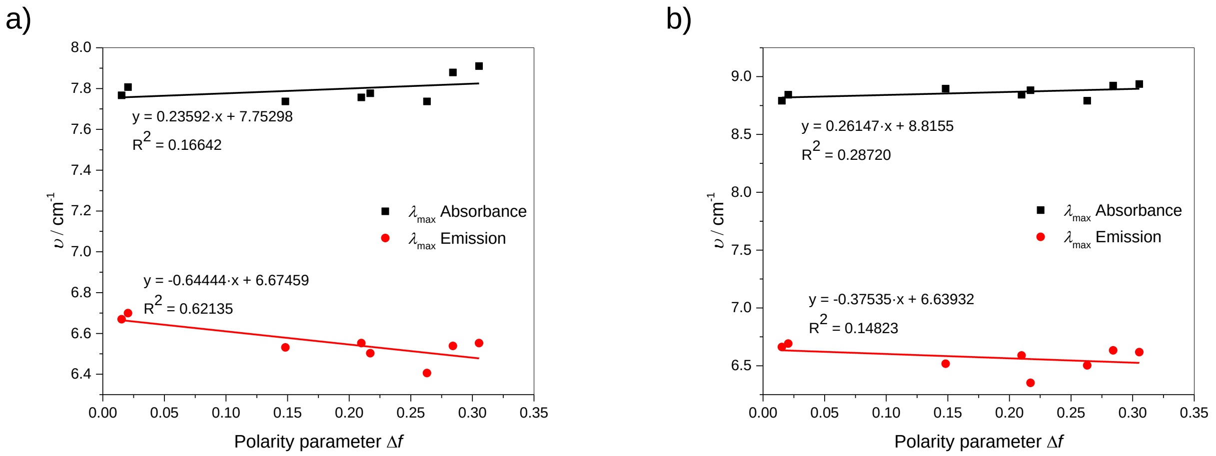

Figure S31: Lippert-Mataga plots[10,11] of a) **(*Z*)-CN-OPE** and b) **(*E*)-CN-OPE**. The Lippert-Mataga plot is used to display the dependency of different excited states by plotting the respective Wavenumber of λ_{max} and λ_{Em} against the polarity parameter, which was obtained using the equation[10] $\Delta \boldsymbol{f} = \boldsymbol{f}(\boldsymbol{e\varepsilon}) - \boldsymbol{f}(\boldsymbol{n}^2) = \frac{\boldsymbol{\varepsilon}-1}{2\boldsymbol{\varepsilon}-1} - \frac{\boldsymbol{n}^2}{2\boldsymbol{n}^2-1}$.

3.3. Cycloaddition studies

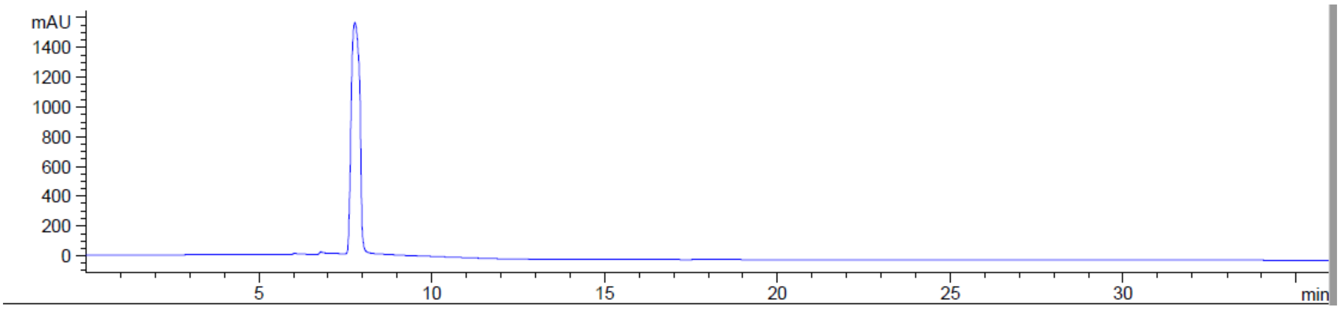

Figure S32: HPLC of the photoproduct using a Daicel Chiralpak AS-H (0.46 cm * 25 cm) column with n-hexane/i-propanol (98/2, 0.5 mL/min) as the eluent.

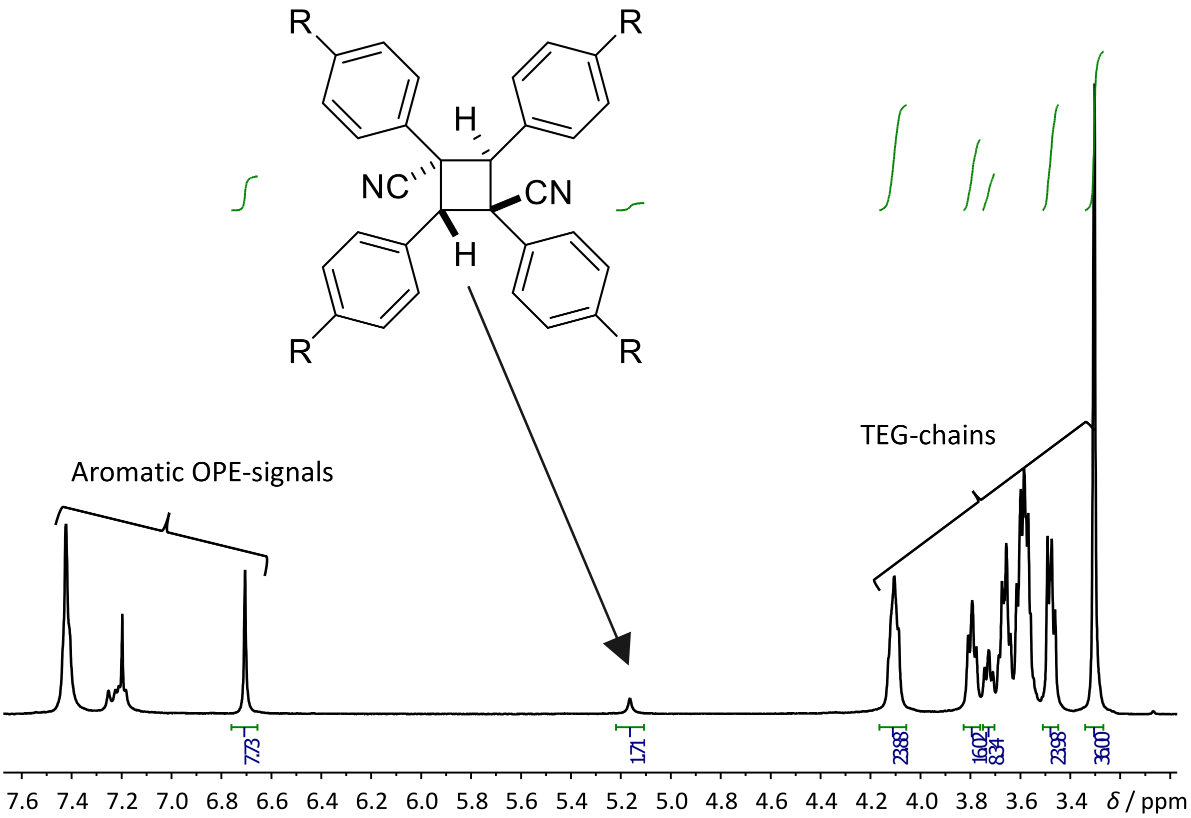

Figure S33: ^{1}H NMR (300 MHz, $CDCl_3$, 298 K) of the obtained photoirradiation product.

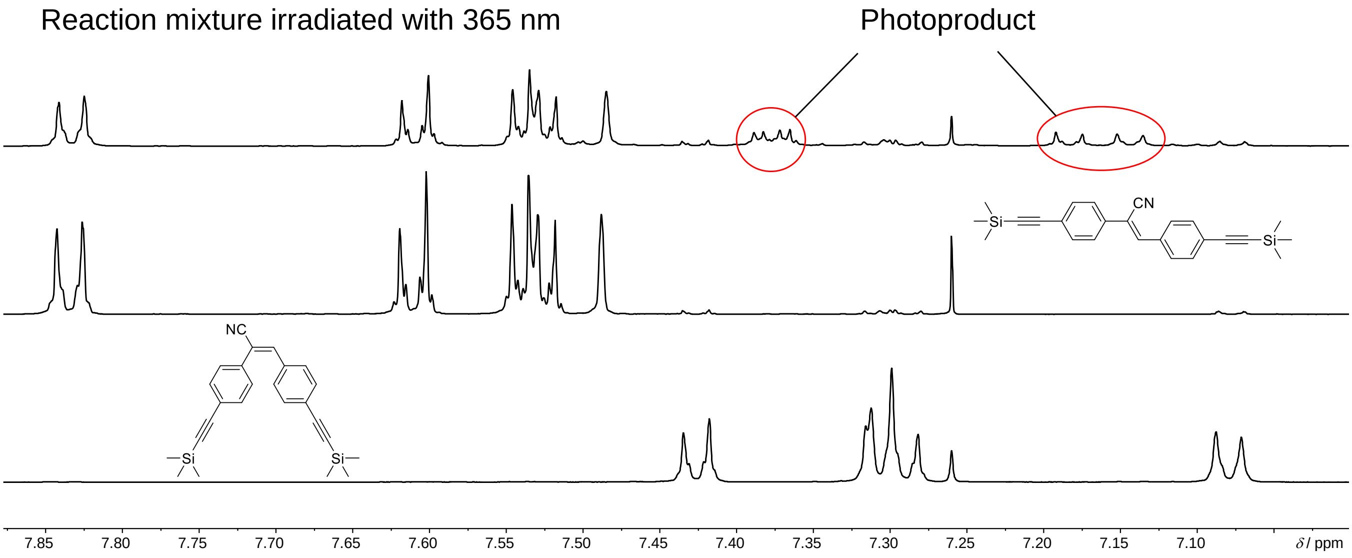

Figure S34a: Top: Aromatic region of the ^{1}H NMR ($CDCl_3$, 500 MH, 299 K) of the irradiation reaction with λ_{exc} = 365 nm using **8** as test system. Middle: Aromatic region of the ^{1}H NMR ($CDCl_3$, 500 MH, 299 K) of **8**. Bottom: Aromatic region of the ^{1}H NMR ($CDCl_3$, 500 MH, 299 K) of (*E*)-2,3-bis(4-((trimethylsilyl)ethynyl)phenyl)acrylonitrile.

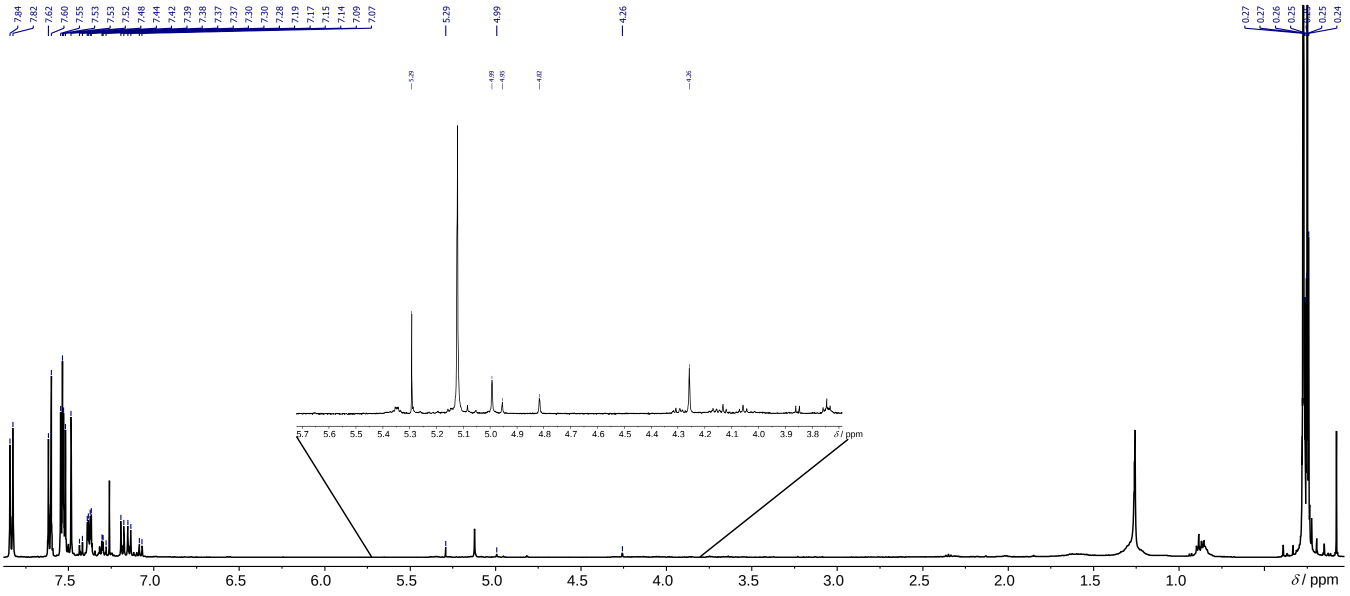

Figure S34b: ^{1}H NMR ($CDCl_3$, 500 MH, 299 K) of the irradiation reaction with λ_{exc} = 365 nm using **8** as test system.

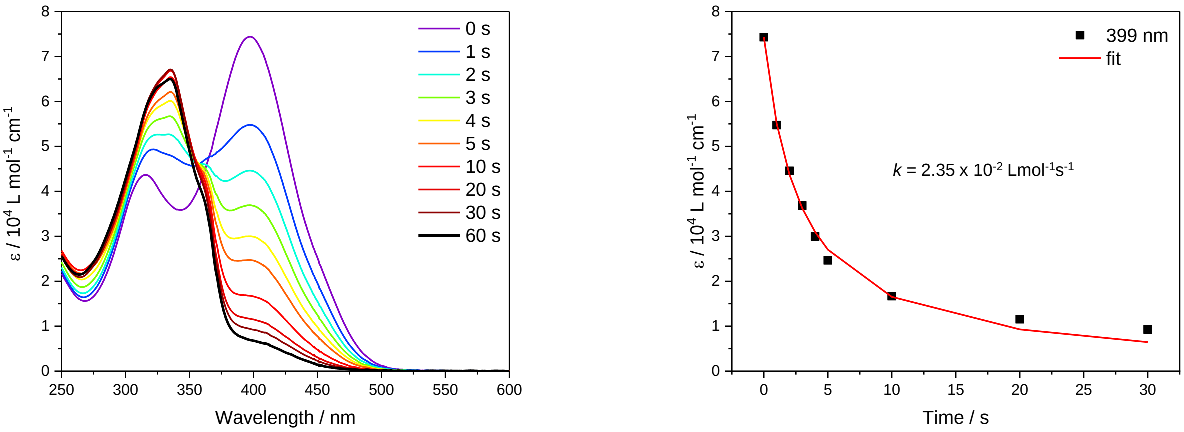

Figure S35a: Left: UV-Vis spectra of **(*Z*)-CN-OPE** in water at *c* = 10^{-5} M monitored at different intervals of exposure to light with λ_{exc} = 365 nm. Right: Plot of the absorbance at λ_{max} = 399 nm as a function of time and fit to second order kinetics.

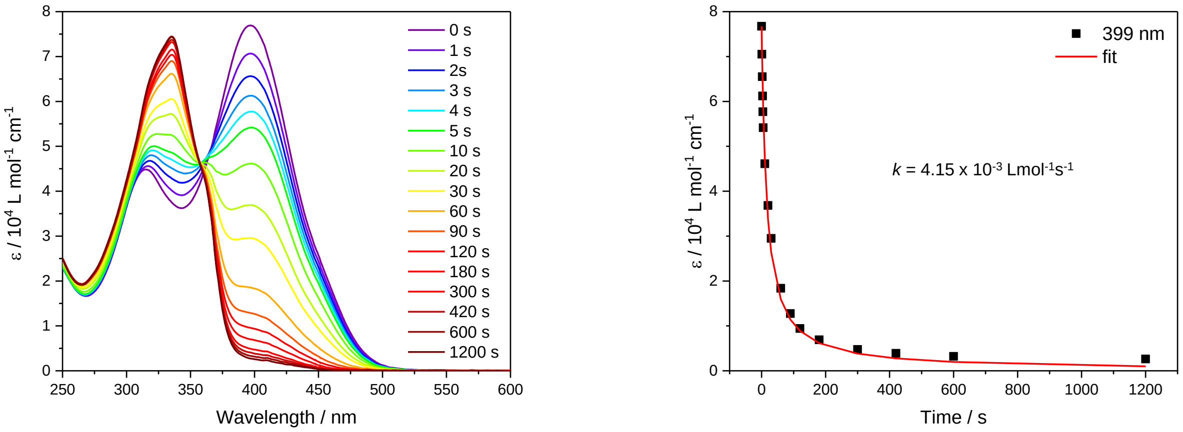

Figure S35b: Left: UV-Vis spectra of **(*Z*)-CN-OPE** in water at *c* = 10^{-5} M monitored at different intervals of exposure to light with λ_{exc} = 465 nm. Right: Plot of the absorbance at λ_{max} = 399 nm as a function of time and fit to second order kinetics.

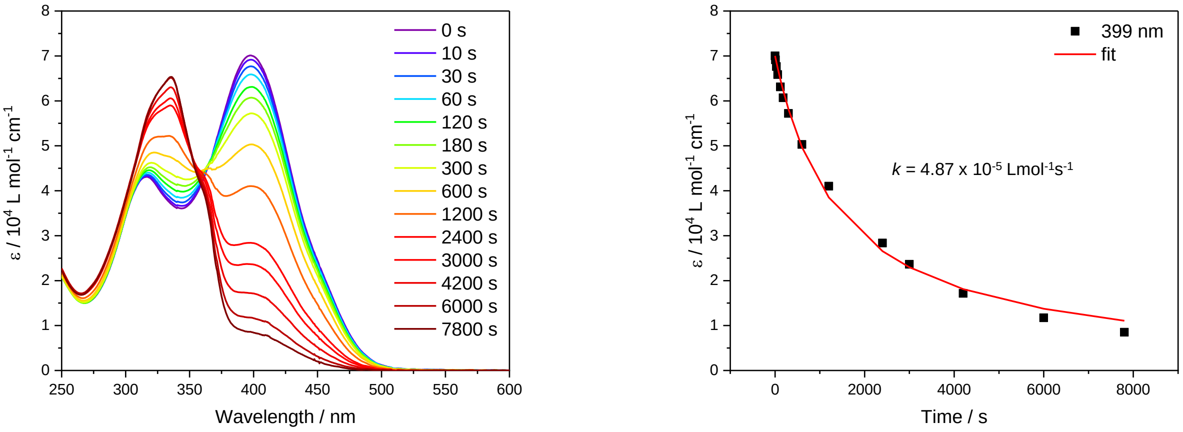

Figure S35c: Left: UV-Vis spectra of **(*Z*)-CN-OPE** in water at *c* = 10^{-5} M monitored at different intervals of exposure to light with λ_{exc} = 520 nm. Right: Plot of the absorbance at λ_{max} = 399 nm as a function of time and fit to second order kinetics.

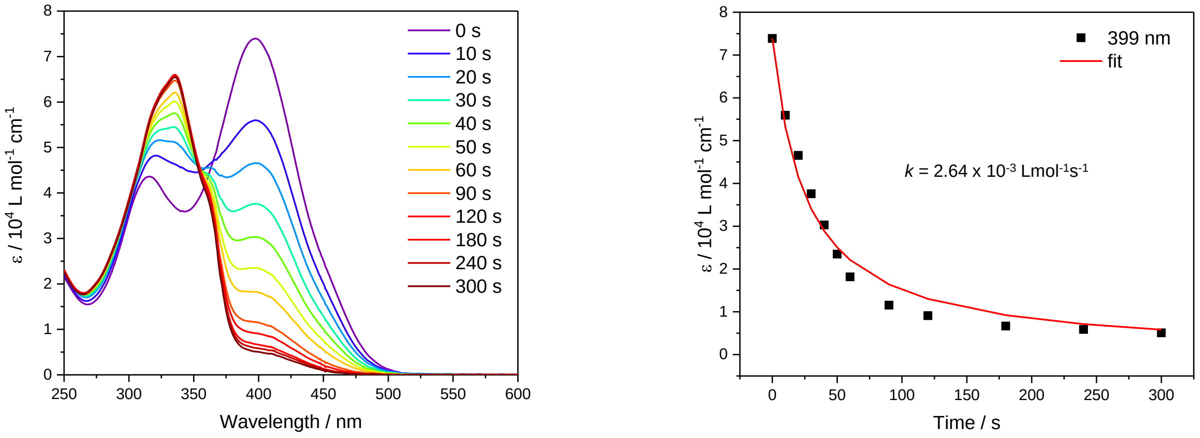

Figure S35d: Left: UV-Vis spectra of **(*Z*)-CN-OPE** in water at *c* = 10^{-5} M monitored at different intervals of exposure to sunlight. Right: Plot of the absorbance at λ_{max} = 399 nm as a function of time and fit to second order kinetics.

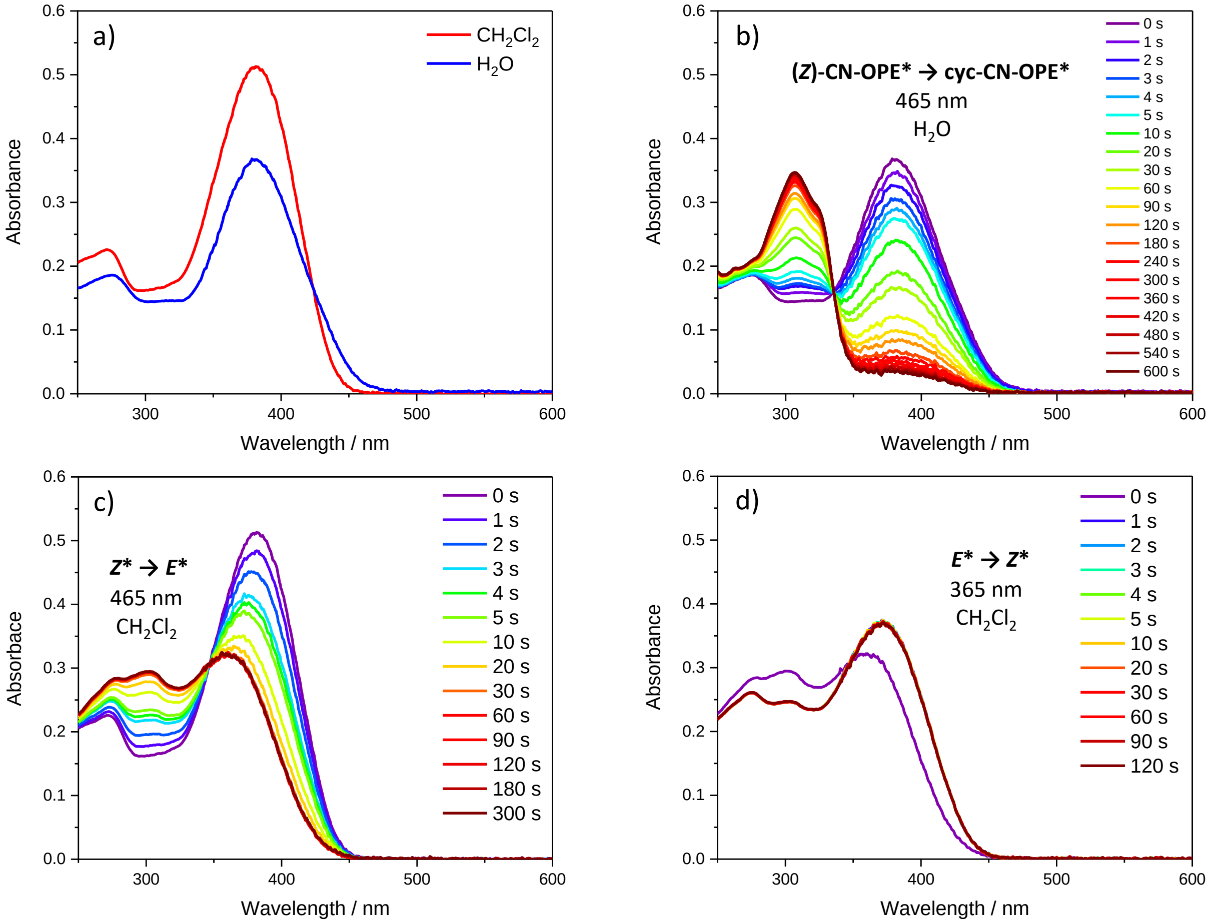

Figure S36: Spectroscopic key features of the reference compound **(*Z*)-CN-OPE*** in 10^{-5} M solutions at 298 K. a) Comparison of the absorption spectra of monomeric (DCM) and aggregated (H_2O) solution. b) Irradiation of an aqueous solution with λ = 465 nm. c) Irradiation of a solution in DCM with λ = 465 nm. d) Irradiation of a solution in DCM with λ = 365 nm.

4. References

1 H. Maeda, Y. Ito, Y. Haketa, N. Eifuku, E. Lee, M. Lee, T. Hashishin and K. Kaneko, *Chem. Eur. J.*, 2009, **15**, 3706.

2 M. Yoshimoto, K. Honda, S. Kurosawa and M. Tanaka, *J. Phys. Chem. C*, 2014, **118**, 16067.

3 C. Rest, M. J. Mayoral, K. Fucke, J. Schellheimer, V. Stepanenko and G. Fernández, *Angew. Chem. Int. Ed.*, 2014, **53**, 700.

4 A. Florian, M. J. Mayoral, V. Stepanenko and G. Fernández, *Chem. Eur. J.*, 2012, **18**, 14957.

5 B. Hu, X. Lv, J. Sun, M. Ouyang, Z. Fu and C. Zhang, *J. Electrochem. Soc.*, 2013, **160**, H173-H178.

6 U. Vogeli and W. von Philipsborn, *Org. Magn. Reson.*, 1975, **7**, 617.

7 H. M. M. ten Eikelder, A. J. Markvoort, T. F. A. de Greef and P. A. J. Hilbers, *J. Phys. Chem. B*, 2012, **116**, 5291.

8 A. J. Markvoort, H. M. M. ten Eikelder, P. A. J. Hilbers, T. F. A. de Greef and E. W. Meijer, *Nature communications*, 2011, **2**, 509.

9 D. Cambié, C. Bottecchia, N. J. W. Straathof, V. Hessel and T. Noël, *Chem. Rev.*, 2016, **116**, 10276.

10 N. Mataga, Y. Kaifu and M. Koizumi, *BCSJ*, 1955, **28**, 690.

11 A. Kawski, *Z. Naturforsch. A*, 2002, **57**.